5104-38

Solar Thermal Power Systems
Point-Focusing
Distributed Receiver Technology Project

DOE/JPL-1060-16
Distribution Category UC-62

A Preliminary Assessment of Small Steam Rankine and Brayton Point-Focusing Solar Modules

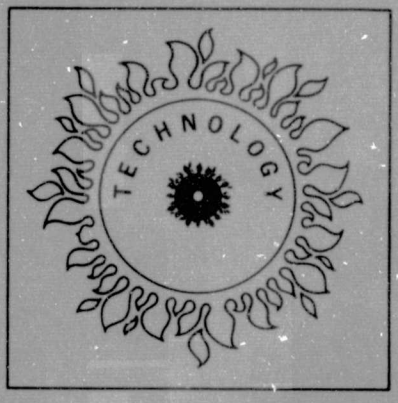

March 1, 1979

Prepared for
U.S. Department of Energy
Through an agreement with
National Aeronautics and Space Administration
by
Jet Propulsion Laboratory
California Institute of Technology
Pasadena, California
and
NASA Lewis Research Center
Cleveland, Ohio

(JPL PUBLICATION 79-21)

5104-38
Solar Thermal Power Systems
Point-Focusing
Distributed Receiver Technology Project

DOE/JPL-1060-16
Distribution Category UC-62

A Preliminary Assessment of Small Steam Rankine and Brayton Point-Focusing Solar Modules

E. J. Roschke
L. Wen
H. Steele
N. El Gabalawi
J. Wang

March 1, 1979

Prepared for
U.S. Department of Energy
Through an agreement with
National Aeronautics and Space Administration
by
Jet Propulsion Laboratory
California Institute of Technology
Pasadena, California
and
NASA Lewis Research Center
Cleveland, Ohio

(JPL PUBLICATION 79-21)

Prepared by the Jet Propulsion Laboratory, California Institute of Technology, for the U.S. Department of Energy by agreement with the National Aeronautics and Space Administration.

The JPL Solar Thermal Power Systems Project is sponsored by the U.S. Department of Energy and forms a part of the Solar Thermal Program to develop low-cost solar thermal electric generating plants.

ABSTRACT

A preliminary assessment of three conceptual point-focusing distributed solar modules is presented in this report. The basic power conversion units consist of small Brayton or Rankine engines individually coupled to two-axis, tracking, point-focusing solar collectors. An array of such modules can be linked together, via electric transport, to form a small power station. Each module also can be utilized, on a stand-alone basis, as an individual power source.

In the present study the technical evaluation and economic analysis were treated separately. Each system concept was optimized by maximizing the thermal output per unit of concentrator area. System performance was then simulated based on the insolation data recorded at Barstow, California (in 1976). Parametric studies concerning concentrator quality and power conversion efficiency were conducted to provide relevant sensitivity relationships and trade-off information. Hardware cost targets were assessed according to the system energy production rate (kWe-hr/yr), and a range of projected energy cost levels (mills/kWe-hr). The trade-off relationship can be utilized as a realistic guideline for establishing concentrator manufacturing requirements and power conversion development targets.

The objective of this investigation is to provide a method of screening candidates for Point-Focusing Distributed Receiver Solar Thermal Systems. Reliable hardware cost estimates are not available at the present time. It is expected that system cost projections will have large uncertainties because they are strongly affected by technology advancement and market penetration situations. The approach adopted in the present study is to calculate the capital investment that would be justified to supply energy at a range of energy costs, assuming a range of performance factors. These relationships can be used whenever updated hardware costs are obtained or whenever proven component performance data are obtained (e.g., improvements in concentrator quality and power conversion efficiency). The strategy is to screen out the least cost effective options that occur within the specified time frame, considering the technological maturity of different power conversion schemes and the degree of readiness of the concentrator manufacturing industry.

The justified capital cost of small (15 kWe output) gas Brayton systems at 816°C (1500°F) and steam Rankine systems at 538°C (1000°F) has been compared for a range of energy cost values. Accurate values for the efficiency of small power conversion subsystems are not available. However, the current assessment is approximately 35% for Brayton power conversion efficiency, and 25 to 30% for steam Rankine. The results obtained indicate that the Brayton system merits a higher capital cost than the Rankine system for an energy cost target of 50 mills/kWe-hr, if the concentrator quality is in the range of 1 to 4 mrad. It is expected that the cost of Brayton concentrators will be greater than the Rankine concentrators.

ACKNOWLEDGMENTS

The guidance and support of V. C. Truscello, Thermal Power Systems Project Manager, and J. W. Lucas, Point-Focusing Distributed Receiver (PFDR) Technology Technical Manager, are gratefully acknowledged. Valuable review inputs and suggestions were obtained from them, as well as from W. Carley, J. Bowyer, T. Fujita, and W. Owen. The authors wish to thank R. Summers and G. Parker for their contributions during the early phase of this study.

The cooperation and support of M. Bailey and J. Heller, of NASA Lewis Research Center are much appreciated for their power conversion subsystem development and performance estimation. Special thanks to J. Sheldon and L. Flinn for their efforts in editing and publishing this report.

This study was performed by the Systems Engineering Task group of the PFDR Technology Project. The authors appreciate the support of the DOE Division of Solar Energy, and particularly the assistance of J. Rannels and M. Gutstein.

CONTENTS

(APPENDIX A, Continued)

Figures

Tables

NOMENCLATURE

A_c	Area of Concentrator Aperture
A_o	Receiver Cavity Opening Area (Aperture)
A_w	Receiver Cavity Wall Area
B	Coefficient of Thermal Expansion
CI_{pv}	Present Value of Capital Investment
C_p	Specific Heat at Constant Pressure
CRF	Capital Recovery Factor
CR	Geometrical Concentration Ratio
D	Concentrator Aperture Diameter
d	Number of Years
E	Recuperator Effectiveness
EC	Levelized Busbar Energy Cost
f	Focal Length
f_g	Gouffe's View Factor
FCR	Annualized Fixed Charge Rate
G	Shading/Blocking Factor
g	Gravitational Constant
g_i	General Rate of Inflation
Gr	Grashof Number
H	Forced Convection Coefficient
h_f	Free Convection Coefficient
h_c	Coefficient of Heat Transfer Through Insulation
h_{fr}	Convective Heat Transfer at Front Surface
h_{back}	Convective Heat Transfer Coefficient for the Back Surface of a Flat Plate
h_h	Coefficient of Heat Transfer of a Horizontal Plate
h_v	Coefficient of Heat Transfer of a Vertical Plate

NOMENCLATURE (contd)

I	Direct Normal Insolation
I_o	Design Point Insolation
J	Local Flux Intensity
K	Thermal Conductivity
l	Concentrator Characteristic Length
L	Receiver Length
MNT_{pv}	Present Value of the Annual Maintenance Cost
$\hat{n}$	Surface Normal Vector
Nu	Nusselt Number
OP_{pv}	Present Value of Annual Operating Cost
$P(r)$	Probability Function
P_e	Electric Power Production
Pr	Prandtl Number
Q_c	Net Thermal Power Collected by Receiver
Q_r	Receiver Heat Loss
Q_t	Transport Heat Loss
Q_{cond}	Conductive Heat Loss through Receiver Insulation
Q_{conv}	Convective Heat Loss (Receiver Aperture)
Q_{rad}	Radiative Heat Loss (Receiver Aperture)
R	Receiver Aperture Radius
R_1, R_2	Reflectance Coefficient
r	Receiver Cavity Wall Radius
T_r	Effective Receiver Radiative Temperature
T_e	Effective Receiver Convective Heat Loss Temperature
T_a	Ambient Temperature
T_w	Absorber Tube Wall Temperature
T_{fl}	Working Fluid Temperature

V	Wind Speed
W	Annual Electric Energy Production
x, y, z	Cartesian Coordinates

GREEK SYMBOLS

α_s	Solar Absorptance
α_{eff}	Effective Solar Absorptance
ϵ	Surface Emittance
ϵ_{eff}	Effective Emittance
ϵ_p	Pointing Error
η	Power Conversion Efficiency
η_o	Rated Conversion Efficiency
$\xi_r(I_o)$	Rated Receiver Efficiency
$\xi_c(I_o)$	Rated Collector Efficiency
ψ	Concentrator Rim Angle
ζ_{cal}	Calorimetric Efficiency
μ	Micron
ρ	Reflectance
ρ_d	Density (Air)
ϕ	Interception Factor
ϕ^*	Spherical Cavity Aperture Half Angle
σ	Stefan Boltzmann Constant
σ_s	Surface Slope Error
σ_w	Specularity Function
$\Delta\theta$	Specular Spreading Angle
ν	Kinematic Viscosity of Fluid
τ	Receiver Tilt Angle

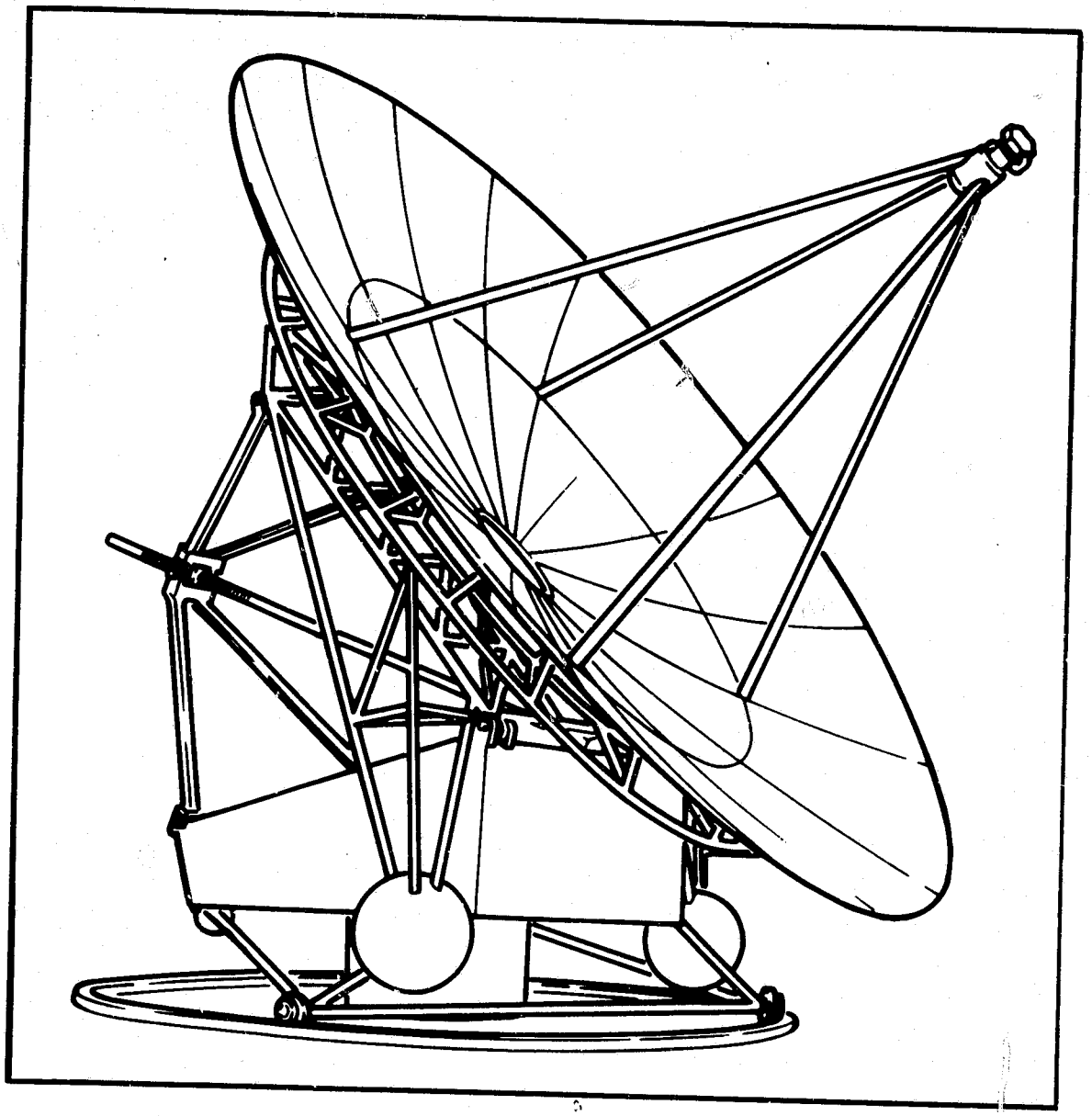

Frontispiece

SECTION I

INTRODUCTION

Distributed solar power generation concepts with modules consisting of two-axis, tracking, point-focusing collectors are considered a viable and attractive method of producing electric power and for providing process heat. The major merit of the concept lies in its high performance capability and its use of subsystems that can be mass-produced at low cost. In addition, modules can be assembled in the quantity needed to achieve the power requirements at a particular site, with modules added as the load requirements grow. JPL currently is conducting projects for the Department of Energy for development of low-cost, high performance options of point-focusing distributed systems. A number of power conversion and energy transport options have been considered (Refs. 1 and 2). The current phase of investigation is limited to electrical transport concepts with near-term power conversion technology utilizing Brayton and Rankine cycles.

A representative point-focusing distributed solar thermal module (see frontispiece) consists of two major subsystems: the solar collector and the power conversion unit. The conversion process of solar energy into electric power is illustrated in Figure 1-1. Direct normal insolation that impinges on a two-axis, tracking concentrator is reflected to the receiver/absorber assembly, where thermal energy is transferred to the working fluid. The net thermal power is then utilized to operate a heat engine and generator to generate electricity at each individual module. Electric power production, P_e is determined by the collector thermal optical performance and the power conversion efficiency

$$P_e = Q_c \cdot \eta \qquad (1.1)$$

where

P_e = electric power production

Q_c = net thermal power delivered from receiver to power conversion subsystem

η = power conversion efficiency at the operating condition.

The economic viability of a solar thermal power conversion system depends primarily on the cost effectiveness of the collector design and the power conversion efficiency. Current activities of the Point Focusing Distributed Receiver (PFDR) Technology Project are concentrated on industrial development of critical subsystems; namely, concentrators, receivers, and power conversion units (Ref. 3). Systems engineering efforts are concentrated in three general areas: (1) participation in design team activity to coordinate and to integrate subsystem development and specifications, (2) establishment of hardware cost and performance targets, and (3) system definition.

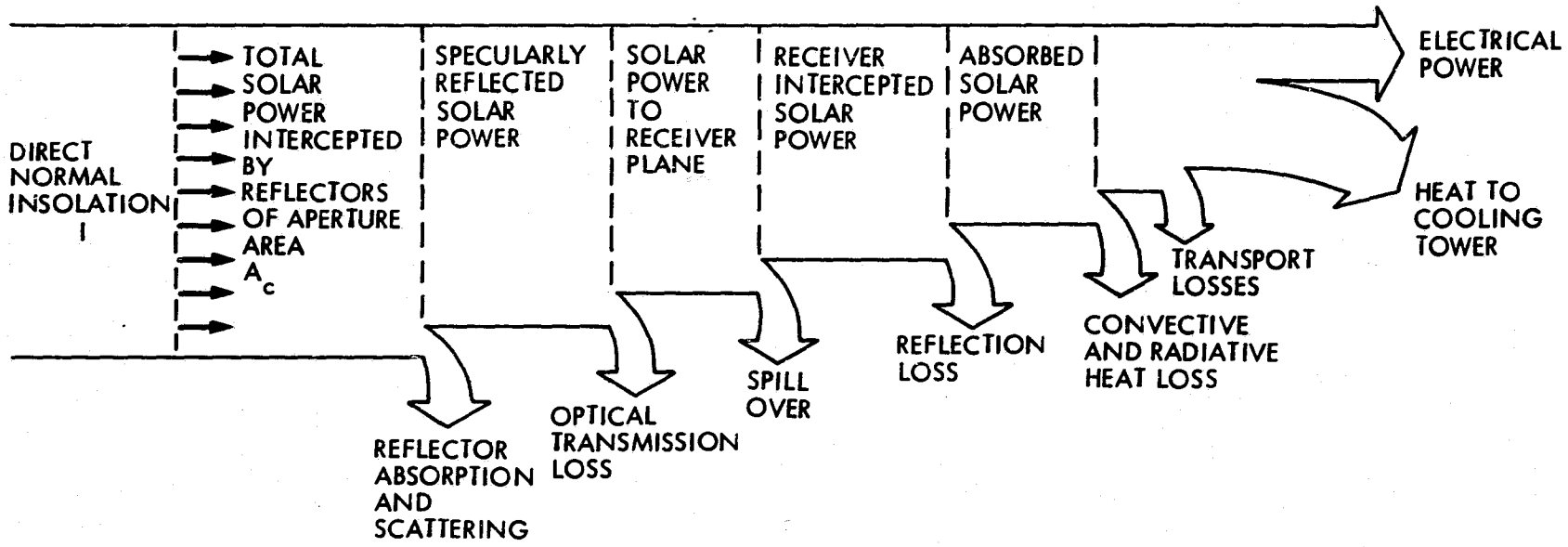

$$\left[\begin{array}{c}\text{COLLECTED THERMAL POWER TO ENGINE}\\ Q_c\end{array}\right] = \left[\begin{array}{c}\text{REFLECTED SOLAR POWER}\\ \rho I A_c G\end{array}\right] \times \left[\begin{array}{c}\text{INTERCEPTION FACTOR OF RECEIVER}\\ \phi\end{array}\right] \times \left[\begin{array}{c}\text{EFFECTIVE RECEIVER SOLAR ABSORPTANCE}\\ \alpha_{eff}\end{array}\right] - \left[\begin{array}{c}\text{RADIATIVE + CONVECTIVE HEAT LOSS RATE}\\ Q_{rad} + Q_{conv}\end{array}\right] - \left[\begin{array}{c}\text{CONDUCTIVE + TRANSPORT HEAT LOSS}\\ Q_{cond} + Q_t\end{array}\right]$$

$$\left[\begin{array}{c}\text{ELECTRIC POWER}\\ P_e\end{array}\right] = \left[\begin{array}{c}\text{THERMAL POWER}\\ Q_c\end{array}\right] \times \left[\begin{array}{c}\text{POWER CONVERSION EFFICIENCY}\\ \eta\end{array}\right]$$

Figure 1-1. Solar Thermal Energy Balance Relationship

The objective of system definition is to select, based on projected commercial cost and performance, small power system options that will provide the most favorable life-cycle cost per unit of useful energy produced.

This study presents a preliminary assessment of small (approximately 15 kWe output) point-focusing distributed receiver solar modules without storage. Steam Rankine and gas Brayton systems were selected for analysis because currently they are the candidates for the PFDR Technology Project (Ref. 3). In contrast, previous studies addressed a variety of distributed receiver concepts with internal or external storage for power plants in the size range of 10 to 50 MWe (Ref. 4) and, more recently, in sizes less than 10 MWe (Ref. 5).

Technical aspects of the principal subsystems (concentrators, receivers, and power conversion units) are reviewed in the Appendices. This information was used to assist in making subsystem selections for the candidate systems chosen for study herein. Concentrators have been reviewed in some depth because they are the most critical and costly subsystem for solar thermal power systems. Power conversion subsystem information was supplied by the NASA Lewis Research Center.

A. OBJECTIVES

The main purpose of this investigation is to establish a cost/performance frame of reference for candidate point-focusing distributed receiver solar thermal systems that are to be developed for use in the early to mid 1980s time frame. One goal is to relate specific system configurations to justified capital investment. The specific objectives are to:

- Develop a methodology appropriate for preliminary screening of candidate systems on the basis of performance and cost.
- Demonstrate the methodology by application to baseline steam Rankine and gas Brayton systems.
- Present results which are not based on specific assumptions of subsystem capital costs. Later, the results can be utilized when such costs become available.

B. APPROACH AND METHODOLOGY

All solar thermal systems are characterized by the fact that they require a high initial capital investment. The selection of a relatively low cost, high performance system involves detailed system optimization that maximizes the cost effectiveness of all candidate options. Such a complicated trade-off process requires an accurate system performance analysis and reliable cost information. Because the solar energy industry is still in a very early developmental stage, reliable mass production cost estimates are not now available.

Until better production cost information can be established by the manufacturing industry through subsystem development programs (such as the Low Cost Concentrator contracts currently underway between JPL and several companies), it is necessary to separate the cost and performance issues to compare different solar thermal concepts. One realistic and useful approach is to establish relevant cost/performance trade-off relationships for the candidate systems. Conditional assessments then can be conducted based on different projections of hardware cost/quality and technology progress.

The proposed approach is significantly different from conventional methodology, in which the projected energy cost (mills/kWe-hr) of a specific system is computed based on system performance simulation and mass production hardware cost estimates. Such system comparative studies may lead to conflicting conclusions arising from inconsistencies in the input hardware costs, which are premature at this time. The adopted methodology is to establish the conditions in hardware cost and quality that enable a specified concept to be competitive under a projected energy cost scenario. These sets of conditions or requirements can be judged against current and projected technology status. Candidate systems can be cataloged according to the anticipated degree of difficulty for the concept to be competitive. The critical information needed for performing system selection is a realistic assessment of the future technology readiness and hardware cost projection. System concepts will be ranked in an order that indicates the likelihood that the subsystem costs will meet the concept goal when the concentrator quality and power conversion efficiency are specified.

Basically, this investigation is focused on a trade-off relationship between three key parameters: concentrator surface quality, receiver temperature, and power conversion efficiency.

C. COST AND PERFORMANCE TARGETS

Initial project cost targets for the various subsystems are shown in Table 1-1. These target costs, in 1978 dollars, include expected reductions due to mass production. For concentrators and receivers the expected reduction for mass production is a factor of five, and for power conversion units is a factor of ten. The values given in Table 1-1 must be realized to achieve an energy cost target of approximately 50 to 60 mills/kWe-hr in the post-1985 time frame. It should be emphasized that these are capital costs per unit size or capacity.

Initial performance targets are shown in Table 1-2. Collector efficiency, which is the product of concentrator and receiver efficiency, includes concentrator reflectivity and blockage, receiver efficiency, and transport losses from receiver to power conversion unit. Of course, transport losses are negligible when the power conversion unit is close-coupled to the receiver mounted at the concentrator focal plane. As will be shown later, it is ambiguous to cite a collector efficiency target unless the insolation design point and the concentrator surface quality also are specified. Also, it is

Table 1-1. Initial Cost Targets for PFDR Technology Project

Subsystem	FY 1982 First Generation	FY 1985 Second Generation
Concentrators	$100-150/m^2	$70-100/m^2
Receivers	$30/kWe	$20/kWe
Power Conversion	$75/kWe	$60/kWe

important to point out that present information is not sufficient to relate concentrator cost to size and surface quality. When this information becomes available more accurate cost and performance targets for PFDR solar thermal systems can be established. Power conversion efficiency at rated or full-load electrical power output is the product of heat engine efficiency and the generator or alternator efficiency; it does not include power conditioning. It will be a challenge to achieve the performance targets given in Table 1-2 for items in large-scale mass production.

The values given in Table 1-2 do not include allowance for thermal (internal) or electric (external) storage. For illustrative purposes, it is useful to relate the relative energy cost with overall system efficiency and collector cost (including receiver) per unit of concentrator area. One such example is shown in Figure 1-2, which is a typical case calculated previously for a 10 MWe power plant with a capacity factor of 0.55. This example indicates the strong effect that collector cost and system efficiency have on energy cost for PFDR solar thermal systems.

Table 1-2. Initial Performance Targets for PFDR Technology Project

Major Subsystem	FY 1982 First Generation	FY 1985 Second Generation
Collector Efficiency	72%	78%
Power Conversion Efficiency	25-35%	35-45%
System (Overall)	18-25%	27-35%

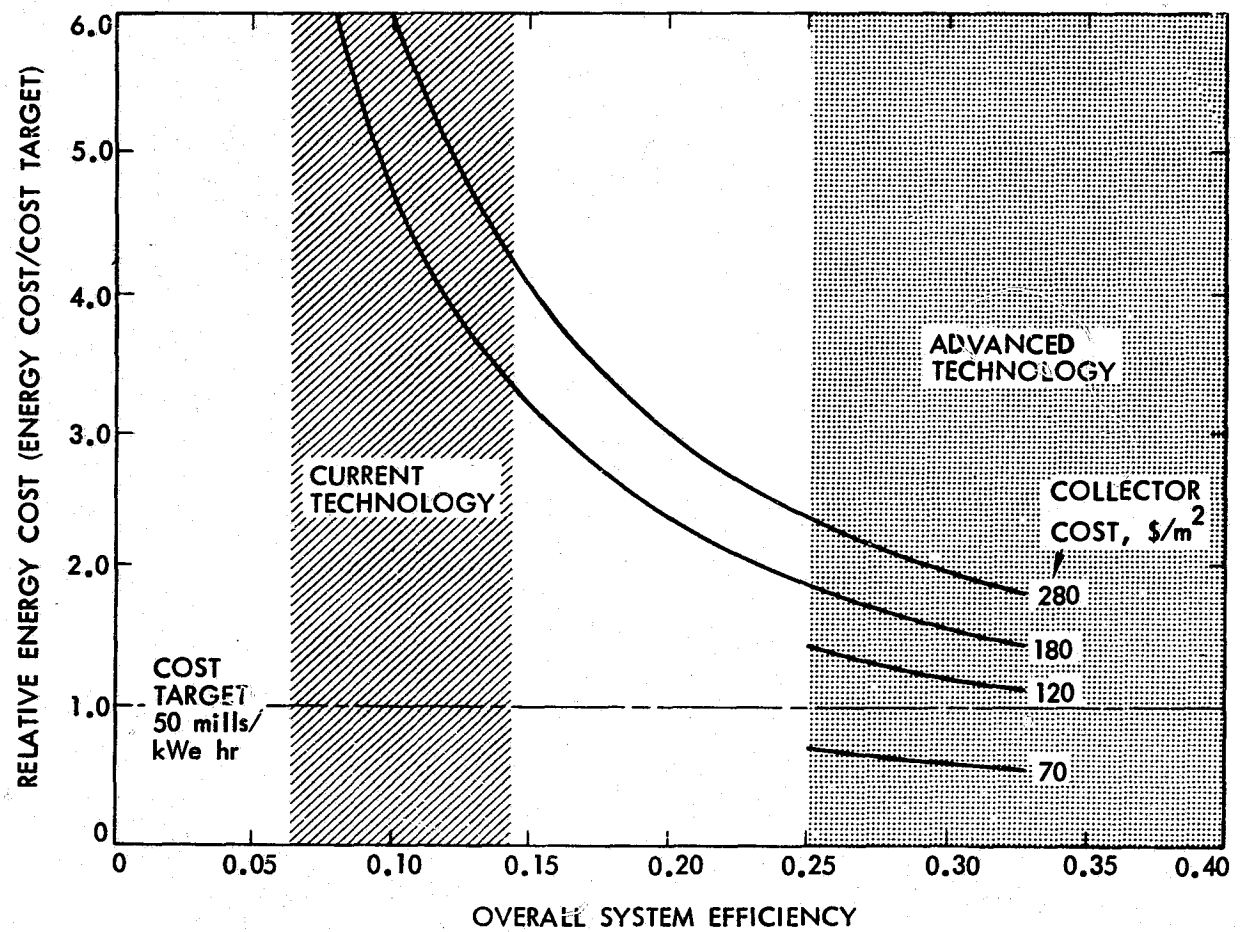

Figure 1-2. Effect of Improvements in System Efficiency on Achievement of Energy Cost Reduction

Apart from an electrical output, PFDR systems can be utilized for thermal output that can be extracted at the exit of the receiver or the thermal transport subsystem for applications such as process heat. There is a unique relationship between energy cost for electrical output and thermal output that depends solely on power conversion efficiency (and appropriate unit conversion factors) irrespective of any economic assumptions. This relationship is shown in Figure 1-3. An energy cost target of $5 per million Btu of thermal output will yield an energy cost target of 50 mills/kWe-hr if the power conversion efficiency is 35%.

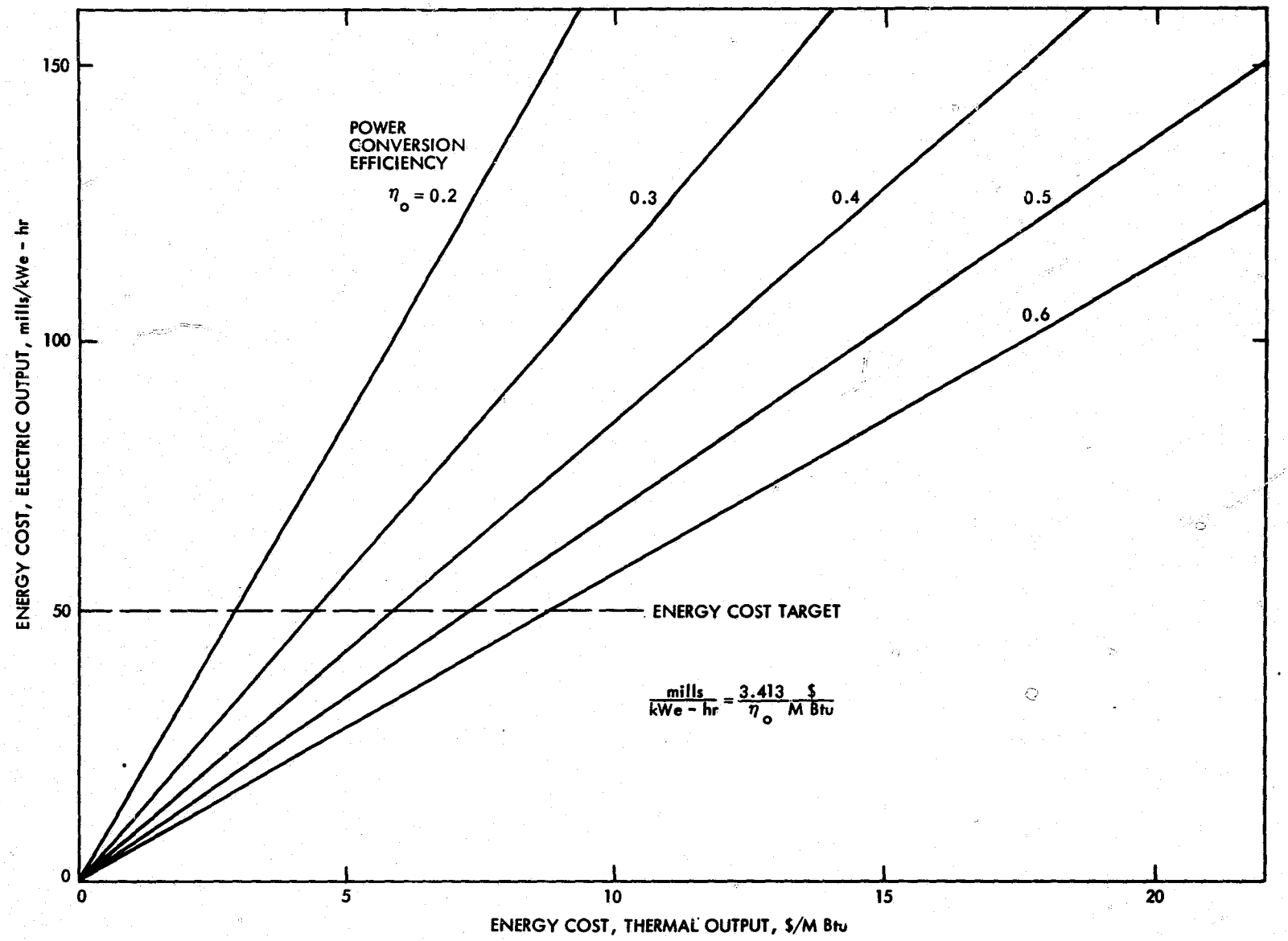

Figure 1-3. Equivalence of Electric and Thermal-Output Energy Cost

SECTION II

SYSTEM PERFORMANCE EVALUATION

A. BASIC CONSIDERATIONS

The methodology for assessing candidate systems were developed in FY 1978 and will be refined, broadened, and improved to meet needs anticipated for the future. Simplifications were introduced to enable a timely approach to achieve early results. Candidate PFDR systems in the nominal range of 15 kWe output were examined initially with regard only to performance and justified capital cost. Emphasis was placed on single-dish modules with the power conversion unit mounted at the focal point. Later, systems consisting of multiple dishes connected to a larger ground-mounted power conversion unit will be analyzed to examine the trade-off between engine size and efficiency, and transport losses.

1. Ground Rules for the Study

Basic ground rules for the study are as follows:

(1) Only solar thermal-electric power production is considered. Hybrid modules utilizing fossil fuels and total energy systems were excluded from consideration.

(2) Only single PFDR modules are considered, not large power plants. Paraboloidal dish-concentrators are utilized.

(3) The baseline modules are assumed to displace energy only, so that thermal/electric storage is not required. This assumption effectively decouples the performance analysis from the economic analysis.

(4) The power conversion unit is assumed to be dish-mounted (close-coupled to thermal receiver) so that transport losses are negligible. This assumption tends to favor Brayton systems, which intrinsically would have higher transport (to ground) losses than lower temperature Rankine systems if dish mounting were not employed.

(5) Candidate baseline systems are steam Rankine and gas Brayton (both open- and closed-cycle). The systems are sized accordingly to yield 60 kWth output from the receiver at design point insolation.

(6) Operating and maintenance costs are not included. This assumption is conditionally valid because it does not affect the results of the parametric approach significantly.

(7) The analysis applies only for quasi-steady operation; transient performance arising from rapidly varying solar insolation (changing cloud cover) is not considered.

(8) Solar insolation data from Barstow, California (1976) is used to determine annual energy production.

(9) Concentrator surface quality is based on the so-called "standard deviation" definition, not the "scatter-sun" definition.

2. Analysis Procedure

Concentrator quality (slope error), operating temperature, power conversion efficiency, and energy cost are treated as variables in a sensitivity analysis. However, operating temperature was selected in accordance with the specified power conversion subsystem, i.e., Rankine or Brayton, and the nominal power output was preselected to be 15 kWe. General steps in the analysis procedure are as follows:

(1) Define the design point for solar insolation.

(2) Specify (and vary) concentrator quality and operating temperature of system module.

(3) Calculate optimum receiver aperture size.

(4) Calculate annual thermal energy collected.

(5) Specify (and vary) power conversion efficiency.

(6) Calculate annual electric output.

(7) Specify (and vary) energy cost.

(8) Calculate justified capital investment.

The results are displayed in a variety of charts.

3. Reference Insolation Environment

Barstow, Calif., where a solar thermal pilot plant will be located, is the insolation data base selected for the present study (Ref. 6) Direct normal insolation was measured with normal incident pyrheliometers in 15 minute intervals, by the Southern California Edison Company acting in conjuction with the West Associates Solar Resource Assessment Project (Ref. 7). Instrument and hardware outages resulted in a data loss of 80 hours in 1976* between 7 a.m. and 7 p.m. These included six complete days (May 12, December 9, 13, 14, 18, 19), and two partial days (May 11 and 13). The total annual accumulated insolation (discounting the missing data) was 2631 kW-hr/m^2. The maximum recorded insolation level was 1.036 kW/m^2, and occurred on March 12, 1976 at 11:45 a.m. Figure 2-1 shows the histogram of insolation levels. The raw recorded data were modified by Aerospace Corporation (Ref. 8) to fill in the missing data using established

---

*A leap year

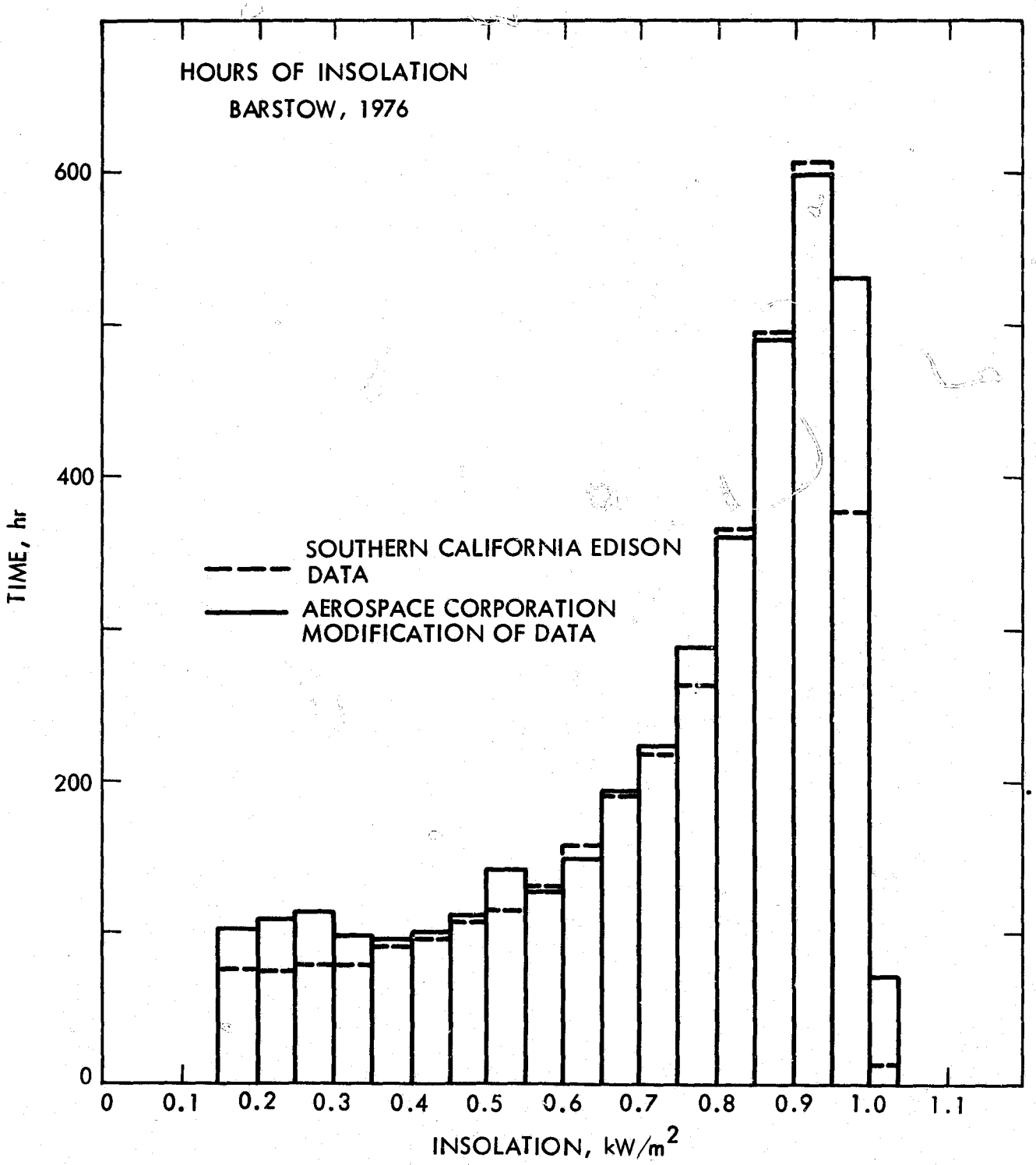

Figure 2-1. Solar Insolation Histogram (Barstow, Calif., 1976)

calculation procedures. Insolation data below 0.15 kW/m^2 was discarded (Figure 2-1) because off-zero night readings were judged to be erroneous; i.e., instrument readings did not return to zero at night. Note that large differences between the raw data and modified data are evident at the high insolation levels (Figure 2-1); this is due to the data modification assumptions used by Aerospace Corporation.

The total accumulated annual insolation using the modified Aerospace data was 2848 kW-hr/m^2, which is 217 kW-hr/m^2 higher than the recorded raw data (approximately 8%). A comparison of the two histograms (Figure 2-1) indicates that the major difference between the recorded raw data and the modified data was in the insolation band between 0.95 to 1 kW/m^2. The daily profiles are illustrated in Figure 2-2 for summer and winter solstices. Note that clouds appeared in the afternoon of December 22, causing a rapid insolation decline. A multiplying factor was used to convert the measured raw data to the absolute scale (Ref. 8). For the present analysis the modified Aerospace Corporation insolation data tape was selected for use. To determine the sensitivity to insolation inputs, however, the raw data also were used to process several cases.

4. General Subsystem Considerations

To place the present study in a more meaningful context a detailed review of concentrators, receivers (together called the collector, in conventional terminology) and power conversion units is given in the Appendices. The interested reader may consult the Appendices for more background information.

Concentrators are discussed in Appendix A with reference to optical transmission characteristics (including surface slope error), existing configuration concepts, and concentrator quality. The last topic includes slope error measurements, flux mapping (at the concentrator focal plane), and calorimetric measurements. Receivers are discussed in Appendix B with reference to cavity radiative characteristics, solar absorber arrangements, and receiver heat losses. A brief review of Brayton and Rankine cycles is given in Appendix C.

A two-axis, tracking, point-focusing solar collector is composed of a dish-type concentrator, a receiver, and associated conduits/piping to transport the working fluid to the power conversion unit. The net thermal power delivered to the power conversion subsystem is expressed as:

$$Q_c = IA_c G \Phi_{eff} - Q_r - Q_t \qquad (2.1)$$

where

ρ = solar reflectance of concentrator mirror
I = direct normal solar insolation
A_c = effective concentrator aperture area
G = geometrical factor for shading and blocking
Φ = receiver interception factor, fraction of the total energy at the focal plane that is intercepted by the receiver aperture

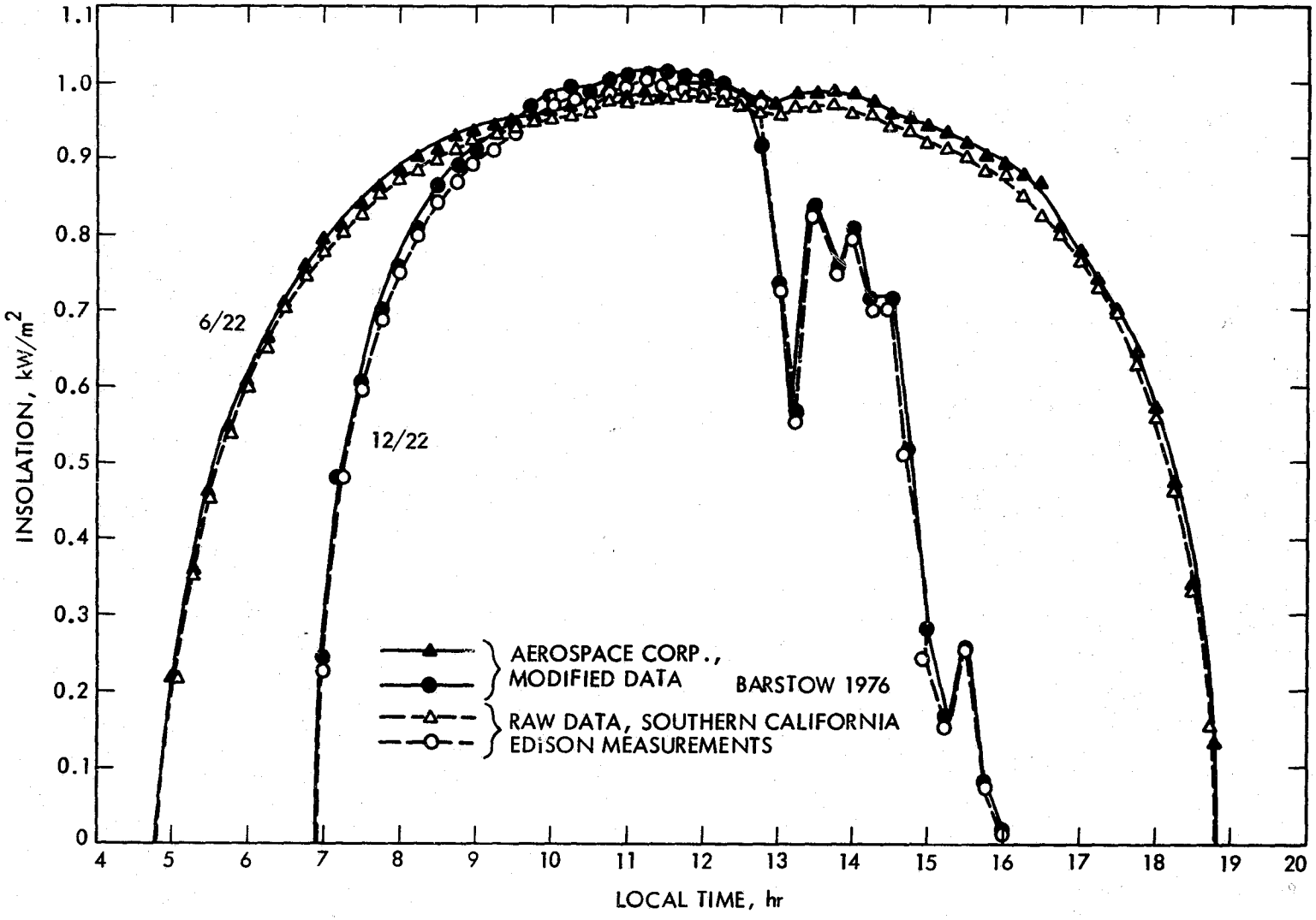

Figure 2-2. Sample Insolation Profile (Barstow, Calif., 1976)

α_{eff} = effective solar absorptance of the receiver cavity
Q_r = receiver heat loss
Q_t = transport line loss

The geometrical shading factor, G, for a point-focusing collector consists of two parts: (1) the shading on reflector surface or blocking of the receiver by supporting structure, and (2) the shading by neighboring concentrators at low solar elevation angles. The structural shading/blocking is determined by the design and would remain unchanged throughout the operating hours. Shading by neighboring concentrators is, on the other hand, a function of the sun position and latitude, the field layout, and the tracking scheme. Conventional tracking schemes generally are based on sequential rotation around orthogonal axes of the surface. In general, two successive rotational motions around two different axes are required to track the sun. Azimuth-elevation mounting, and polar mounting, are the two most commonly employed schemes for two-axis, sun-tracking collectors. Detailed discussion of the tracking/pointing mechanism is given in Reference 9.

Although the present study is confined to single modules, it will be useful to consider briefly the effects of mutual shading by adjacent concentrators in a field array. Figure 2-3 illustrates the shadow pattern of a square concentrator with an Az-El tracking mount (Ref. 10). The minimum distance between the centers of two adjacent concentrators is the concentrator diameter, so there is no mechanical interference during installation, operation and maintenance. In practice, the spacing must be larger. Obviously, sufficient separation must be maintained to minimize shadowing of neighboring concentrators. There is a preference for arranging rows along a north-south direction. Because the shadow lengths are shorter in the north-south direction (Figure 2-3), collectors can be spaced more closely in the north-south direction than in the east-west direction. In general, field layout is important to minimize transport losses and maximize land utilization. These considerations are not relevant to the present preliminary study, which is limited to single modules. In Eq. 2.1, Q_t is zero because the power conversion systems are close-coupled to the receiver at the focal location.

The interception factor Φ in Eq. 2.1 includes the effects of pointing/tracking error, and concentrator surface quality.

B. CANDIDATE SYSTEMS

Three candidate systems for point-focusing distributed receiver solar thermal electric power generating modules are discussed in the following sections. These candidates include baseline steam Rankine and gas Brayton concepts (open-cycle air and closed-cycle air) as reference systems (Ref. 3) and may differ significantly from final system designs adopted by the Project. The basic make-up of a module consists of a two-axis, point-focusing concentrator, a cavity-type receiver and a power conversion subsystem mounted near the receiver.

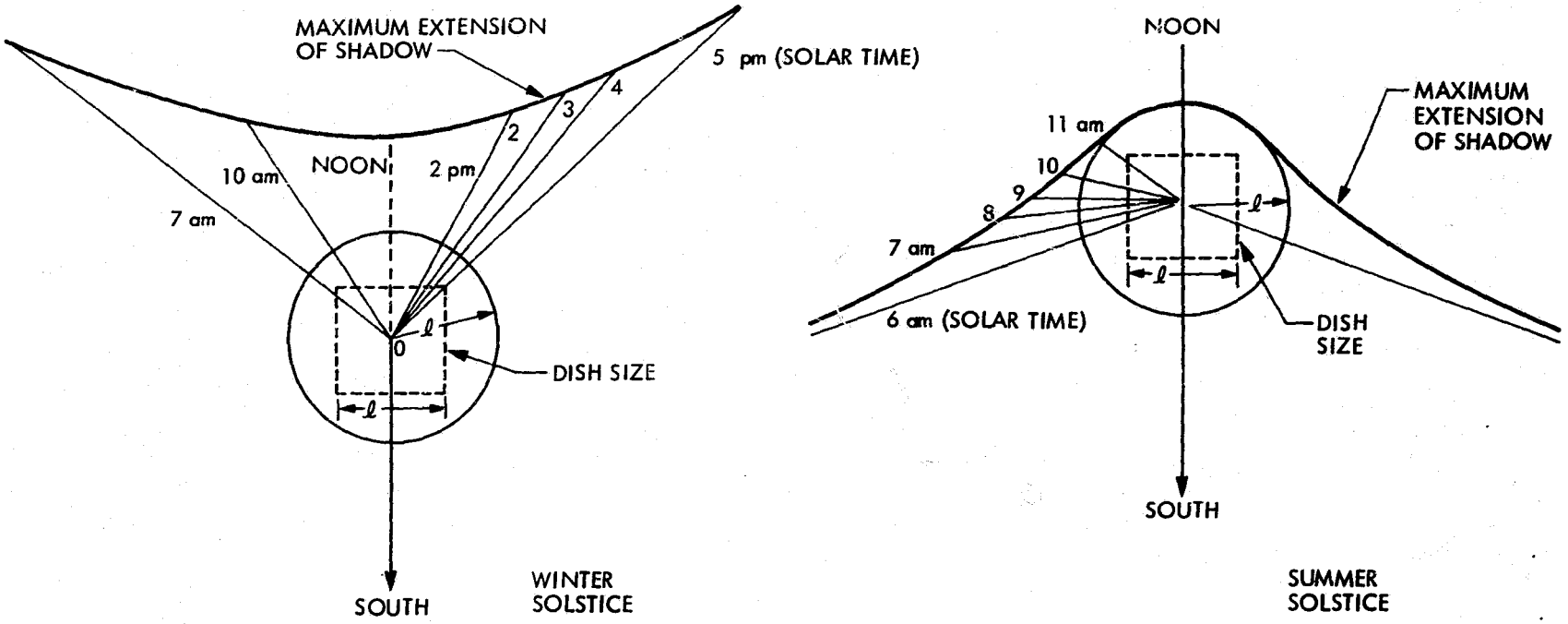

Figure 2-3. Concentrator Shadow Pattern (Latitude 35^{o} N)

1. Baseline Steam Rankine System

The schematic of the baseline Rankine system is illustrated in Figure 2-4 (Ref. 11). The power conversion unit specified uses a two-stage reciprocating steam engine directly coupled to the electric alternator. About 18% of the steam extracted from the high pressure cylinder outlet is fed into the feed water heater directly to add sensible heat and to improve the overall power conversion efficiency. The air-cooled condenser is mounted directly on the engine assembly. Both are mounted to the receiver. The total weight of the power conversion unit is estimated to be 283 kg (625 lb). The condenser unit is air-cooled with a 0.82 kW (1.1 HP) fan. The design specification of the steam Rankine power conversion is listed in Table 2-1. Efficiency can be increased further by employing a reheat cycle in which additional heat from the receiver is furnished to the steam as it passes through the connecting lines between the high temperature and low temperature stages of the expander. Schemes for water-cooling the condenser offer some potential for increasing cycle efficiency and for decreasing the fan power consumption.

The receiver is considered to be a cylindrical cavity with coil-type absorber (Ref. 12). Because the heat transfer characteristics are significantly different for water preheating, boiling and superheating, the design includes a separator between the boiler and the superheater sections. In addition, sufficient transient storage is considered to provide enough thermal inertia for transient operations. The baseline design specification is shown in Table 2-2. The rated efficiency of the receiver is governed by the heat loss, which is dictated by the concentrator quality (see later section, Receiver Aperture Optimization).

2. Baseline Brayton Systems

The schematics of the baseline open-cycle (air) and closed-cycle (air) Brayton systems are shown in Figures 2-5 and 2-6, respectively (Ref. 13). The power conversion units are recuperated turbines with the required variable gear ratio to drive an alternator. The turbocompressor unit weighs around 91 kg (200 lb) and the alternator weighs less than 91 kg (200 lb). Both systems (with recuperators) have nominal operating temperatures at 816°C (1500°F). For open air cycle operation, ambient air is passed through a filtered evaporative cooler at 27°C (80°F) before entering the compressor. In the recuperator, the compressed air receives thermal energy from the hot turbine exhaust before entering the receiver. The recuperator exit to ambient temperature is around 149-204°C (300-400°F) depending upon the effectiveness of the recuperator. For closed-cycle operation, the working fluid is compressed, heated to an intermediate temperature in the recuperator, and heated finally to the required temperature of 816°C (1500°F) in the receiver. The gas is then expanded through a turbine. Turbine exhaust gas is first cooled in the recuperator, and then in the cooler (radiator), to the minimum temperature before delivery back to the compressor. The design specifications and operating conditions of the baseline open- and closed-cycle Braytons are compared in Table 2-3.

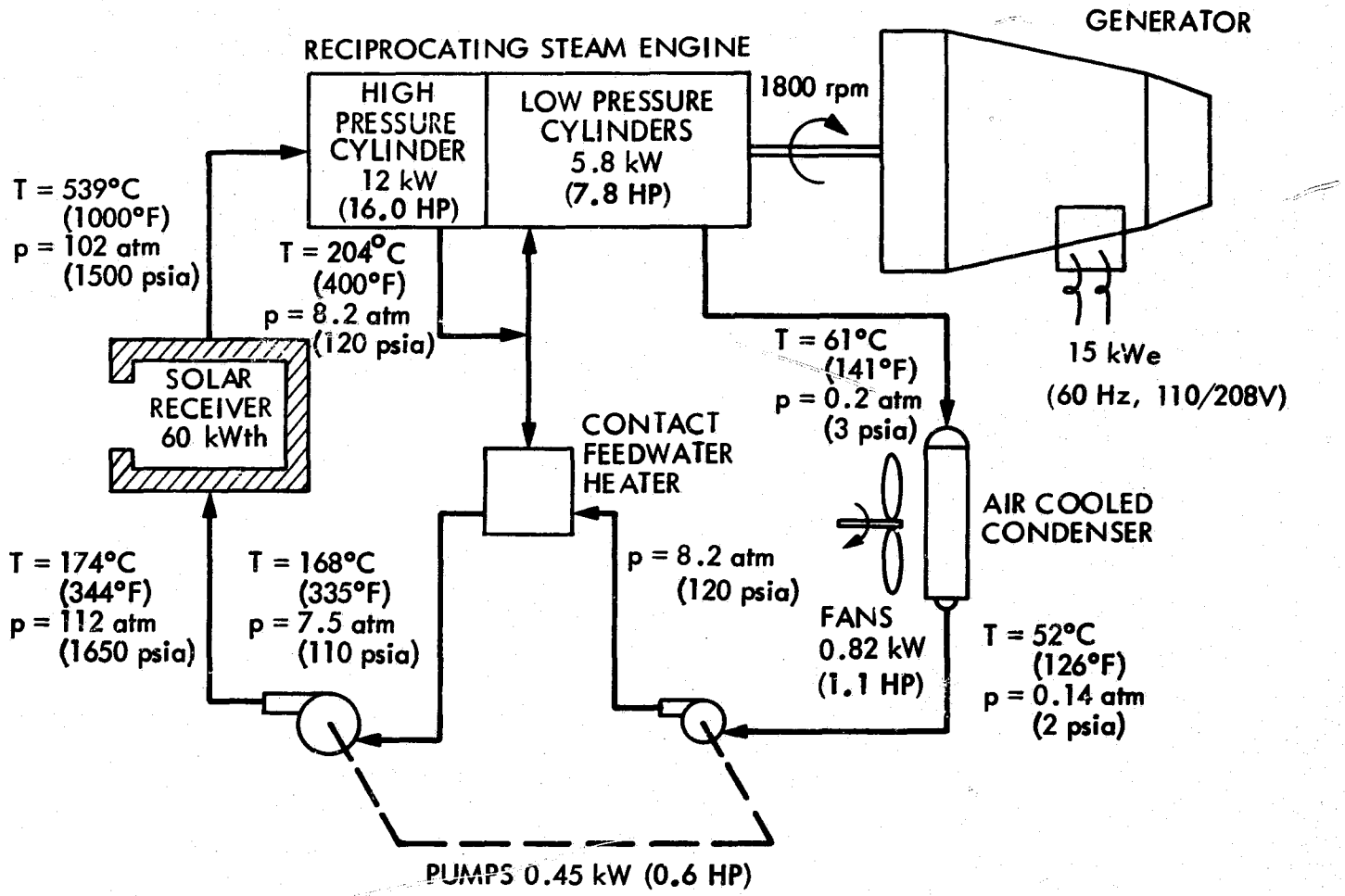

Figure 2-4. Schematic of Baseline Steam Rankine System

Table 2-1. Baseline Specifications of Steam Rankine Power Conversion Subsystem

Defined Parameters (reciprocating steam Rankine cycle direct shaft coupled to 60 Hz alternator):

Rated Capacity	20 kWe ± 5 kWe	
Overload capability	120%	
Overall power conversion efficiency (including AC generator and auxiliary power requirements for fluid pumping and condenser cooling fan. No reheat included)	25% ± 5%	
Mass flow rate to high pressure (HP) side of engine	79 kg/hr	(174.3 lb/hr)
Engine HP inlet temperature	538°C	(1000°F)
Engine HP inlet pressure	102 atm	(1500 psia)
Enthalpy at engine HP inlet	3458 $\frac{\text{kW-sec}}{\text{kg}}$	(1490 Btu/lb)
Engine HP outlet temperature	204°C	(400°F)
Engine HP outlet pressure	8.2 atm	(120 psia)
Enthalpy at engine HP outlet	2845 $\frac{\text{kW-sec}}{\text{kg}}$	(1226 Btu/lb)
Mass flow rate to low pressure (LP) side of engine	64.3 atm	(141.7 lb/hr)
Condenser inlet temperature	61°C	(141°F)
Condenser inlet pressure	0.2 tm	(3.0 psia)
Enthalpy at condenser inlet	2413 $\frac{\text{kW-sec}}{\text{kg}}$	(1040 Btu/lb)
Condenser outlet temperature	50°C	(126°F)
Condenser outlet pressure	0.14 atm	(2.0 psia)
Enthalpy at condenser outlet	218 $\frac{\text{kW-sec}}{\text{kg}}$	(94 Btu/lb)
Feedwater inlet pressure	8.2 atm	(120 psia)
Steam extraction flow rate to feedwater heater	14.8 kg/hr	(32.6 lb/hr)
Feedwater preheater outlet temperature	169°C	(335°F)
Feedwater preheater outlet pressure	7.5 atm	(110 psia)
Feedwater pump power required	0.45 kW	(0.6 Hp)
Condenser cooling fan power required	0.82 kW	(1.1 Hp)
Operating speed		1800 rpm
Alternator efficiency		0.91
Generated power		110/208 volts AC 60 Hz
Engine weight including feedwater system and condenser	129 kg	(285 lb)
Generator weight	131.5 kg	(290 lb)
Mounting brackets and hardware	22.7 kg	(50 lb)
Total estimated weight	283 kg	(625 lb)

Table 2-2. Baseline Steam Receiver Specification

Solar Receiver (cavity type):		
Defined Parameters		
Power production	60 kWth	
Outlet steam temperature	538°C	(1000°F)
Outlet steam pressure	102 atm	(1500 psia)
Steam flow rate	76 kg/hr	(174.3 lb/hr)
Weight	90.7 to 181 kg	(200 to 400 lb)
Derived Parameters		
ΔT between working fluid and tubes	22°C	(50°F)
Total pressure drop	10.2 atm	(150 psia)
Inlet water temperature	173°C	(344°F)
Inlet water pressure	112 atm	(1650 psia)
Inlet enthalpy	732.7 $\frac{kW\ sec}{kg}$	(315 Btu/lb)
Fluid flow rate	79 kg/hr	(174.3 lb/hr)
Outlet enthalpy	3458 $\frac{kW\ sec}{kg}$	(1490 Btu/lb)
Enthalpy added (Δh)	2727 $\frac{kW\ sec}{kg}$	(1175 Btu/lb)

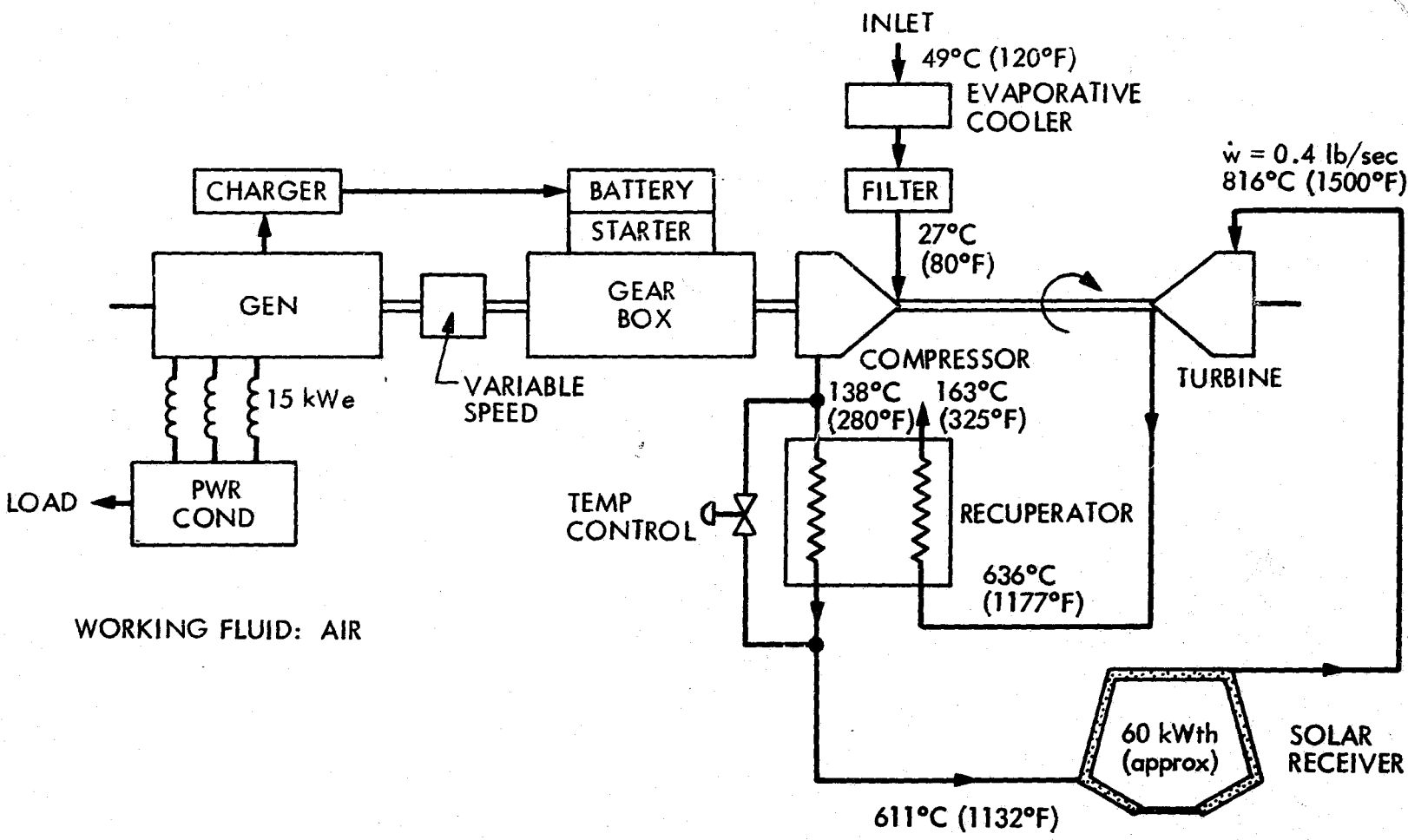

Figure 2-5. Schematic of Baseline Open Air Brayton System

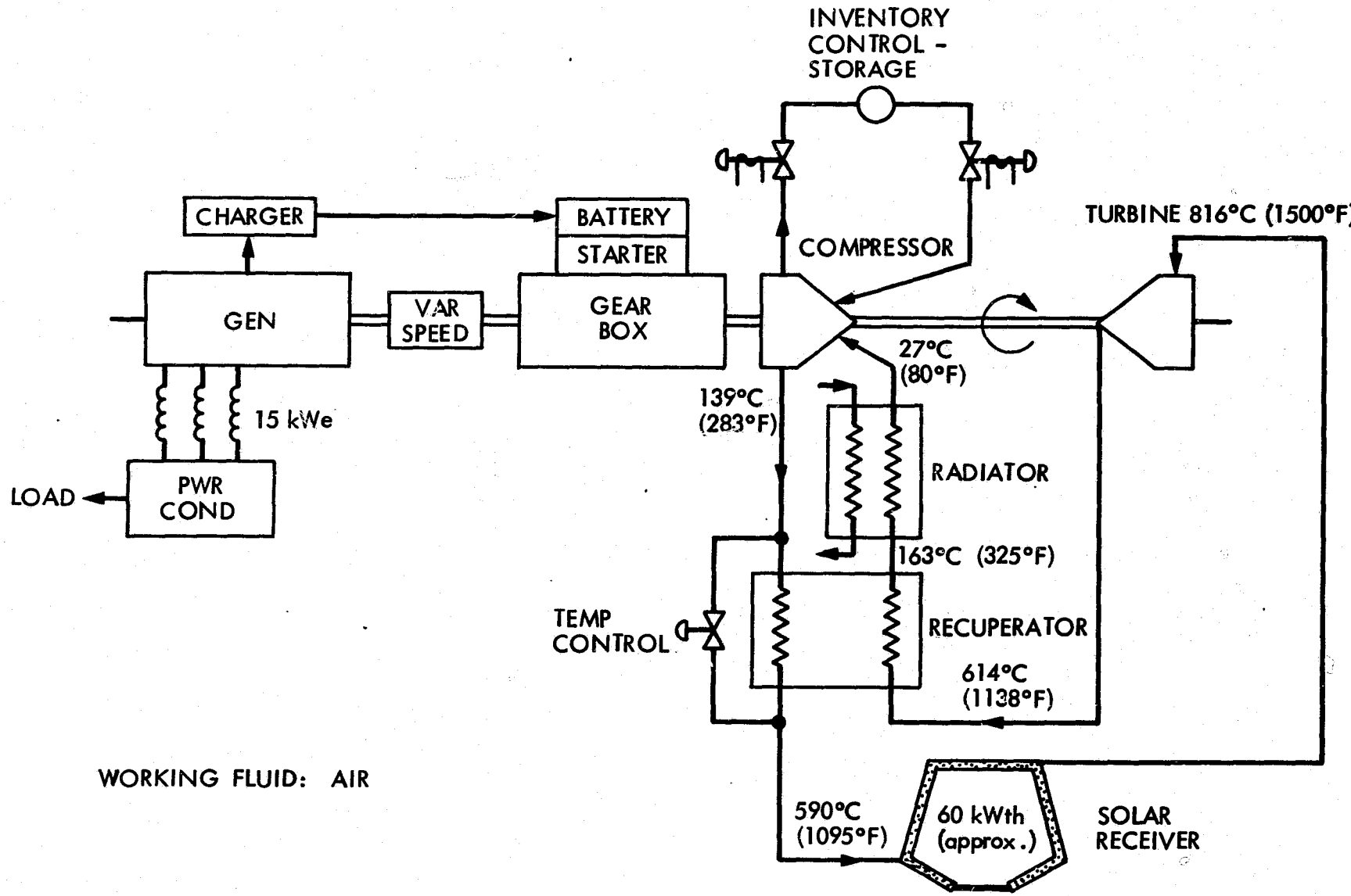

Figure 2-6. Schematic of Baseline Closed-Cycle Air Brayton System

Table 2-3. Baseline Specification of Brayton Cycle Systems

Rated output	15 kW ± 5 kW
Overload capacity	120%
Turbine inlet temperature	816°C (1500°F)
Generated power	120/240 ± 2% volts AC 60 Hz, 3 phase, 4 wire
Turbine, compressor and gear box weight	91 kg (200 lb)
Recuperator effectiveness	0.9
Recuperator weight	91 kg (200 lb)
Alternator weight	91 kg (200 lb)

	Open-Cycle Air	Closed-Cycle Helium
Turbine inlet pressure	2.4 atm (35.3 psia)	2.4 atm (35.3 psia)
Cycle pressure drop $\Delta p/p$	0.08	0.10
Turbine exhaust pressure	1.03 atm (15.1 psia)	13.6 atm (200 psia, base pressure)
Turbine exhaust temperature	636°C (1177°F)	546°C (1015°F)
Inlet temperature at recuperator	138°C (280°F)	193°C (380°F)
Recuperator exhaust temperature	188°C (370°F)	211°C (412°F)

Open- and closed-cycle systems each have their advantages and disadvantages. Open air systems do not require system seals or radiative cooling, thus they would be more reliable and less complex. Furthermore, they allow relatively low recuperator exit temperature and pressure, which permits thinner absorber tube designs that result in more effective system performance. Previous studies of solar Brayton modules (Refs. 14 and 15) favored open-cycle over closed-cycle systems mainly because of higher reliability (less O&M) and lower operating pressure. The closed-cycle Brayton system usually has a slightly higher cycle efficiency (2 or 3 percentage points), and the machinery is generally more compact compared to the open-cycle system. The closed-cycle system generally has a somewhat better part-load characteristic as well, which is particularly significant for solar applications. Working fluids, such as helium have better heat transfer properties than air, but higher system pressure levels are necessary because of the low molecular weight. All considered, the choice between open- and closed-cycle systems will depend on their future technology development, and the type of application.

Brayton solar receivers, in general, differ significantly from steam receivers. First of all, high temperature materials such as Inconel, Hasteloy, or even ceramic absorbers may be needed. The high flow rate and low coefficient of heat transfer characteristics require a large heat transfer area and a large flow cross-sectional area. Typical Brayton receiver designs may employ a multiple tube arrangement, e.g., the so-called "bird-cage" type. Furthermore, phase change materials such as lithium fluoride or lithium chloride may be employed as a heat storage medium inside the receiver for transient operations (Refs. 16, 17, 18). The baseline specifications of the Brayton receivers are listed in Table 2-4.

3. Power Conversion Part-Load Performance

The power conversion efficiency of an engine subsystem typically is evaluated under specified, rated conditions. Because local insolation level varies with time (Figure 2-2), it is likely that a significant portion of solar thermal conversion will occur at conditions other than the design point. The engine part-load characteristics may vary substantially according to the type of engine, engine size, and mode of operation, e.g., constant speed or constant temperature. Three representative part-load engine characteristics are used in the present study for the three baseline systems (see Figure 2-7). The steam Rankine and open-cycle air Brayton characteristics were provided by NASA Lewis Research Center (Refs. 11 and 13, respectively). The closed-cycle Brayton part-load curve is represented by a 10 kWe Garrett-AiResearch gas turbine with constant turbine inlet temperature (Ref. 19). For convenience in computer simulation, the relative engine efficiency is expressed in terms of thermal heat input (from the receiver) rather than the more conventional power output. Of course, the basic relationship expressed in Eq. 1.1 remains true. Actual part-load characteristics may differ significantly from those shown here (Figure 2-7); nevertheless, these representative curves can be used to demonstrate the effects of off-design point operation.

Table 2-4. Baseline Brayton Receiver Specification

Thermal Energy Production	60 kWth at I_o = 0.8 kW/m^2	
Outlet Temperature	816°C (1500°F)	
Weight	91 kg (200 lb)	
	Open-Cycle Air	Closed-Cycle Helium
Flow Velocity	15 to 30 m/sec (50 to 100 ft/sec)	15 to 30 m/sec (50 to 100 ft/sec)
Total Heat Transfer Area Required (approx.)	2 m^2 (21 ft^2)	0.6 m^2 (6.4 ft^2)
Mean Temperature Differential	93°C (200°F)	93°C (200°F)
Absorber Tube I.D.	0.48 cm (0.188 in)	0.48 cm (0.188 in)
Tube Length	73 cm (2.4 ft)	73 cm (2.4 ft)
No. of Tubes	180	55

Generator/alternator efficiency also varies with part-load and in the same manner as gear boxes used with high speed machines (see Ref. 20 and Appendix A of Ref. 5). A promising development for eliminating gear boxes is the field-modulated alternator (Ref. 21), which is a small, light weight, low cost, high speed device.

4. Concentrator Specification

The solar concentrator design selected for analysis is a dish that resembles a paraboloid. It may be any of the nine basic types discussed in Appendix A. The reflector surface is a second surface mirror that covers most of the concentrator surface except for a 3 m diameter area directly beneath the receiver. The general specifications of the concentrator are listed in Table 2-5. The slope error and dish size requirements are interrelated and will be discussed in a later section.

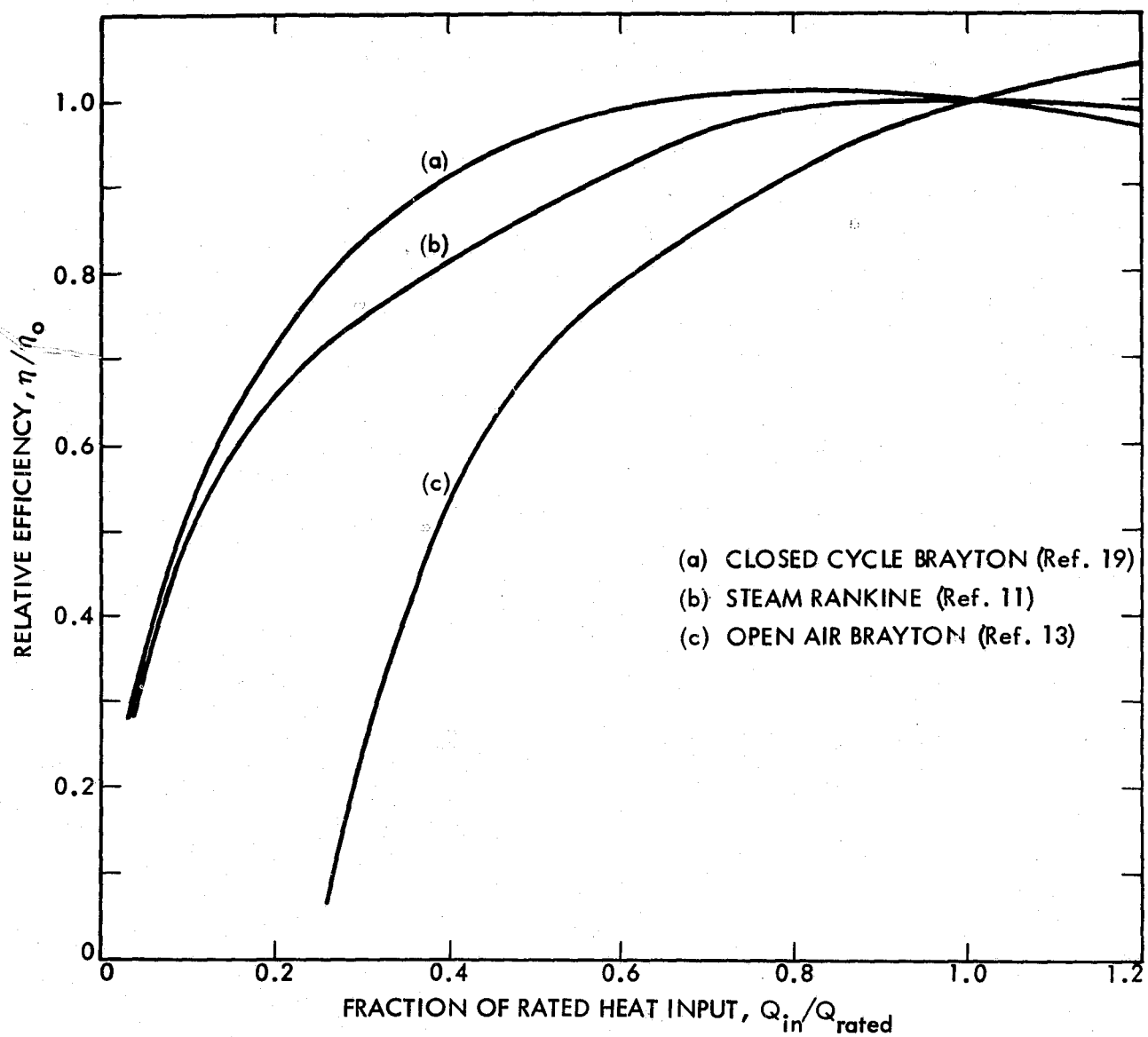

Figure 2-7. Representative Part-Load Engine Performance Characteristics

Table 2-5. Concentrator Design Parameters

Reflector	Laminated float glass second surface mirror reflectance = 0.83
Focal length to diameter ratio (f/D)*	0.6
Structural Shading	4%
Pointing Error	0.1° RMS
Slope Error	1 mrad to 10 mrad
Dish Diameter	10 to 15 m
Weight supporting capability at the focal point	455 to 628 kg (1000 to 1500 lb)

*See Appendix A, Eq. A.2.

C. SYSTEM DESIGN CONSIDERATIONS

1. Module Size

Each module of a point-focusing distributed system consists of a mechanically and thermally integrated set which includes a concentrator, a receiver, and a power conversion unit. One of the critical system design requirements is that the components be compatible with each other so that the entire module operates efficiently. Two factors determine the optimum module size from a cost-effective point of view. The governing factor lies in constructing a concentrator with the diameter that corresponds to a minimum cost per unit area ($/m^2). Empirical relationships established at JPL (Ref. 22) during construction of many microwave antennas for the Deep Space Network (up to 60 m diameters or 212 ft) indicated that there is an optimal size for the antenna-type structure. For solar concentrators, the relationship is more complex because different types of configurations will have differing structural requirements and differing cost sensitivities.

The second factor that affects the module size optimization is the cost/performance of receivers and power conversion units. Power conversion efficiency increases with the design power output. Fewer trackers, receivers, and power conversion units will be required for the entire system if a larger concentrator is used. Consequently, it is desirable to employ large solar concentrators within the limit that the cost-performance benefit can off-set the cost increase due to structural and wind load requirements. A detailed trade-off between

module capacity and concentrator size is complex and involves many parameters, such as concentrator quality, engine type, operating temperature, etc.

Most of the information required to select an optimum cost effective module size is not available at the present time. Current subsystem development contracts let by the PFDR Technology Project utilize basically general guidelines instead of definitive specifications. The Low Cost Concentrator (LCC) development (Ref. 23) required the concentrator size to be in the range between 5 and 15 m (in diameter). Consequently, the receiver conceptual design must cover a range of capacities. Similarily the engine/generator assembly in development is considered to be rated at a nominal, approximate net power output of 15 kWe at the generator terminals. Because the hardware descriptions still are loosely defined, further alterations and adjustments of subsystem specifications to ensure compatibility between subsystems are anticipated during the developmental phase.

The so-called Test Bed Concentrator (TBC), is the Mod 0 design and will be the earliest module developed for the PFDR Technology Project. It will precede the LCC or Mod 1 design (Ref. 3). The TBC has a nominal 11 m diameter dish concentrator. Without specifying the power conversion efficiency, which may vary somewhat during the development phase, a specification of 15 kWe engine output does not provide sufficient information to design a matching solar collector. On the other hand, it would be unrealistic to design a receiver to fit an 11 m diameter concentrator without specifying the dish quality (surface slope error). At the present time, the module size is characterized best by expressing the kilowatt thermal capacity of the receiver, and not by specifying the capacity of the power conversion unit or the concentrator size. In the present study, the nominal module size will correspond to a receiver thermal output of 60 kWth at a given operating temperature and insolation design point. The value of 60 kWth is chosen merely for illustrative purposes; the final value, optimized for actual hardware, may differ from this.

2. Insolation Design Point Selection

The area required for a concentrator to provide a specified receiver output is a function of the design point insolation and the collector effectiveness. Figure 2-8 shows the concentrator area requirements as functions of the design insolation level, I_o, to provide a 60 kW net thermal power to the engine. Two levels of heat loss coefficients, Q_r/A_c = 0.01 and 0.1 kW/m^2, are considered to illustrate the collector effectiveness. It is clear that significantly different concentrator sizes may be required depending on the design point selection.

When the actual insolation level, I, is lower than the selected design pont, I_o, it will be necessary to reduce the flow rate to maintain constant receiver outlet temperature. This implies that the engine will be operated at a part-load condition with a correspondingly degraded efficiency (Figure 2-7). However, when the actual insolation value is higher than the design value, the receiver output will exceed the rated capacity. If the limit (which corresponds to 120% of the rated engine capacity in this study) is

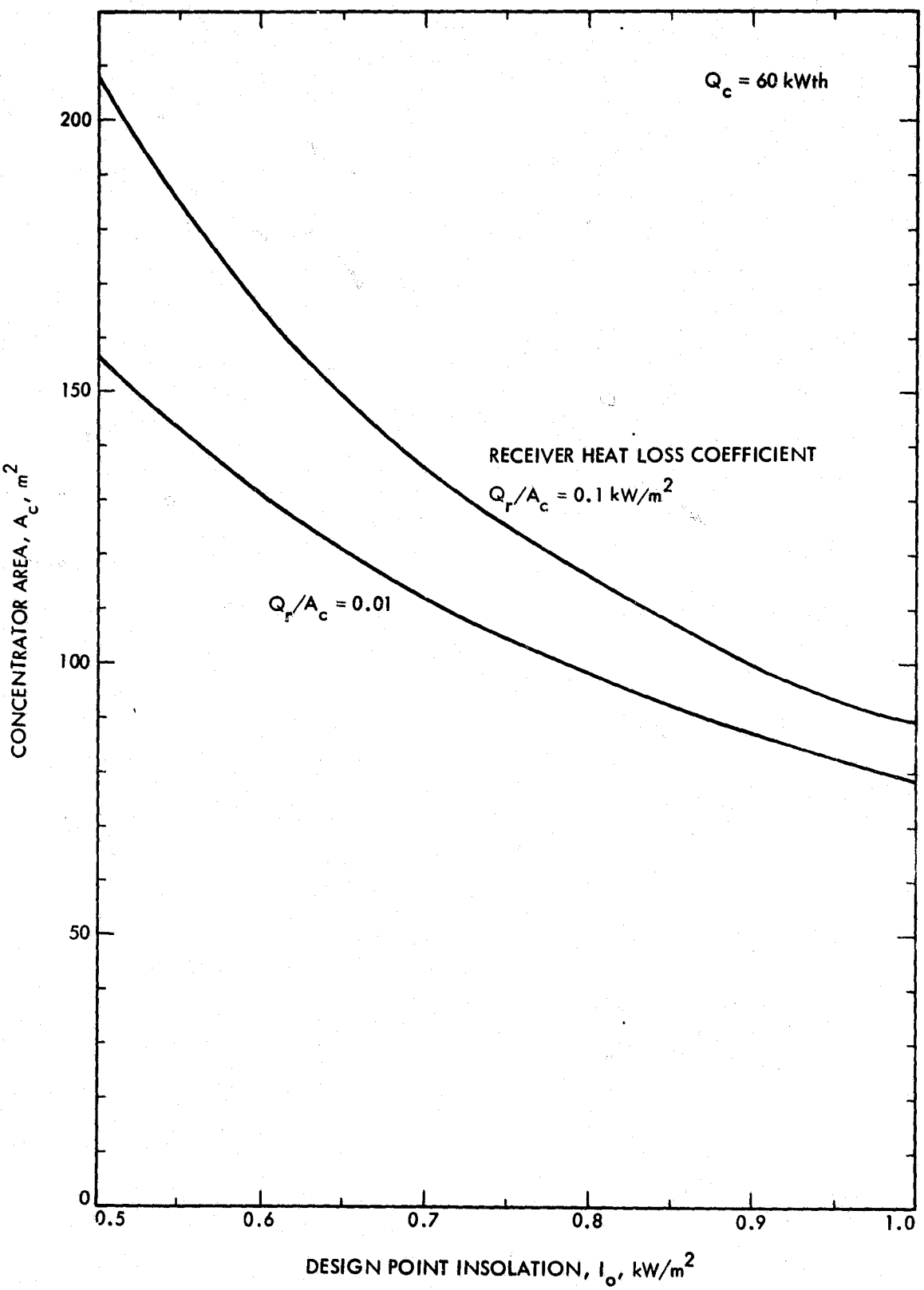

Figure 2-8. Concentrator Area Dependence on Insolation Design Point Selection

exceeded, the excess thermal energy must be discarded upstream of the engine to prevent resultant damage to the generator/alternator assembly.

Annual energy production, W, is the accumulation of the time-varying electric power generation taking into account the variation in insolation and engine part-load characteristics. The integration process accounts for the time period that positive net thermal energy can be collected:

$$W = \eta_o \int \left[\left\{ I_\rho \; G \; \Phi \; \alpha_{eff} - Q_r/A_c \right\} \quad A_c \; \eta/\eta_o \right] dt \qquad (2.2)$$

for

$$I_\rho \; G \; \Phi \; \alpha_{eff} > Q_r \qquad (2.3)$$

where

W = annual electric energy production
η_o = rated power conversion efficiency
η = part-load power conversion efficiency
Q_r/A_c = receiver heat loss coefficient.

Figure 2-9 shows the normalized integrated annual thermal energy production based on different engine part-load characteristics. The results were computed for 15 minute intervals using Barstow insolation data. It can be seen that the insolation data modification varies the annual energy collection by approximately 10%; however, this does not significantly change the design point selection. Similarly, the differences in collector effectiveness change the annual plant output levels but yield almost the same optimal design point insolation.

The optimal design point selection may be affected by the local insolation characteristics, the actual engine part-load characteristics, and the collector effectiveness. However, from the results shown in Figure 2-9, a selection of I_o = 0.8 kW/m^2 would be a good compromise choice for all two-axis, point-focusing distribution systems considered herein. The maximum mismatch would be expected to be less than a few percentage points. Note that there is a crossover in curves (Figure 2-9) at approximately I_o = 0.8 kW/m^2. The crossover between the open-cycle and closed-cycle Brayton systems probably is due to the crossover in engine part-load characteristics used herein, see Figure 2-7. The part-load characteristic for the open-cycle system is relatively poor at low heat input but very good at high heat input, where it exceeds the closed-cycle curve; the opposite is true for the closed-cycle characteristic. The trends are partially offsetting.

3. Receiver Aperture Optimization

The performance of a collector is dominated by the quality of the concentrator, particularly the surface slope error, σ_s. It is shown in Appendix A that a large value of concentrator surface error produces a widely spread solar image and thus requires a large

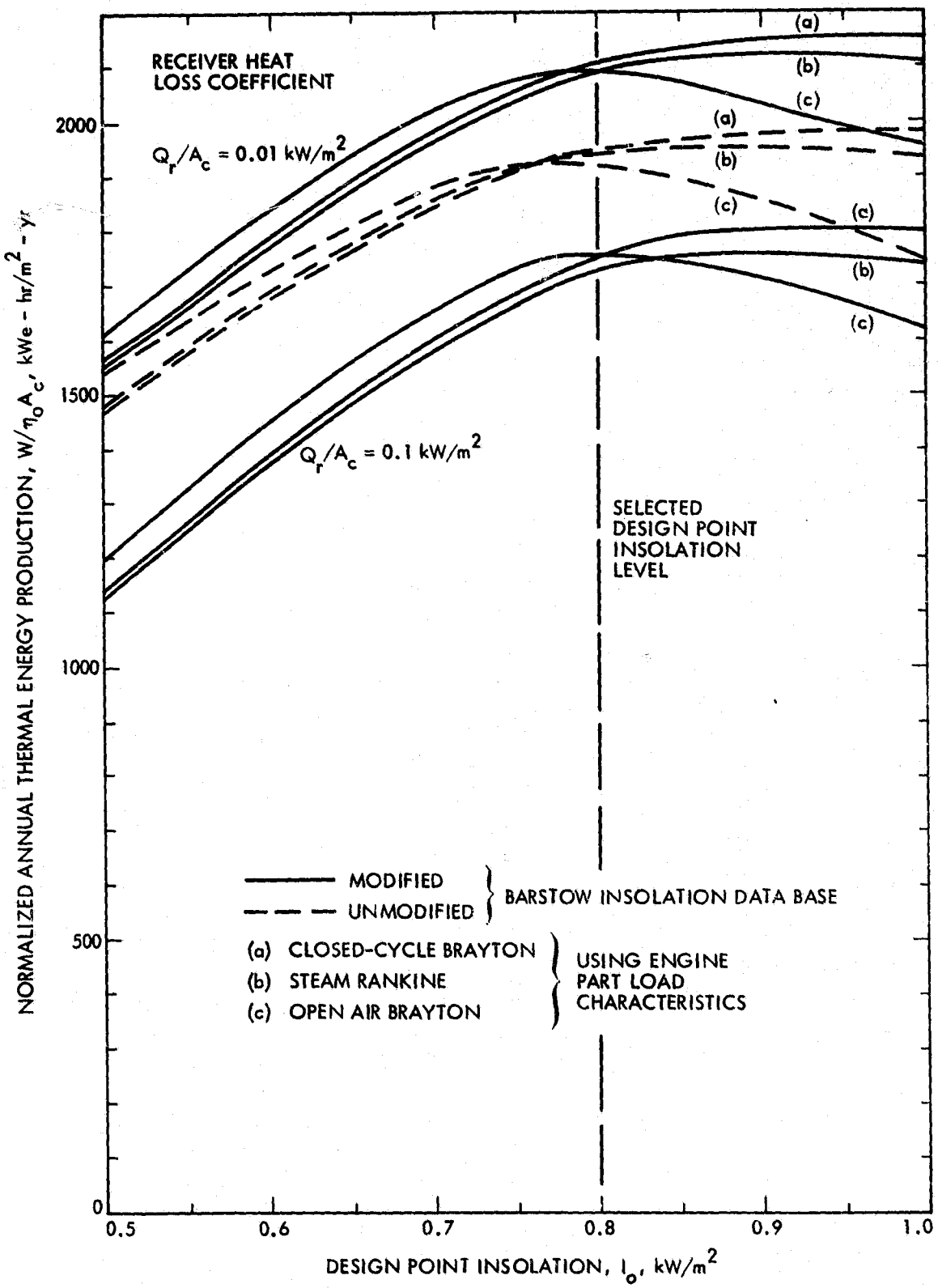

Figure 2-9. The Effect of Design Point Insolation on Annual Energy Production Rate for a 60 kW Thermal System

receiver aperture. Because the heat loss from the aperture is proportional to the aperture area, the thermal performance of a collector can be related directly to the quality of the concentrator. Although the term "efficiency" is poorly defined for solar thermal systems, the performance of a receiver and a collector often are referred to by their rated efficiencies evaluated at the design condition, I_o. The net energy absorbed by the cavity aperture is partly conducted through the insulation layer to the ambient air and is partly transferred to the working fluid. The rated receiver efficiency, $\xi_r\ (I_o)$, defined in Eq. 2.4, is the ratio of the net energy absorbed compared to the total energy reflected from the concentrator under the design point insolation, I_o.

$$\xi_r\ (I_o) = \frac{Q_c}{I_o\ \rho G\ A_c} = \alpha_{eff}\ \Phi - \frac{Q_r}{\rho I_o\ G\ A_c} \qquad (2.4)$$

The corresponding collector efficiency, $\xi_c\ (I_o)$, is defined in Eq. 2.5.

$$\xi_c\ (I_o) = \frac{Q_c}{I_o\ A_c} = \xi_r\ (I_o) \cdot \rho G \qquad (2.5)$$

The receiver aperture area should be selected to allow maximum net thermal energy collection. The heat loss from the aperture is proportional to the aperture area, A_o. As illustrated in Figure A-12 (Appendix A), the solar flux interception factor Φ would reach a plateau when the radius becomes larger than the central core. Consequently the optimum cavity opening would correspond to an interception factor somewhat less than unity. In the present analysis, the receivers for both power conversion systems are sized to have a 60 thermal-kilowatt capacity.

Figure 2-10 illustrates a specific case to show how receiver efficiency varies with aperture radius. The optimum cavity opening, and thus the rated solar collector efficiency, is governed by the thermal-optical properties of the concentrator (reflectance, surface error, and pointing error) and the effective receiver temperature. The example shown in Figure 2-10 does not take into account the conductive losses through the receiver walls.

In the present study, the steam receiver has a water inlet temperature of 174°C. The absorber consists of a single tube coil with a heat transfer area of 0.435 m^2. The mean temperature difference between the tube surface and the working fluid is 28°C. The receiver design for the open-air Brayton system is significantly larger. Because of the low heat transfer coefficient of the working fluid and the high mass flow rate, the absorber requires nearly 200 tubes with a total heat transfer area in excess of 3 m^2 (for a mean temperature difference of 110°C). The external surface of the

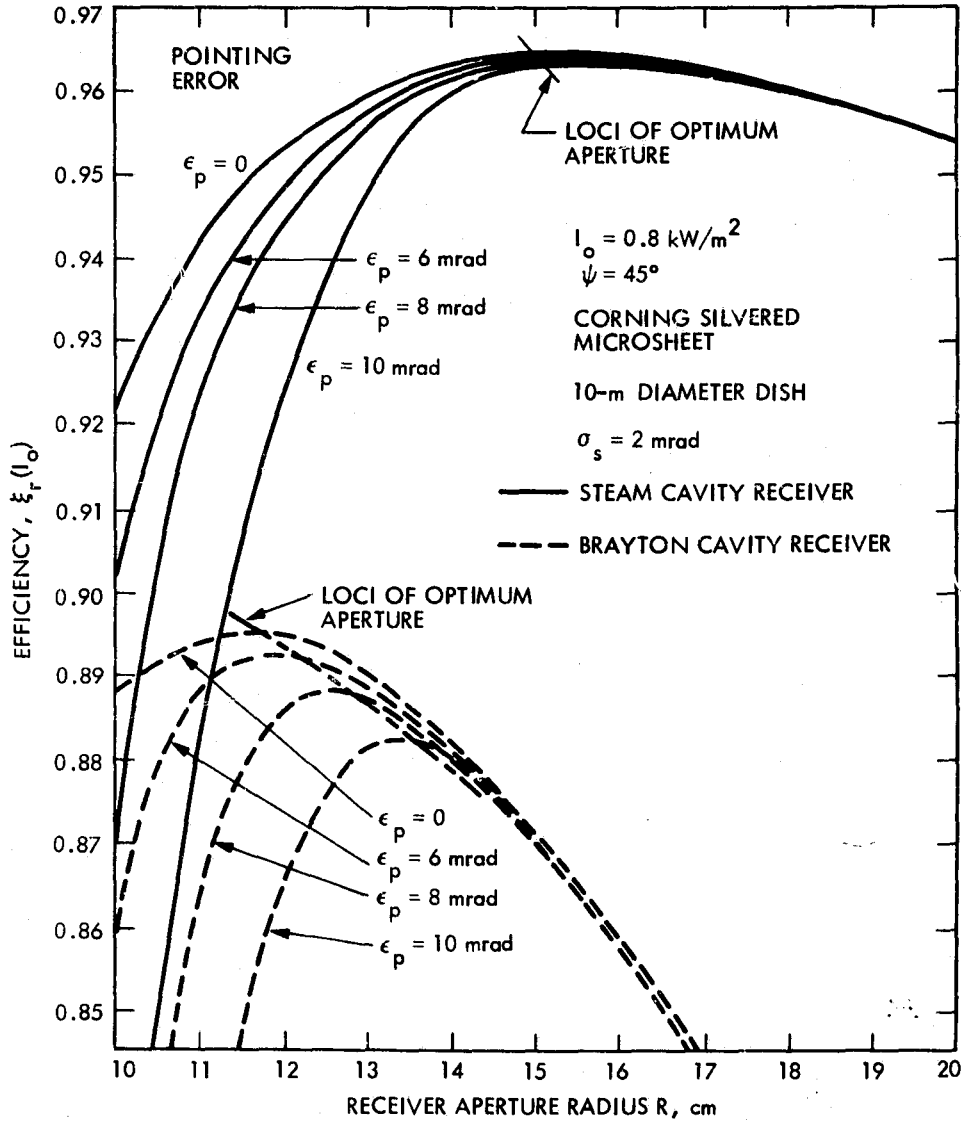

NOTE: THIS ILLUSTRATIVE EXAMPLE INCLUDES ONLY HEAT LOSSES FROM THE RECEIVER APERTURE AND NOT THE CONDUCTIVE LOSSES THROUGH THE WALLS.

Figure 2-10. Receiver Aperture Optimization

cavity receiver is covered with a 13-cm layer of insulating material (with an average thermal conductivity of 0.052 W/m-°C) to reduce the conductive heat loss.

D. PERFORMANCE SIMULATION

The performance of a point-focusing solar thermal power plant is affected by many variables, each having its own cost relationship and performance sensitivity. However, three of the design parameters, namely concentrator quality, receiver temperature, and engine efficiency, have a dominating significance. They not only are the major factors governing the system performance and capital investment, but they also are strongly influenced by the state of technology advancement. This investigation is focused on the trade-off relationship of these three key parameters because they control the optimal selection of solar thermal power system concepts.

For all system concepts, the effect of mirror reflectance has a nearly linear relationship with the system performance. For the present analysis a representative reflectance value of 0.83 is assumed, and concentrator quality is considered to be characterized by just the surface slope error. The operating temperatures selected for baseline Rankine and Brayton systems are 538°C (1000°F) and 816°C (1500°F), respectively. Consequently, the major trade-off parameters become concentrator surface error, σ_s, and rated power conversion efficiency, η_o.

1. Rated Collector Performance

The rated receiver efficiency (at I_o = 0.8 kW/m^2) is shown in Figure 2-11 as a function of the concentrator slope error for an effective steam receiver temperature of 500°C, and an effective Brayton receiver temperature of 900°C. As the concentrator surface slope error increases the optimal aperture area also increases, which implies larger heat loss. Figure 2-12 shows that the corresponding interception factor also decreases. The net effect is reduction of the receiver efficiency and the rated collector efficiency. Figure 2-13 shows the concentrator area requirements to provide 60 kWth (thermal power) under the rated conditions.

The rated receiver efficiency and the collector efficiency were evaluated under an insolation level of 0.8 kW/m^2. During system operations the actual insolation values may vary significantly, as would the collector efficiency. Figure 2-14 shows a sample variation of collector efficiency with the insolation level for various values of slope error. It can be seen that a specification of collector efficiency would lead to ambiguous conclusions unless the rated insolation and surface quality also were specified. In Figure 2-15, the collector efficiency at the value of design point insolation is plotted as a function of surface slope error. For the steam Rankine system, a value of approximately σ_s = 4 mrad or better would be required to achieve the 1982 collector performance target value of 0.72 (Table 1-2); the Brayton system would require σ_s <2 mrad.

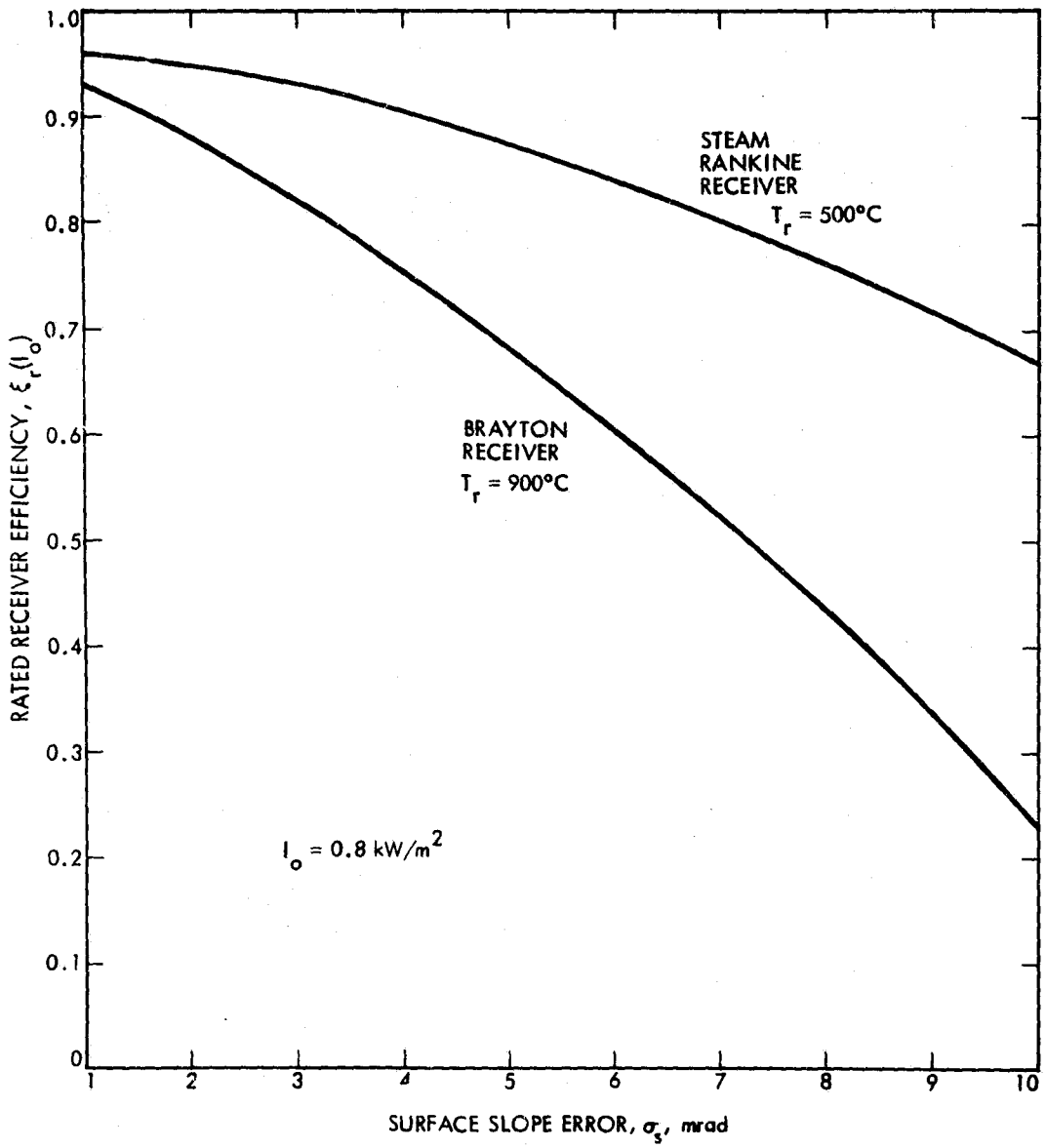

Figure 2-11. Rated Receiver Efficiency

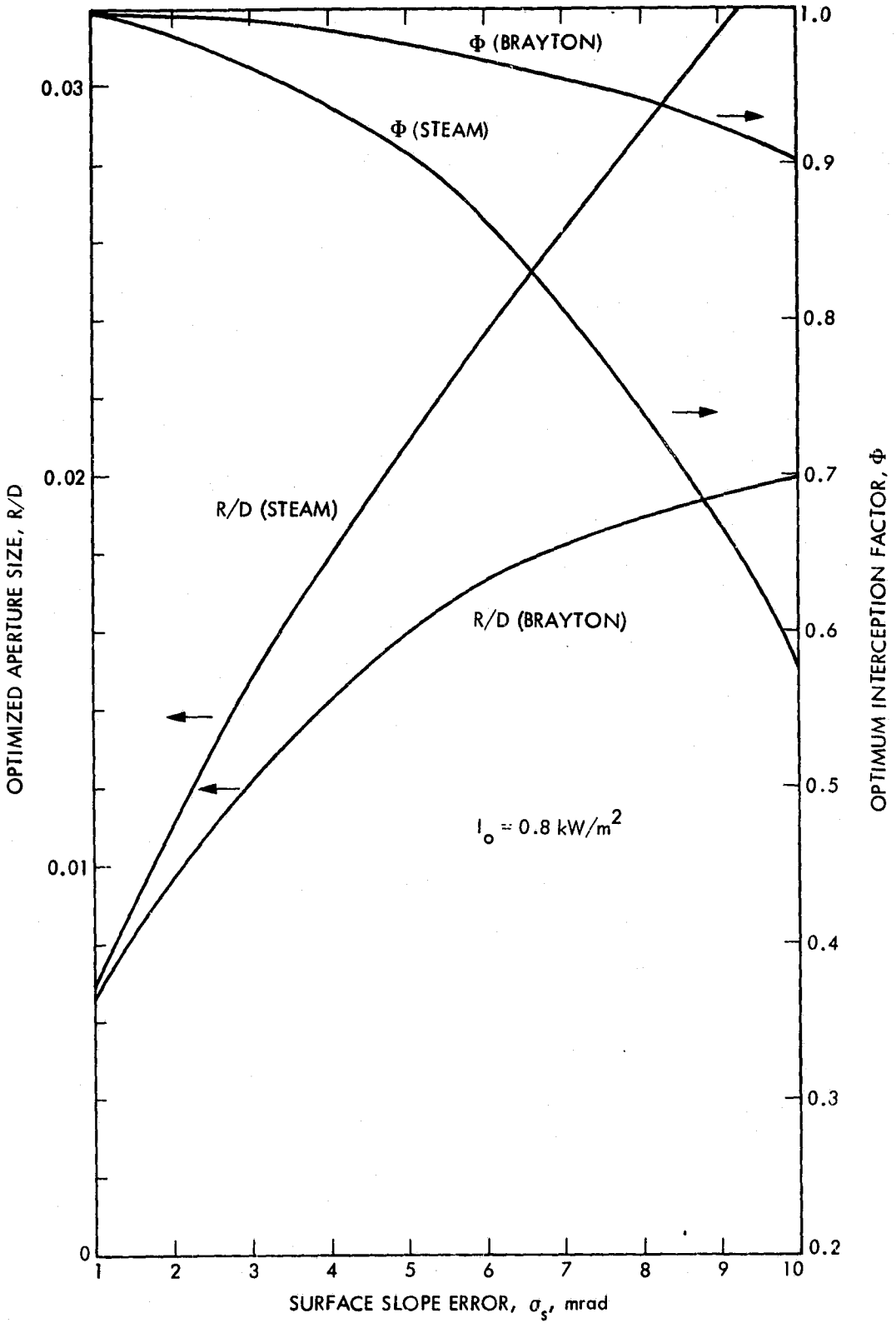

Figure 2-12. Optimal Aperture Sizes and Corresponding Interception Factors

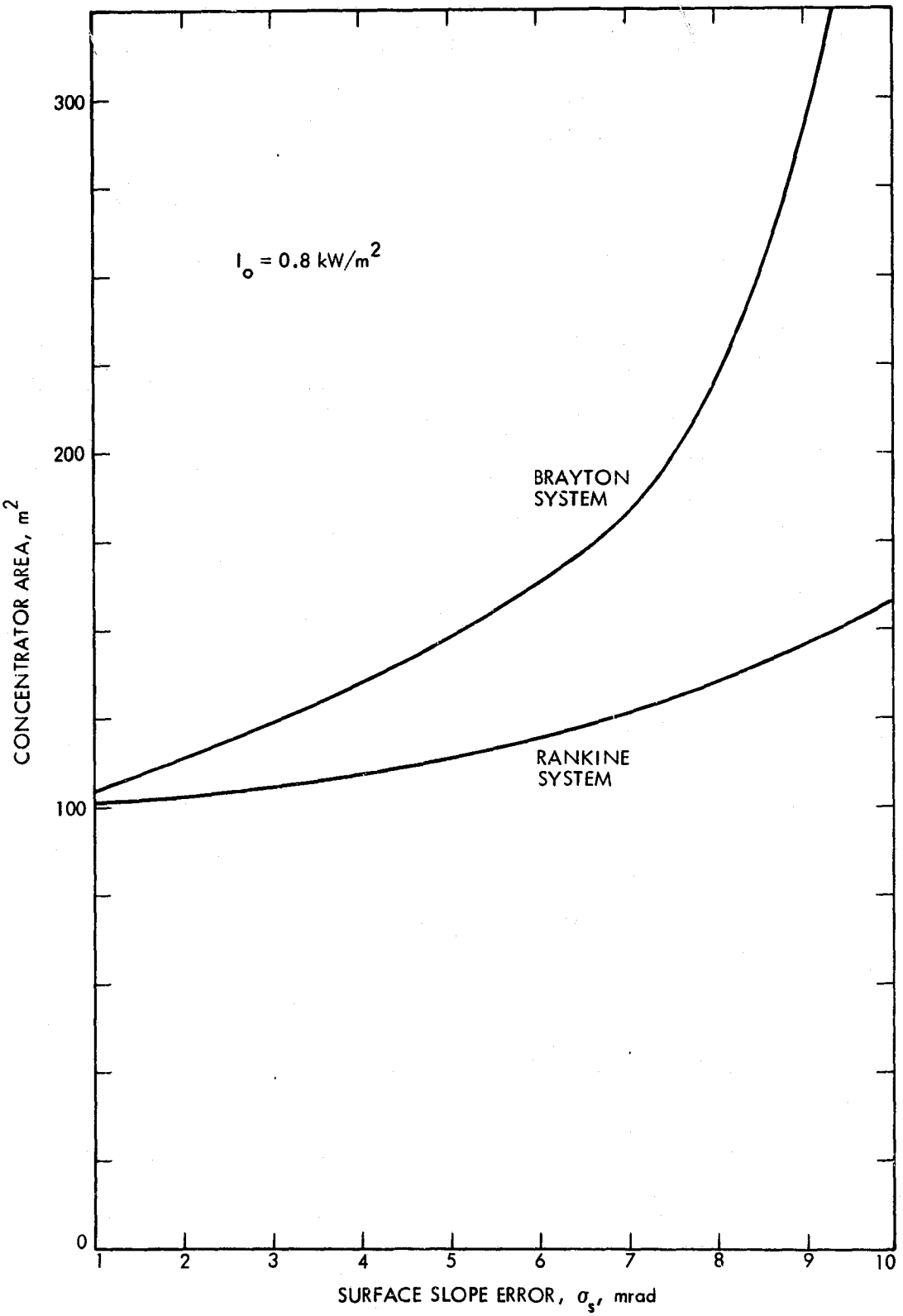

Figure 2-13. Concentrator Area Requirement for a Receiver of 60 kWth Rated Capacity

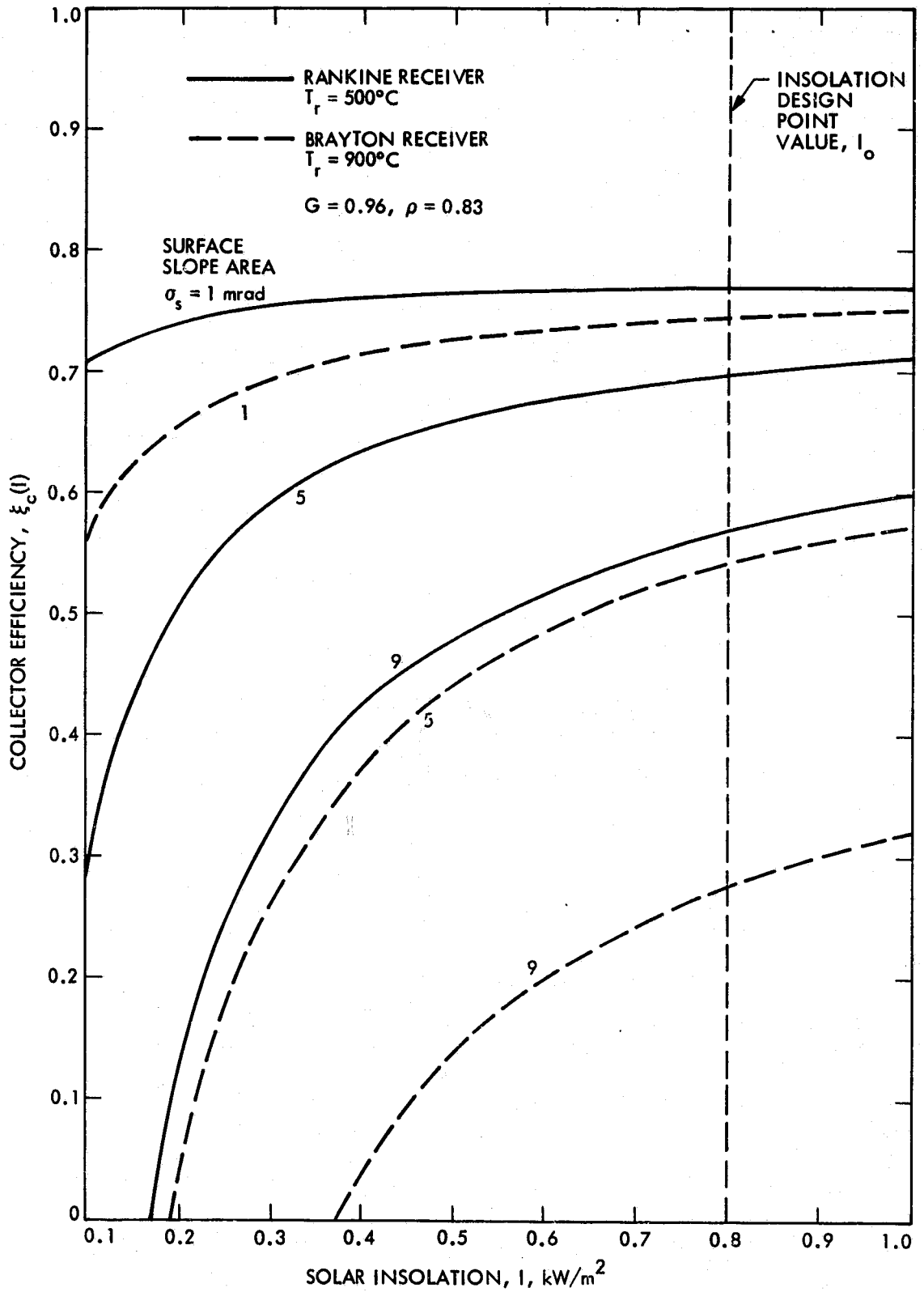

Figure 2-14. Collector Efficiency versus Insolation Level

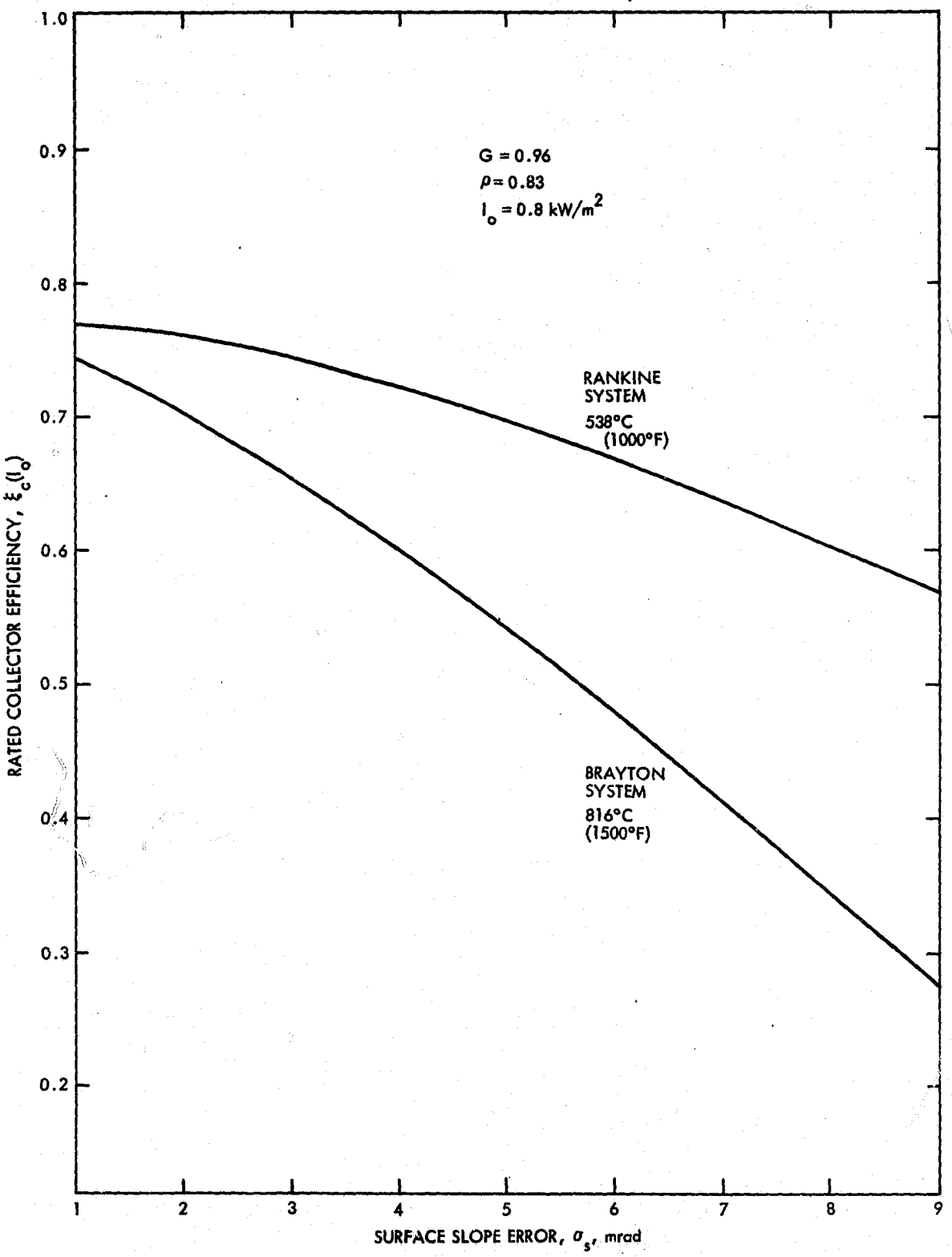

Figure 2-15. Collector Efficiency versus Surface Slope Error at Design Point Insolation

2. Annual Electrical Energy Production

The annual integrated electric energy production rates, W, are computed on the basis of the referenced Barstow insolation data as modified by Aerospace. The results are presented per unit of concentrator area, kWe-hr/m^2-yr, so the merits of different system concepts can be evaluated on a comparable basis. Figures 2-16, 2-17, and 2-18 show the energy production rate as a function of the concentrator surface slope error and power conversion efficiency for steam Rankine, open-cycle air Brayton and closed-cycle helium Brayton systems, respectively. The performances of open-cycle air Brayton and closed-cycle helium systems are almost identical (Figures 2-17 and 2-18).

It should be emphasized that the results obtained for these sample baseline systems are to be used as reference frames for more detailed design trade-off investigations in the future. The analyses were simplified by neglecting transport losses, system outage, scheduled maintenance, unscheduled repair, and dirt buildup/cleaning cycles. For simplicity, the baseline power plant is considered to displace energy only. In other words, the cost performance trade-off is based solely on annual energy production with no consideration of storage requirement. One result of this is that economic analysis is independent of the performance analysis. The next section describes the economic analysis.

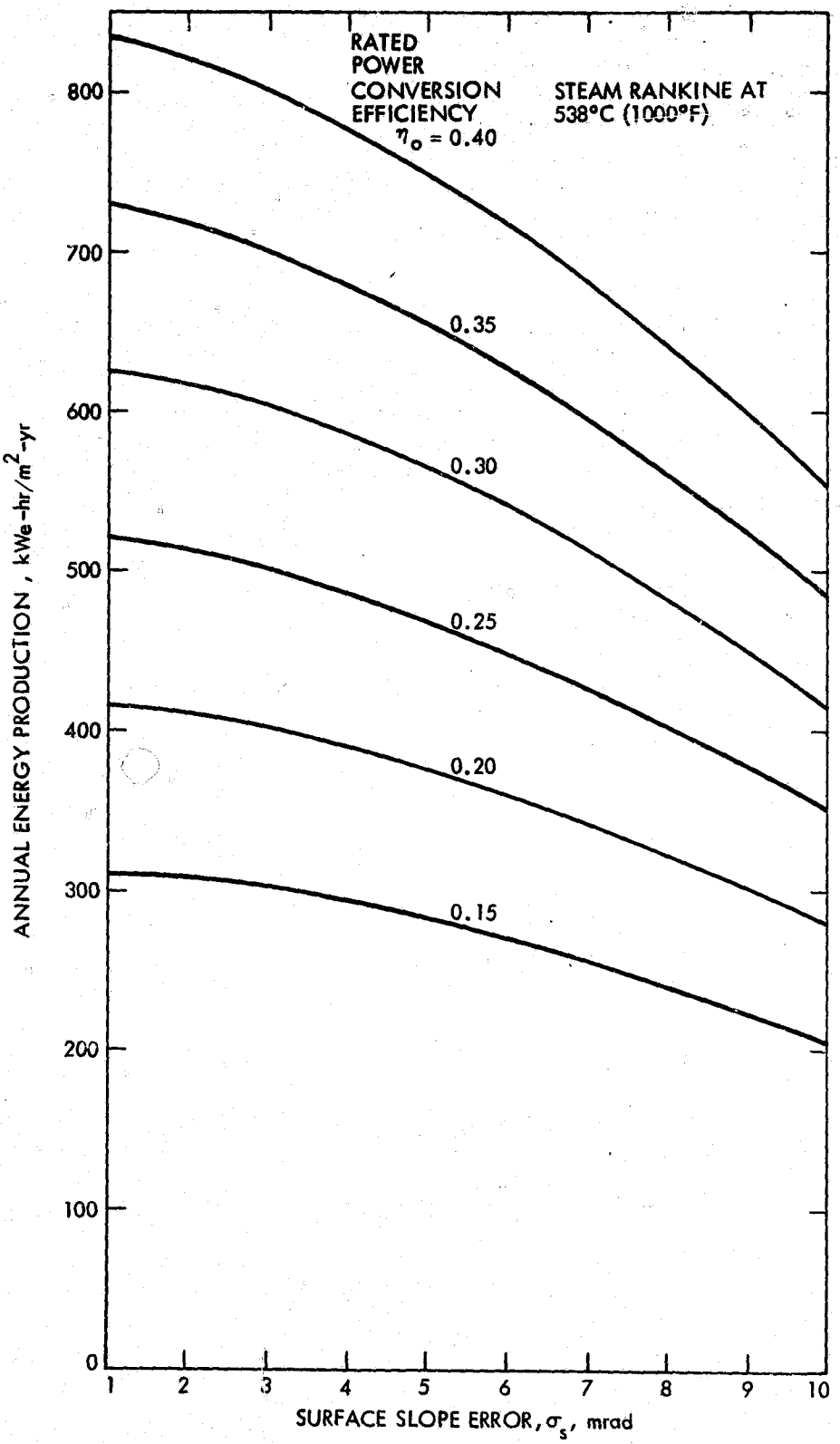

Figure 2-16. Annual Electric Energy Production for the Baseline Rankine System

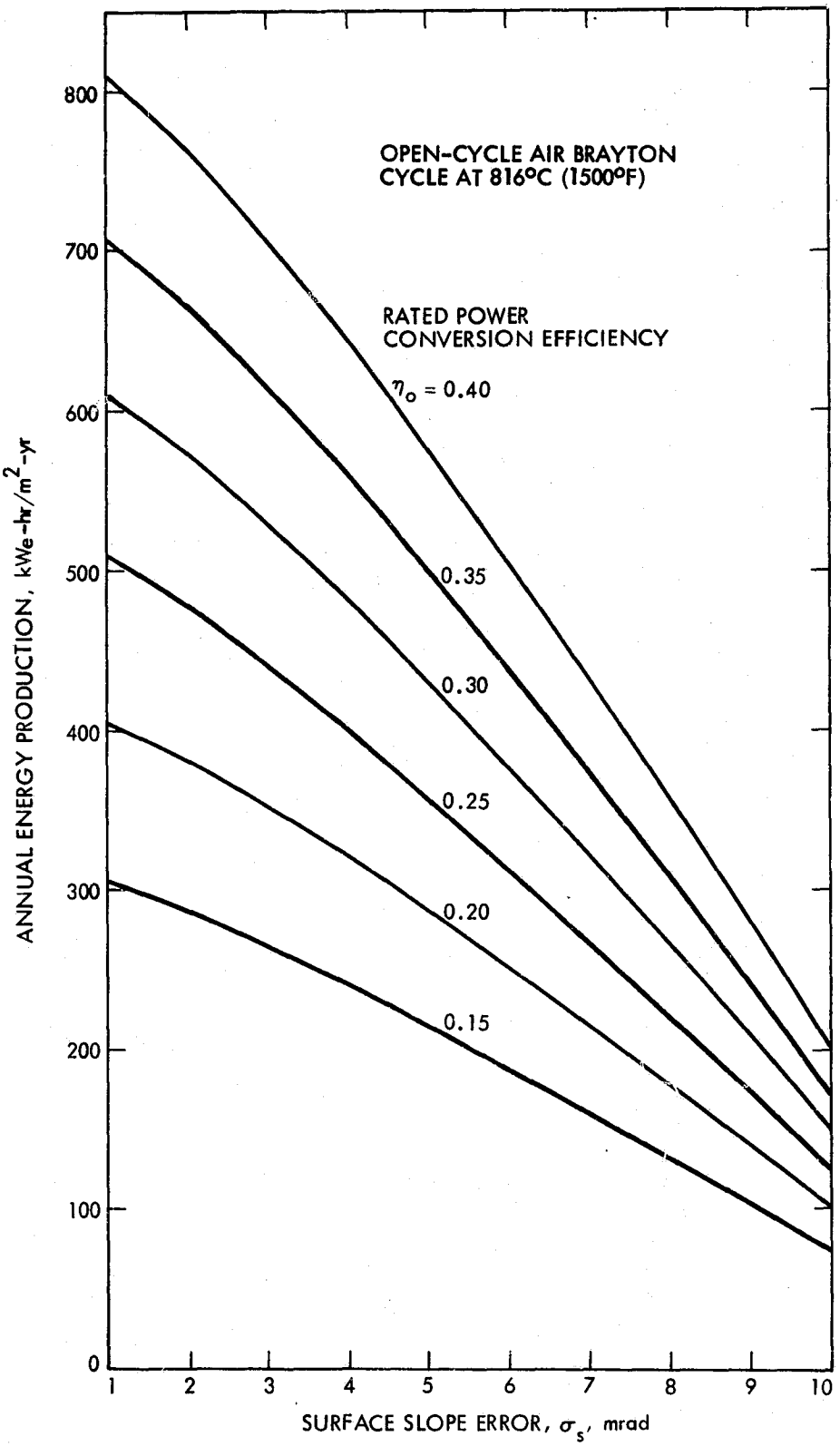

Figure 2-17. Annual Electric Energy Production for the Baseline Open-Cycle Air Brayton System

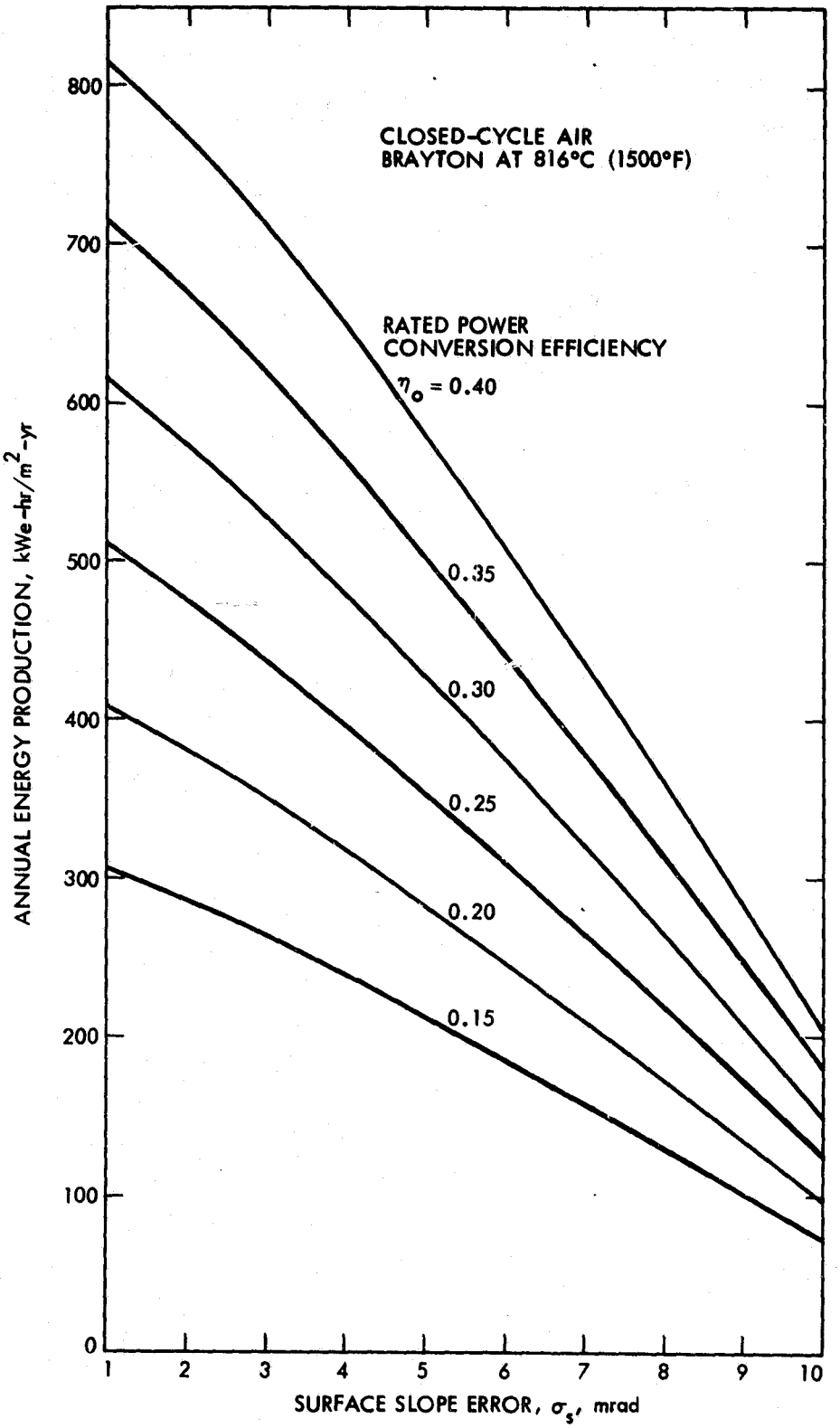

Figure 2-18. Annual Electric Energy Production for the Baseline Closed-Cycle Air Brayton System

SECTION III

ECONOMIC ANALYSIS

A. METHODOLOGY

The economic analysis utilized in this study is a parametric approach that can be applied to any energy production system. The energy cost analysis is based on the approach used at JPL for utility-owned solar electric power plants (Ref. 4). The energy cost equation takes the following form:

$$EC = \frac{(1 + g_i)^{-d}}{W} \left[FCR \cdot CI_{PV} + CRF \, (OP_{PV} + MNT_{PV} + FL_{PV}) \right] \quad (3.1)$$

where

EC	=	levelized busbar energy cost
W	=	plant's annual electric energy production
FCR	=	annualized fixed charge rate
CI_{PV}	=	present value of capital investment
CRF	=	capital recovery factor
OP_{PV}	=	present value of the annual operating cost
MNT_{PV}	=	present value of the annual maintenance cost
FL_{PV}	=	present value of the annual fuel cost
g_i	=	general rate of inflation
d	=	$(Y_{co} - Y_b)$ is the number of years from the base year to the year of commercial operation.

An earlier application of the methodology to solar thermal power systems can be found in Ref. 24. Operating and maintenance (O&M) costs are not included in the energy cost herein, because the baseline systems have not been defined in sufficient detail. The fact that O&M costs are not included in the anlysis does not affect the results of the parametric approach. The cost of fuel, of course, is zero. These assumptions reduce the energy cost equation, Eg. 3.1, to the following form:

$$EC = \frac{(1 + g_i)^{-d} \cdot FCR \cdot CI_{pv}}{W} \quad (3.2)$$

Because all of the economic parameters were kept constant throughout the present analysis (see Table 3-1), the values for g_i, d, FCR and the present value operator also remained constant. For constant W values, the energy cost (EC) therefore is directly proportional to the capital investment (CI). Figure 3-1 presents a family of curves that relate the energy cost, EC, to the capital

Table 3-1. Economic Assumptions

Factor	Value
System Operating Lifetime, years	30
Annual "Other Taxes" as Fraction of Capital Investment	0.02
Annual Insurance Premiums as Fraction of Capital Investment	0.0025
Effective Income Tax Rate	0.40
Ratio of Debt to Total Capitalization	0.50
Ratio of Common Stock to Total Capitalization	0.40
Ratio of Preferred Stock to Total Capitalization	0.10
Annual Rate of Return on Debt	0.08
Annual Rate of Return on Common Stock	0.12
Annual Rate of Return on Preferred Stock	0.08

investment, CI, for various values of the annual energy production, W. The curves are linear because O&M and fuel costs were omitted from consideration. If W is known, or can be determined from prior analysis, then EC can be determined when CI is specified, and vice versa. The latter approach is used herein because CI can not yet be determined accurately for solar thermal power systems.

B. JUSTIFIED CAPITAL INVESTMENT AND COST TARGETS

For solar power plants to be competitive in a commercial market the system cost must be lower than the justified capital investment, which is determined by the power plant energy production and the commercial energy cost rate. The hardware cost includes the concentrator, receiver, power conversion unit, and associated component costs. For convenience, the results are normalized, i.e., the system justified capital investment is expressed per unit of concentrator area. The index can be used to establish hardware cost goals of competitive point-focusing distributed solar thermal system

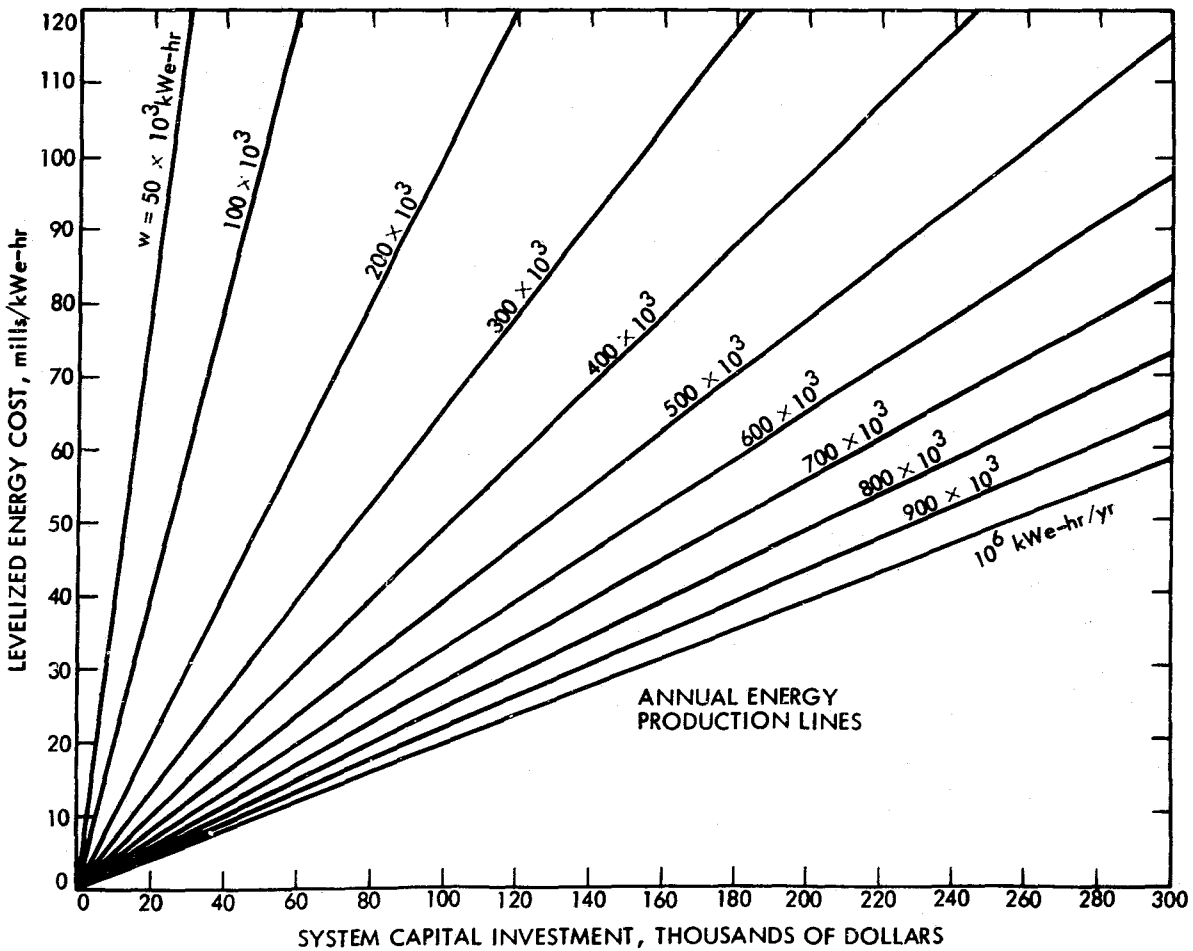

Figure 3-1. Energy Cost versus Capital Investment for Different Annual Power Production Rates

options. Figure 3-2 shows the reference system cost goals for baseline Rankine and Brayton systems. The steep dotted lines in Figure 3-2 indicate loci of equivalent capital investment for the two systems when the Brayton power conversion efficiency is greater than the Rankine efficiency by 5, and 10 percentage points respectively. It is apparent that the justified system capital investment is a strong function of power conversion efficiency, concentrator quality, and the operating temperature. The energy cost target for the PFDR Technology Project is 50 to 60 mills/kWe-hr in the post-1985 time frame.

As an example, a 10 MW steam Rankine solar power plant (rated at I_o = 0.8 kW/m^2, η_o = 25%) consisting of 1000 concentrators (σ_s = 5 mrad), each with a 10-m diameter, produces approximately 3.7 x 10^7 kWe-hr annually. If the average commercial energy cost for the next 30 years, which is the lifetime of the power plant, is 50 mills/kWe-hr, then the justified capital cost for this power plant would be \$9.5 x 10^6. In other words, the condition for this power plant to be economically viable would be that the combined sum of hardware costs and installation must be less than 9.5 million dollars. The unit capital cost would be approximately \$950/kWe, which falls in the range of 600 to 1000 \$/kWe established as a cost target for the PFDR Technology Project in the post-1985 time frame.

A comparison of annual integrated energy production of the baseline open-cycle air and closed-cycle air Brayton engines (Figures 2-16 and 2-17) indicates that, on the average, engine part-load characteristics may not play a significant role in system design or cost/performance trade-offs. This follows because the annual energy production for the two cases is almost identical, even though the engine part-load characteristics are markedly different (Figure 2-7). Yet, this conclusion may be premature because of the unique part-load characteristics used herein, i.e., they have a crossover at high heat input that may be compensatory.

The effect of two different insolation data base inputs on system performance is illustrated in Figure 3-3. The results indicate that the annual energy production is almost directly proportional to the total insolation level. Justified capital investment differences for the two insolation data base inputs are less than 10%. Figure 3-4 shows the justified cost versus concentrator accuracy for two representative systems: a steam Rankine system with 30% power conversion efficiency, and a gas Brayton system with 35% power conversion efficiency. It is apparent that the cost performance trade-off relationship of concentrator accuracy is governed by the system operating temperature and the power conversion efficiency. Concentrators with surface accuracy poorer than 7 mrad would be more suitable for low temperature applications. It would be more effective to select high surface quality concentrators for high temperature applications to achieve low energy cost. System performance is linearly proportional to the power conversion efficiency. However, the sensitivity relationship varies with the operating temperature and the concentrator quality. Figures 3-5 and 3-6 illustrate the increases in justified capital investment due to improvements in power conversion efficiency for representative Rankine and Brayton systems with an energy cost target of 50 mills/kWe-hr.

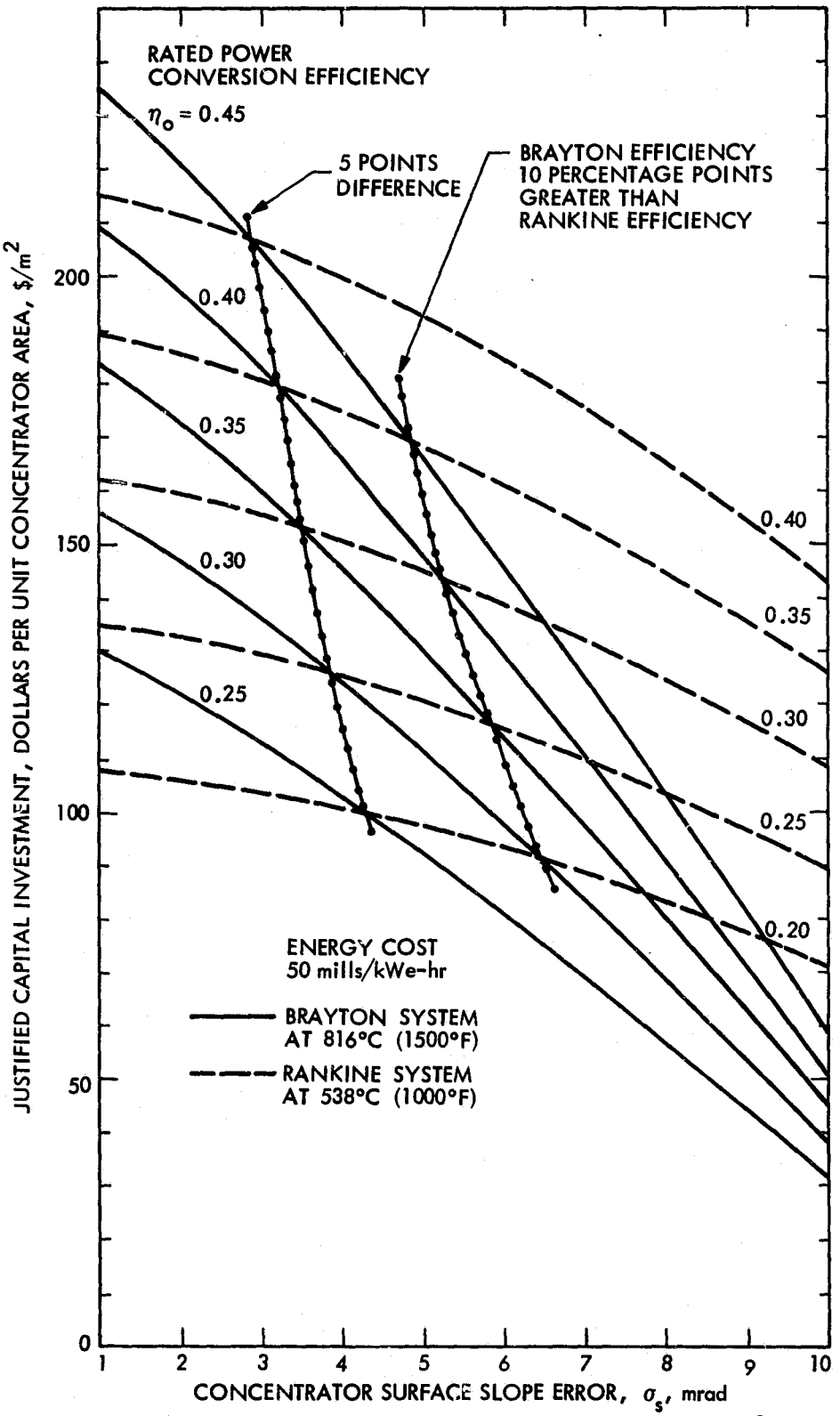

Figure 3-2. Reference System Cost Goals for Baseline Rankine and Brayton Systems

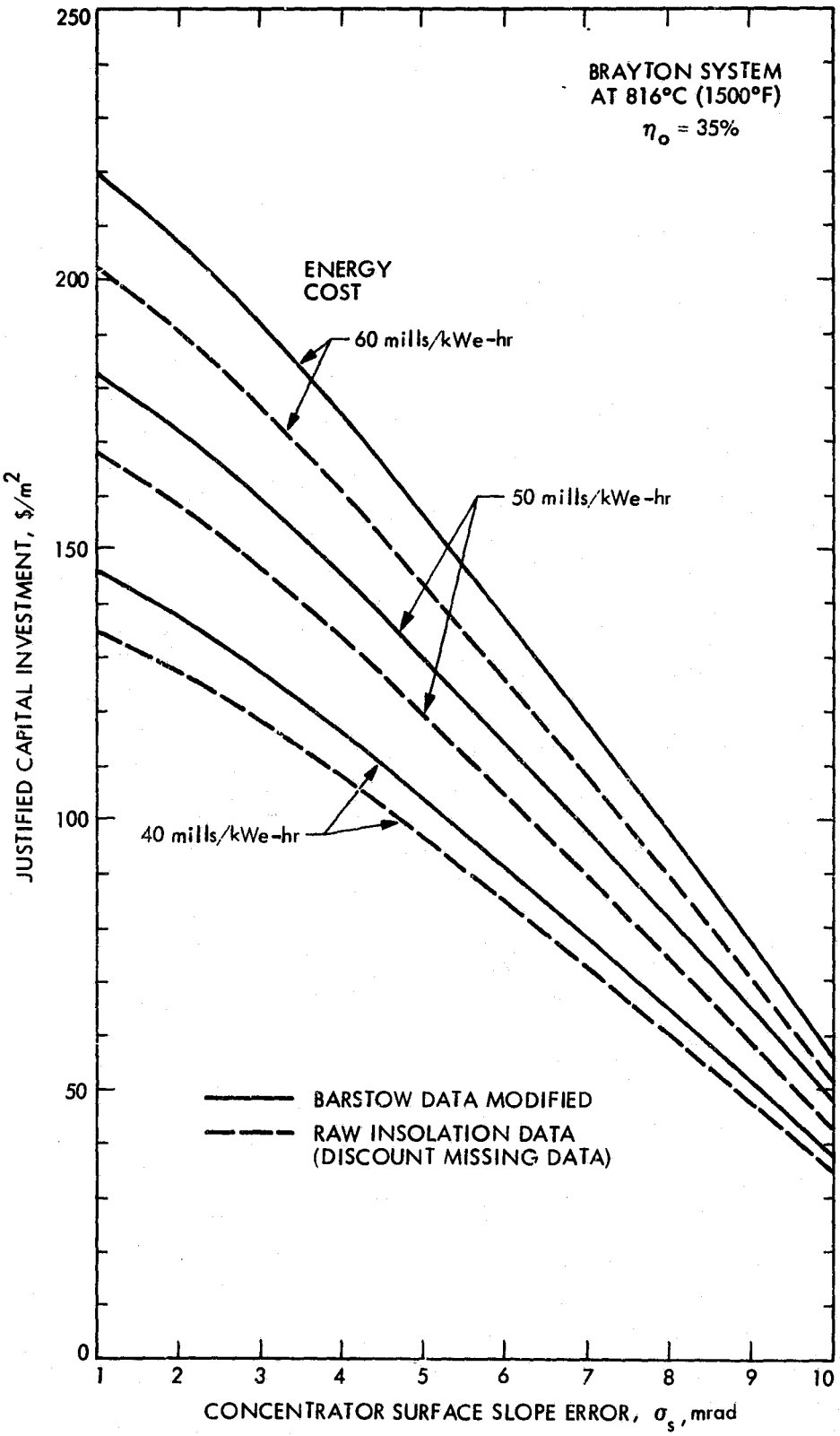

Figure 3-3. Effects of Insolation Data Base on System Performance Computation

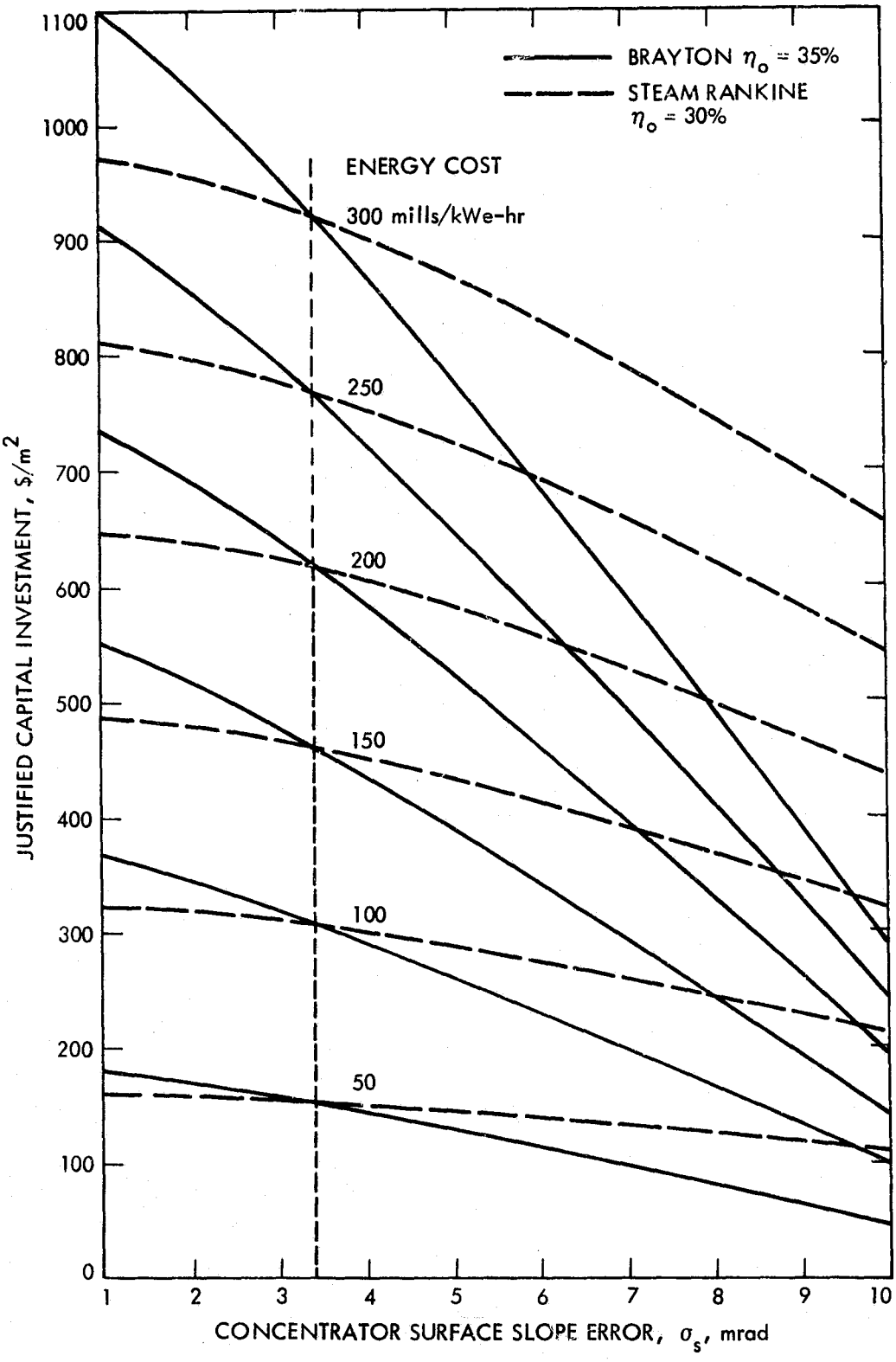

Figure 3-4. Justified Capital Investment versus Concentrator Quality

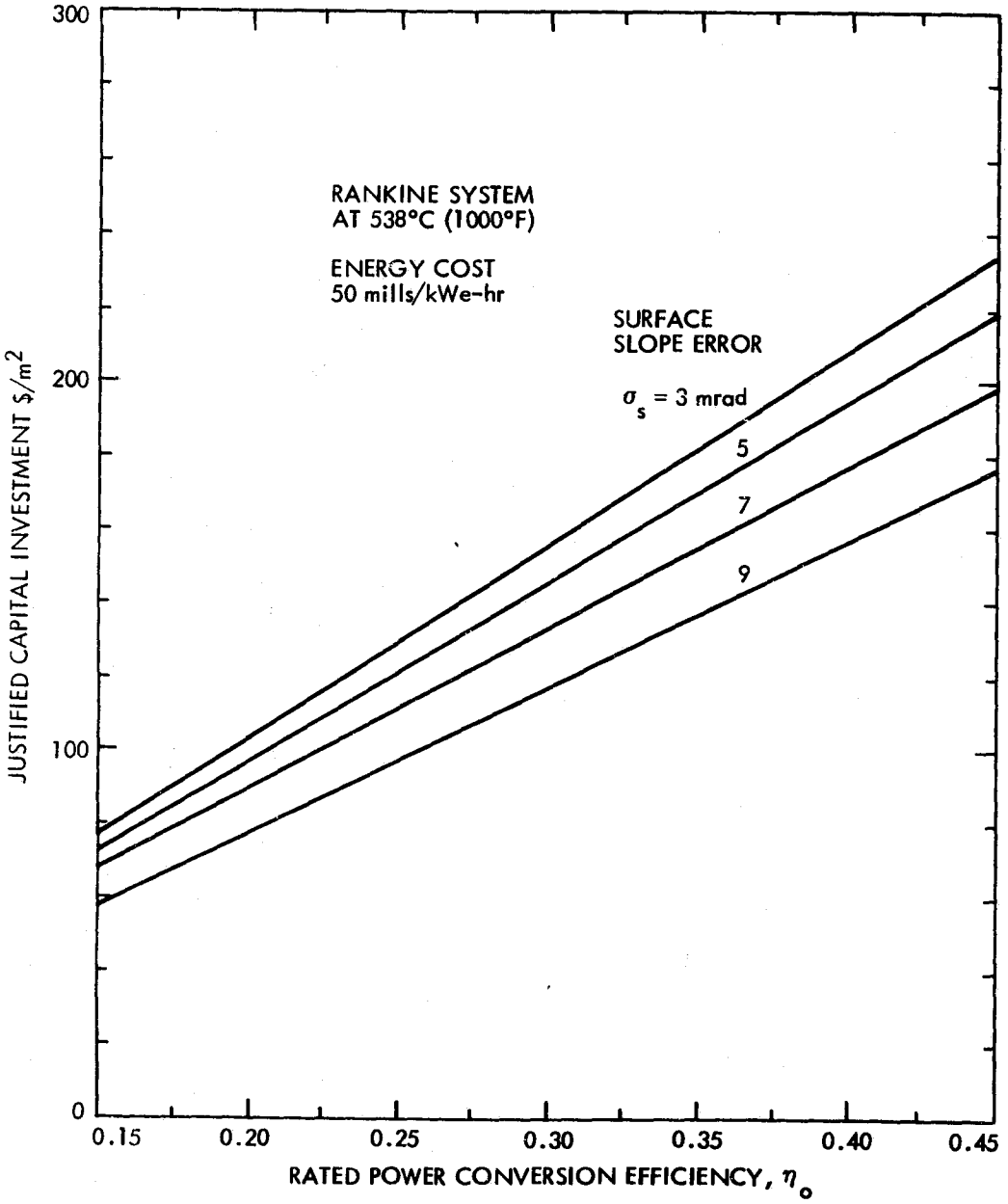

Figure 3-5. Justified Capital Investment versus Power Conversion Efficiency for the Baseline Rankine System

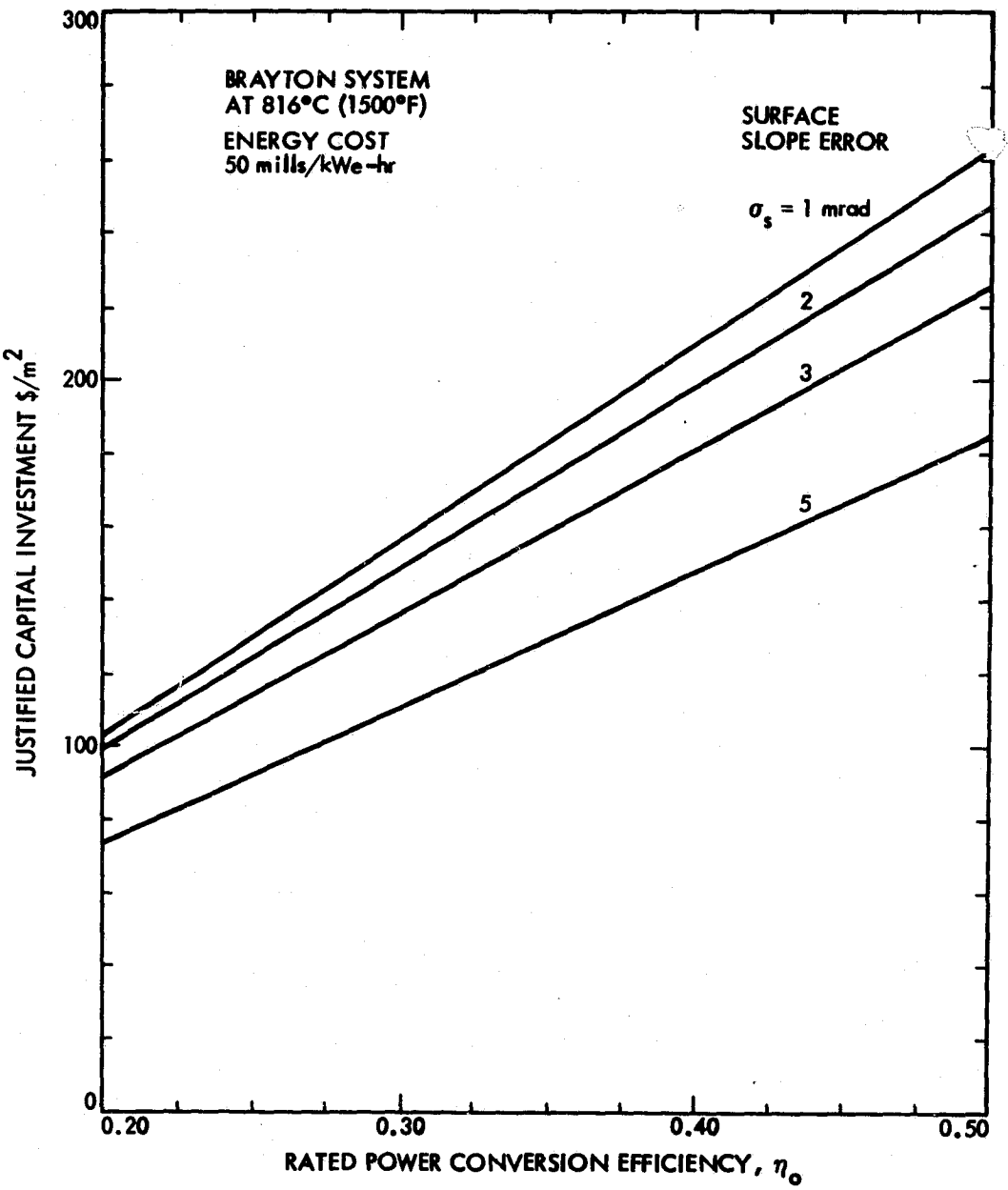

Figure 3-6. Justified Capital Investment versus Power Conversion Efficiency for the Baseline Brayton System

SECTION IV

SUMMARY AND DISCUSSION

The main thrust of the Point-Focusing Distributed Receiver (PFDR) Technology Project is aimed at industrial technology development of the most cost-effective combinations of concentrators, receivers and power conversion units.

The objective of the present investigation was to establish a set of system cost/performance reference frames for simple baseline systems with various levels of energy cost targets. The results, expressed in terms of the "Justified Capital Investment", can be used to compare detailed design variations as well as to provide useful guidelines for hardware development programs. It should be noted that the purpose of the system definition activity is to generate and apply a methodology for screening candidate options with updated hardware cost projections and subsystem performance. Consequently, the trade-off study was limited only to the key parameters that govern the concept selection process.

A. KEY SYSTEM PARAMETERS

The viability of a point-focusing distributed receiver solar power system is governed by its cost effectiveness. System concept selection is influenced by many variables, such as technology advancement and potential market penetration, which influence the mass production hardware cost. However, three key parameters, namely, concentrator quality, system operating temperature, and power conversion efficiency are regarded as setting the pace for the development of point-focusing solar thermal conversion systems. The power conversion efficiency of a thermodynamic cycle improves with increasing temperature. The performance of a solar collector is governed by both the operating temperature and the concentrator surface quality. As the operating temperature increases, the heat loss rate per unit of receiver aperture area also increases. Receiver aperture size requirement for maximum effectiveness under a specified operating temperature is determined by the concentrator quality. A more accurate concentrator implies smaller aperture opening and, thus, higher receiver effectiveness.

Optimum system performance is determined by proper matching of concentrator quality, receiver operating temperature, and engine conversion efficiency. System concept selection involves detailed cost/performance trade-offs among all optimized candidate options. The power conversion efficiency may vary significantly according to the type of thermodynamic cycle and the anticipated improvements from research and development. Because solar thermal power generation is still in a very early developmental stage, the relationship between concentrator cost, size, and quality is yet to be established. Based on a survey of existing prototypes, it appears that the concentrator quality and, possibly, manufacturing cost are directly related to the design concept and material selection.

In this study the operating temperatures were preselected to be 538°C (1000°F) and 816°C (1500°F) for baseline Rankine and Brayton systems, respectively. The choice of concentrator quality and heat engine characteristics are interactive. A high-quality concentrator always improves the system performance, but the improvement becomes more pronounced for higher temperature applications. Consequently, a high-quality concentrator requires a high-temperature, high-efficiency power conversion unit to utilize the full potential of the high-quality dish. The improvement in concentrator surface accuracy probably is associated with an increase in manufacturing cost, which must be justified by a higher system performance in order to be competitive. However, a certain design concept and manufacturing process, established to produce low-cost concentrators with a specific surface accuracy, would create a need for the research and development of a compatible and effective solar heat engine. These two parameters, concentrator quality and engine performance, are both closely related to advancement of the state-of-the-art technology. Their cost/performance trade-off relationships dominate the selection of cost effective solar thermal power system options preceding the detailed system design phase. Other design parameters are less critical and can be grouped into two categories: engineering parameters and functional parameters.

B. ENGINEERING AND FUNCTIONAL PARAMETERS

Engineering parameters include concentrator size, structural support configurations, etc., that may have a major bearing on construction cost and could play an important role in design optimization. For example, concentrator size is a critical factor affecting subsystem compatibility. Larger engines generally exhibit better conversion efficiency. Furthermore, the per-unit-area cost of concentrators decreases with increasing dish diameter because only one tracking system and one receiver assembly are required per dish. However, the structural/wind load considerations may have an even stronger effect on the dish size, from the construction cost point of view. Module size optimization is critical to the development of point-focusing solar power systems; nevertheless, an optimum concentrator size will benefit all system options. These types of parameters have little direct effect on system concept selection.

Functional parameters include mirror reflectance (including surface cleaning), thermal insulation of the receiver and the transport pipelines, etc. The effects of these parameters on the overall system cost/performance are moderate, and the current state-of-the-art is considered to be adequate. Concentrator surface reflectance probably is the most important parameter in this group. The effect of reflectance variation on system performance is nearly linear. Periodic surface cleaning may be required for certain concentrator reflector materials.

C. CONCENTRATOR/REFLECTOR CLEANING AND RELATED IMPLICATIONS

Preliminary test results at Sandia Laboratory (Ref. 25) show that 15 weeks of outdoor weathering of second-surface silvered glass and second-surface aluminized Teflon decreased solar reflectance by approximately 10% and 40%, respectively, due mainly to dirt accumulation. It is clear that concentrator cleaning requirements, and the corresponding O&M cost, could vary significantly. However, with a given system concept selection, the design trade-off of material selection and cleaning strategy can be carried out in a straight-forward manner. For example, the cleaning maintenance cost may be considered as a fraction of the justified capital investment amortized for the lifetime of the system (e.g., 30 years). For second-surface glass, the justified cleaning cost may be equivalent to 10% of the baseline system cost. The value (i.e., 10% of the justified capital investment) may vary from 20 $\$/m^2$ for a high-performance system, with concentrators of 1 mrad surface accuracy, to 5 $\$/m^2$ for a low-performance system.

It is possible that the actual cleaning cost may be higher than the justified allocation. In this situation, it may be more cost effective to accept the reflectance loss by supplying an additional 10% of concentrator surface. In the case of second-surface Teflon, the justified cost for cleaning would be 40% of the baseline system cost. The system would be viable only if the energy cost corresponding to the sum of the baseline system cost and O&M allocation remain competitive. In any event, the optimization process takes place in detailed design trade-off studies, not in the system concept selection process.

D. ASSUMPTIONS FOR THE STUDY

In the present analysis, many assumptions and approximations were made in order to simplify the approach. All engineering parameters and functional parameters either were treated as given constants or were not taken into consideration. Transport losses, storage requirements, and related capacity factor were not considered. Dirt accumulation and associated reflector cleaning cycles were not taken into account. Remarks concerning the reference solar insolation data are warranted.

The reference insolation data used in this study, the Aerospace modified data (Ref. 8), probably is too optimistic. From a practical point of view, the pyrheliometer outage experienced by Southern California Edison during the recording period (see Section II, Part A.3) would reflect realistic system downtime (such as scheduled maintenance and repair). Furthermore, pyrheliometers usually employ an aperture field-of-view ranging from 6° to 15°. This field-of-view would include a significant amount of circumsolar energy, which would not be utilized by highly concentrating devices such as point-focusing collectors. The ratio of circumsolar to total solar radiation ranges from 0.82% to 69.2% (Ref. 26). An assessment from Lawrence Berkeley Laboratory (Ref. 27) indicated that pyrheliometer data would lead to 1 to 5% over-estimation of energy production for

power tower applications. For point-focusing collectors the error probably would be even greater because of the higher concentration ratio. Current selection of the 1976 Aerospace modified data as an insolation reference was based on the desire to maintain a data base consistent with other solar thermal power projects. The cone optics computation used in the present analysis considered the ratio of circumsolar to total radiation to be 2.9% (Ref. 28). All considered (system outage and circumsolar, etc.), the energy production calculation probably has an uncertainty less than 15%.

E. HARDWARE SUBSYSTEM DEVELOPMENT

As pointed out earlier, current PFDR Technology Project activities are directed towards industrial technology development of critical subsystems: concentrators, receivers, and power conversion units. From a system selection point-of-view, the relative importance of the three hardware development programs is distinctly different.

1. Concentrators

Concentrator development probably is the most important, and definitely the most uncertain, factor affecting the selection of two-axis, point-focusing solar energy conversion options. Because concentrators are the major cost item in the system, their development will have high pay-off potential. The rating of a point-focusing concentrator depends upon many factors such as surface slope error, tracking accuracy, size, optical surface durability, maintenance requirements and, most of all, the manufacturing and installation costs. Depending upon the options of the power conversion unit and the operating temperature, a low-quality concentrator may be preferred if the cost is low enough. In other words, the key criterion for concentrator development may be low cost instead of technology excellence. Technology development within the next few years will determine whether or not this viewpoint is correct.

It should be emphasized that every concentrator design concept, large or small, highly accurate or with large slope errors, could be a viable choice if the cost is competitive with the system justified capital investment. Current information concerning concentrator quality, size, and mass production cost is not available. The main objective of low-cost concentrator development programs should be to establish this critical data base.

2. Power Conversion Units

Engine development centers on improvements in power conversion efficiency. Engine efficiency, however, can play only an ancillary role in solar energy applications. An optimistic target may be to double the current state-of-the-art efficiency. Nevertheless, such a major technology advancement cannot, by itself, improve the system cost/performance relationship to the required level of justified capital investment, which is an order of magnitude lower than present hardware cost. If point-focusing solar power generation systems are

to become competitive it appears that co-development of low-cost concentrators and high-performance power conversion units will be required.

Advanced engine development could modify concentrator trade-off relationships. For example, the development of a highly efficient Brayton or Stirling engine at 816°C (1500°F) could substantially increase the associated justified system cost and create additional incentive for manufacturing high-quality concentrators with surface accuracy around 3 mrad. If the manufacturing industry could develop a very inexpensive process to construct umbrella-type concentrators (around 12 mrad), then there will be a need to accelerate the research and development of a medium temperature, 260°C to 371°C (500° to 700°F) organic Rankine system, which would be best suited to operate with this type of concentrator.

According to the compatibility requirements between operating temperature and concentrator quality, current estimates of mass-produced concentrator accuracy (3 mrad to 12 mrad) would suggest that engine development probably should be directed towards the low to medium temperature range, 260°C to 816°C (500°F to 1500°F). Advanced systems with high-temperature, high-efficiency engines may be attractive on paper but probably will not be practical from a system and cost effective point-of-view. For example, if the concentrator quality is 3 mrad or worse, a 1371°C (2500°F) Brayton system with power conversion efficiency of 55% would produce less electric energy than a 538°C (1000°F) Rankine system with 40% conversion efficiency (Ref. 29). The development of high-temperature solar heat engines should be well-coordinated with the development of high-quality concentrators. The matching concentrator quality for a 1371°C (2500°F) engine would be 0.5 mrad or better. This corresponds to the small monolithic-type designed for thermionic applications. The associated cost to manufacture this type of concentrator probably is prohibitive for practical point-focusing solar power generation.

3. Receivers

Receiver development plays an entirely different role from concentrator and engine development. The receiver is an indispensible critical component that links the engine and the concentrator together. Yet, the performance of a solar receiver is dominated by its aperture opening, which is governed by the operating temperature and the concentrator quality, and not the receiver design concept. Reliable receivers with long service lifetime are critical to the success of point-focusing solar thermal systems, but their development does not strongly influence the selection of viable system options. In fact, for each specific system concept, the receiver should be custom designed to match the concentrator and the power conversion unit. The design criteria are usually functional/operational requirements such as safety features, transient storage requirement, etc. Important design features such as absorber arrangements, material selection, heat pipe/storage-bath applications are related to tube temperature differential limits, pressure drop considerations, durability/lifetime, etc., and not to receiver performance.

The implementation of receiver design/construction would be an explicit engineering task to meet predetermined requirements according to the system design specifications. Before critical system selections are made, receiver development activities should be divided into two areas. One activity would emphasize basic heat tranfer and materials research, planned to address the anticipated receiver design requirements. The other activity would be continued participation in the early hardware implementation programs currently planned in the PFDR Technology Project. In the hardware demonstration phase, the critical subsystems may not be optimally matched. However, the main purpose of hardware demonstration is to gain operational experience, to confirm system analytical predictions, and to show technology feasibility. In this context, the near-term activity of receiver development may deserve more attention than other subsystems because of its many critical functional requirements: safety, durability, controls, and transient operation.

F. COST/PERFORMANCE SUMMARY

The systems considered here were sized so that the receiver would provide 60 kWth output to the engine. The required concentrator area is a function of the design point insolation (selected as 0.8 kW/m^2 from Figure 2-9) and collector efficiency, which depends on the concentrator surface slope error and receiver operating temperature. Details of the analysis were described previously and will not be repeated here. The annual energy production is calculated for varying insolation, using the assumed part-load engine characteristics and rated engine efficiency.

The justified capital investment used herein is the present value of an electricity-generating module (calculated from Eq. 3.2 for an assumed lifetime of 30 years) per unit of concentrator area. The justified capital investment can be used as a tool to establish preliminary system cost targets, i.e., to place an upper bound on the system costs, including hardware manufacturing and system installation costs, that will be required to meet specified energy cost targets. The principal results were shown in a series of charts (Figures 3-2, 3-4, 3-5 and 3-6) that illustrate the justified capital investment plotted as a function of concentrator surface slope error and power conversion efficiency for baseline steam Rankine and gas Brayton systems.

A rough estimate of the surface accuracy of mass-produced low-cost concentrators would be somewhere between 3 mrad and 12 mrad. Figure 4-1 shows the justified capital investment for a baseline Brayton system employing concentrators with 3 mrad surface accuracy, and power conversion efficiencies of various values. The justified capital investment for the system is in the range of $150 to $180 per unit of concentrator area to meet an energy cost target of 50 mills/kWe-hr. An equally attractive alternative would be to develop low-quality concentrators with very low cost, in contrast to attempts at developing high-quality concentrators with low cost. Concentrators, such as the film-type or inflatable designs, were estimated to be in the $\$50/m^2$ range for mass-produced items. Figure 4-2 shows that the

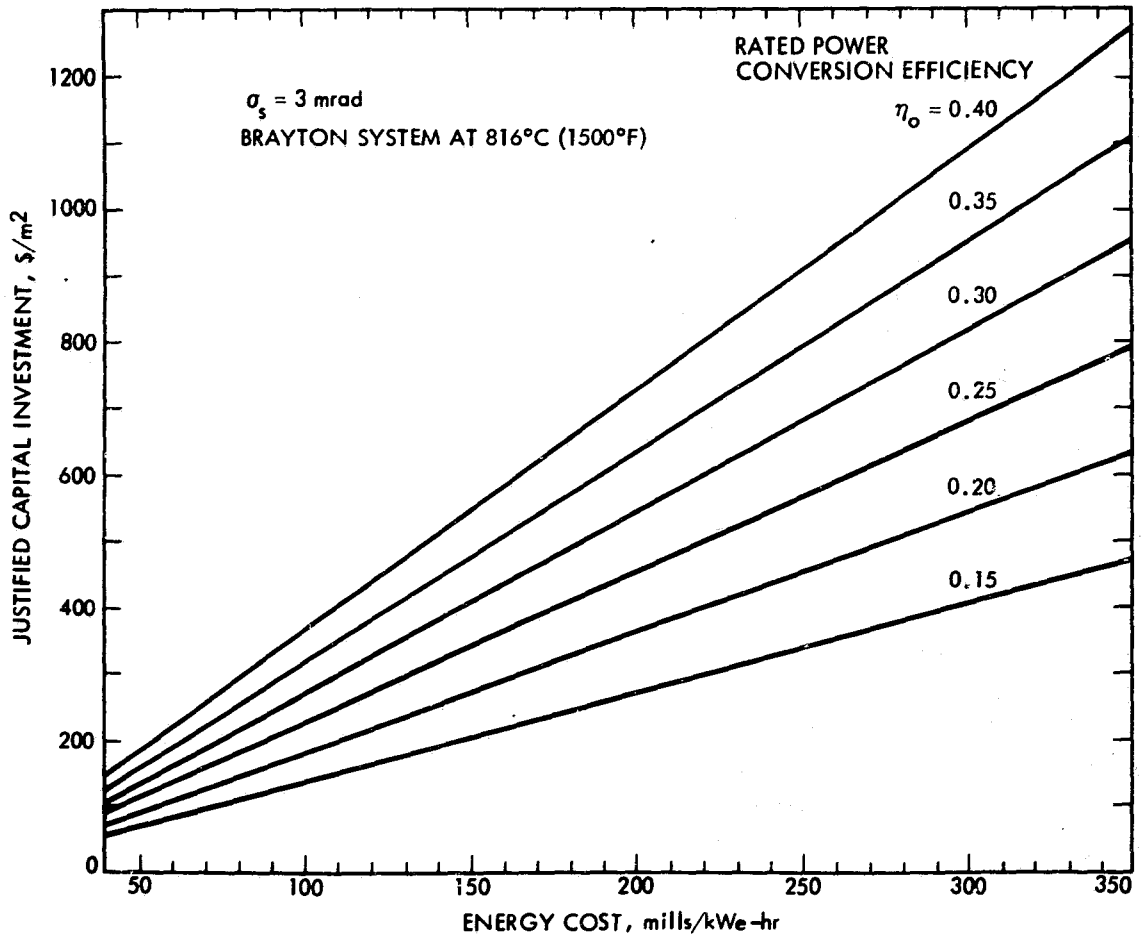

Figure 4-1. Justified System Investment for a Brayton System with a 3 mrad Concentrator

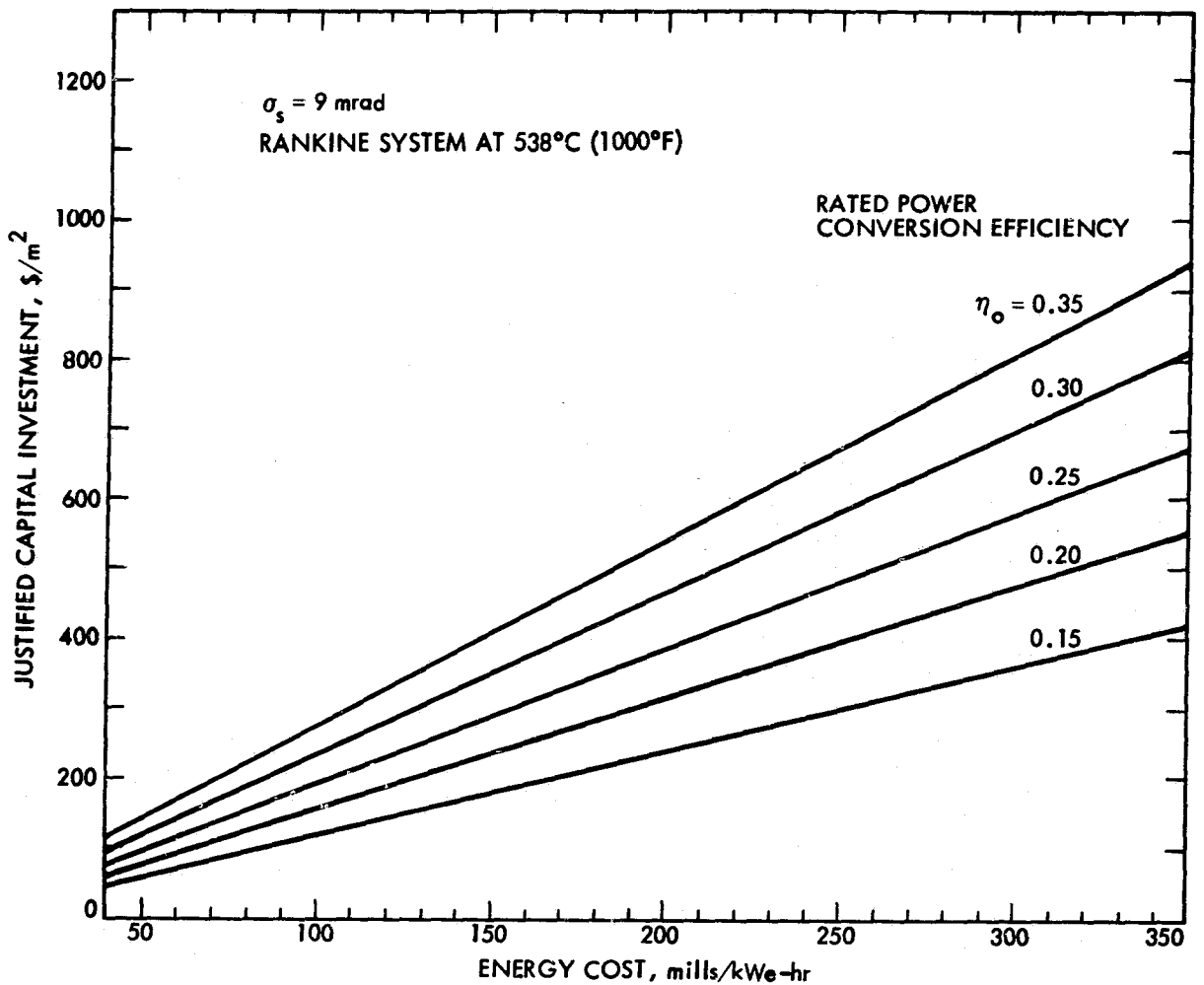

Figure 4-2. Justified System Investment for a Rankine System with a 9 mrad Concentrator

system justified capital investment for a Rankine system, with a concentrator quality of 9 mrad, is approximately 50 to 100 $/m^2 depending on the power conversion efficiency. If the cost projections are correct, then this combination would be a viable option.

It is useful to compare a Brayton system with a concentrator quality of 3 mrad to a steam Rankine system with a concentrator quality of 7 mrad because the required concentrator area (Figure 2-13) and the rated collector efficiency (Figure 2-15) are nearly the same for these two cases. The results can be presented in a format similar to the cost target presentation in Figure 1-2. Figure 4-3 shows the comparison; note that the parameter value $/m^2 is the system justified capital cost, not the collector cost per unit of area. The upper, horizontal, scale for overall system efficiency is based on an approximate value of $\xi_c = 0.64$ for the collector efficiency, as obtained for the two systems at design point insolation (Figure 2-15). Curves for constant system capital investment are nearly the same for the two cases. However, for the same relative energy cost, the Brayton system allows a higher justified capital investment than a steam Rankine system with lower power conversion efficiency. Figures 4-3 and 1-2 are remarkably similar if it is assumed that collector cost is roughly half the system cost.

Further system comparisons are shown in Table 4-1. A Brayton system with $\sigma_s = 3$ mrad, and values $\eta_o = 0.35$ and 0.40, is compared to two steam Rankine systems with $\sigma_s = 7$ mrad and $\sigma_s = 9$ mrad, each for values $\eta_o = 0.30$ and 0.35. Actual hardware costs must be equal to, or less than, the system justified capital investment. The justified capital cost is the larger for the Brayton system when expressed in $/m^2; however, values expressed in $/kWe are nearly the same for all six cases. The Rankine system for $\sigma_s = 9$ mrad seems to be the poorest of the three cases because its concentrator is the largest and its justified costs are the lowest. Overall, under the assumptions of this study, the Brayton system appears to have a slight edge because of its highest annual energy production. It is seen that large improvements in power conversion efficiency will have increasingly less effect on energy cost when the values of energy cost approach or fall below the target value (See Figure 4-3).

Comparisons with the commercial Omnium-G module are of interest in the present context. The Omnium-G concentrator is 6 m in diameter, has an effective aperture area of 27 m^2, and is estimated to have a surface slope error of approximately 3 mrad (Figure A-13 of Appendix A). The module presently is fabricated to order, and is not in mass production. Current selling prices are $29,500 for the tracking concentrator and $41,500 for the OG-7500 module/system, which are equivalent, per unit of concentrator area, to $1090/m^2 and $1540/m^2, respectively. If site preparation, shipping and installation costs are included, the total system cost is approximately $1650/m^2. The latter cost corresponds roughly to a range of $6000 to $11,000/kWe (due to current uncertainty in system performance of the Omnium-G module). Thus, the current costs of the concentrator and the system are a factor of 10 to 15 greater than 1985 target values. JPL presently is estimating mass-production costs for the Omnium-G module.

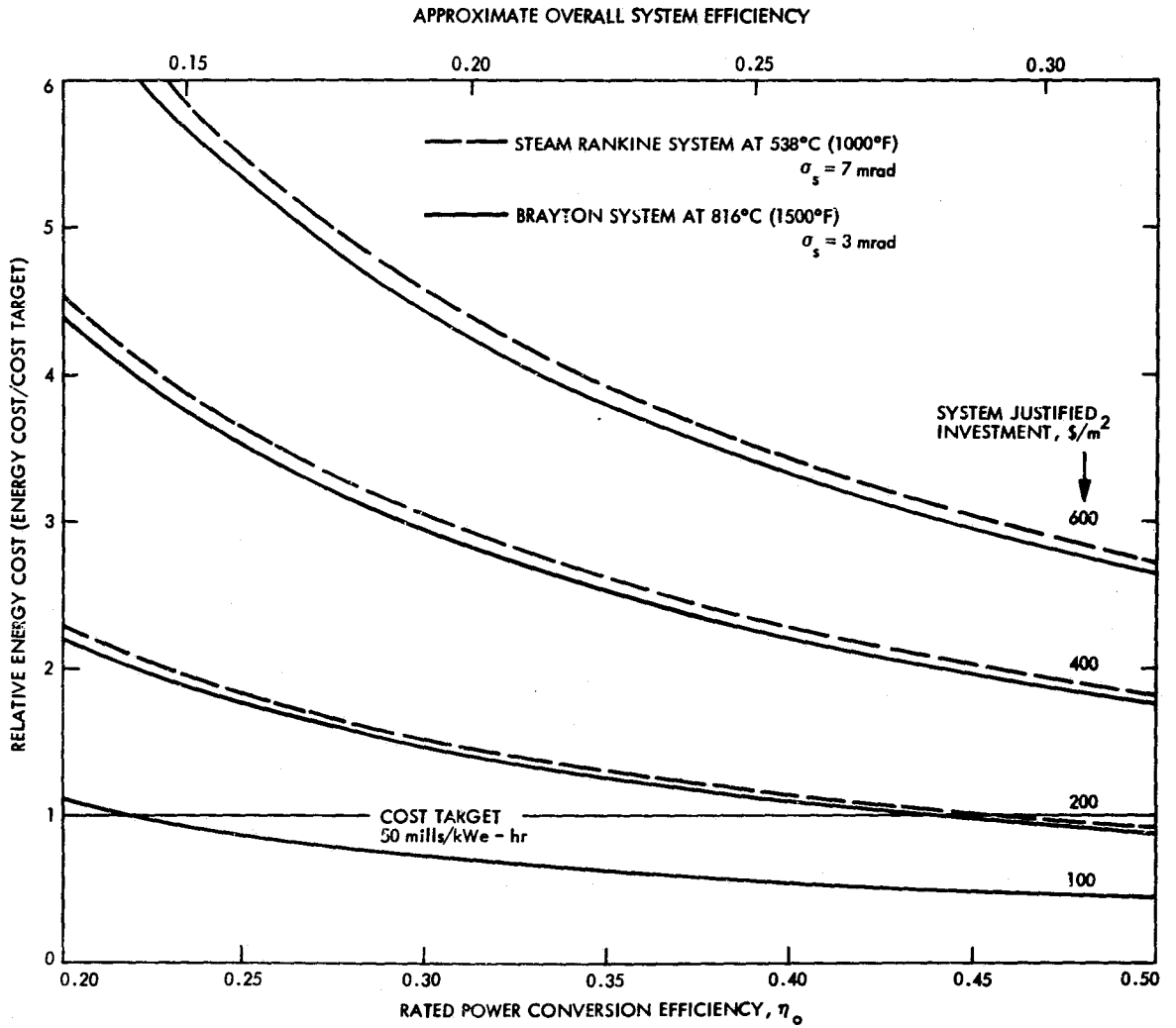

Figure 4-3. Effect of Power Conversion Efficiency on Relative Energy Cost

Table 4-1. Representative Scenarios for Baseline Systems with an Energy Cost Target of 50 mills/kWe-hr

DESIGN POINT INSOLATION, I_o = 0.8 kW/m^2
RECEIVER THERMAL OUTPUT ≅ 60 kWth
ENERGY COST TARGET = 50 mills/kWe-hr

	BRAYTON SYSTEM 816°C (1500°F)		STEAM RANKINE SYSTEM 538°C (1000°F)			
	σ_s = 3 mrad		σ_s = 7 mrad		σ_s = 9 mrad	
ASSUMED POWER CONVERSION EFFICIENCY, η_o	0.35	0.40	0.30	0.35	0.30	0.35
CONCENTRATOR AREA, A_c, m^2	125		127		146	
ANNUAL ENERGY PRODUCTION, kW-hr/m^2-yr	616	707	514	596	450	523
ANNUAL ENERGY PRODUCTION (TOTAL), kW-hr/yr	77,000	88,380	65,280	75,690	65,700	76,360
MEAN CAPACITY, kWe*	21.6	24.8	18.3	21.3	18.4	21.4
SYSTEM JUSTIFIED CAPITAL INVESTMENT, $/m^2	159	182	132	153	116	135
SYSTEM JUSTIFIED CAPITAL INVESTMENT (TOTAL), $	19,880	22,750	16,760	19,430	16,940	19,710
SYSTEM JUSTIFIED CAPITAL INVESTMENT, $/kWe	920	917	916	912	920	921

*CALCULATED FROM ANNUAL ENERGY PRODUCTION ASSUMING 3560 HOURS OF OPERATION PER YEAR.

SECTION V

CONCLUSIONS

The main objective of this study was to establish a methodology for comparing small power system modules using a consistent approach and input assumptions. The results, expressed in terms of the justified capital investment, can be used to compare detailed design variations as well as to provide guidelines useful for hardware development programs. Many assumptions were employed to simplify the cost/performance analysis; thus the results should be regarded strictly as preliminary. Better results will be obtained only when subsystem mass production cost estimates become available, particularly for concentrators.

- The viability of point-focusing distributed receiver modules is governed by three key parameters: concentrator quality, operating temperature, and power conversion efficiency. For systems with pre-selected operating temperature, concentrator quality and engine performance dominate the cost/performance trade-off relationships.

- Engineering and functional parameters are not critical to cost/performance trade-offs; however, concentrator reflectance is the most important of these parameters.

- The solar insolation model (Barstow, 1976, data modified by the Aerospace Corp.) used in this study probably is too optimistic, by an amount of at least 5%.

- Any concentrator design, large or small, high or low quality, could be a viable choice if it is cost-competitive and in accordance with the system justified capital investment. However, a key criterion for concentrator development may be low cost and not technology excellence.

- Module/concentrator size is critical to all point-focusing solar power systems and an optimum concentrator size will benefit all systems. Optimum size cannot be determined until the relationship between size, surface accuracy, and cost first has been decided. Trade-offs will occur between concentrator cost and module (system) cost.

- Compared to other subsystems, receiver development is not considered critical for the long-term outlook. However, near-term development merits careful attention because of critical requirements such as safety, durability, controls, transient performance, etc.

- In the first approximation, power conversion efficiency has a linear effect on the justified capital investment for a given energy cost target, and should be pursued in

technology development. However, the benefits of higher conversion efficiency diminish rapidly as system cost targets are approached.

- From the standpoint of annual electricity production and justified capital investment there is little difference between the Brayton open-cycle air systems and closed-cycle air systems even though the engine part-load characteristics were markedly different for the two cases. Further work is needed to establish the effect of the part-load characteristics..

- A range of concentrator surface accuracy of roughly 3 to 5 mrad (surface slope error) separates selection of steam Rankine and open-air Brayton systems. High-temperature Brayton systems require high-quality concentrators, whereas the opposite is true for Rankine systems.

- For the same energy cost target and overall system efficiency, a 3 mrad Brayton system and a 7 mrad steam Rankine system yield about the same justified capital investment. However, granting that the Brayton system has a higher performance potential, it will always have the higher justified capital investment and annual electricity production.

- At the present time, there is no clear choice between gas Brayton and steam Rankine systems. Concentrator development will have the largest influence on this choice. Thus, a key input to system selection will come from industry as they develop mass-production cost estimates and prototype hardware for low-cost concentrators.

SECTION VI

RECOMMENDATIONS

Recommendations are addressed both to the restrictions of this analysis as well as to anticipated changes of direction for point-focusing solar thermal power systems. Some are general, some are specific.

- The present study was confined to two levels of operating temperatures (1000°F steam Rankine and 1500°F gas Brayton). The study should be extended to other temperature levels to establish a more definitive understanding of the effects of this parameter.

- In the development of high-temperature systems (greater than 1500°F), if and when that appears desirable, the development of high-temperature solar heat engines should be coordinated closely with the development of high-quality (accuracy) concentrators.

- The main objective of low-cost concentrator development programs should be to establish a data base relating concentrator size, quality, and mass-production cost.

- A concentrator costing study should be initiated at the earliest opportunity. The objective of such a study would be to assess the cost of a variety of concentrator concepts on a relative basis using consistent assumptions and input data. Information from this study would be useful for making decisions regarding candidate power conversion subsystems.

- The various possible paths to PFDR technology development, e.g., a high-performance and possibly high-cost path versus a very low-cost concentrator path, should be established and explored in greater detail.

- A trade-off study of transport losses against potential gains in higher-performance and lower-cost power conversion units should be performed for dish clusters utilizing large, ground-mounted engines.

- A transient analysis (for varying cloud cover) should be performed to determine the response of a "real" receiver to fluctuating thermal energy input as well as system performance.

- Hybrid systems using fossil fuel should be studied with respect to such issues as (1) parallel versus series operation with the solar thermal system, (2) internal versus external combustion, (3) integration problems, (4) controls, (5) fuel constraints, (6) potential electric

storage requirements, (7) mirror contamination, (8) environmental effects, and (9) waste heat rejection as a source of interference for optical transmission.

SECTION VII

REFERENCES

1. Caputo, R., "An Initial Study of Solar Power Plants Using a Distributed Network of Point Focusing Collectors," JPL Internal Document No. 900-724, Jet Propulsion Laboratory, Pasadena, Calif., July 1975.

2. Selcuk, M. K., et al., "Preliminary Evaluation of a Parabolic Dish - Small Heat Engine Central Solar Plant," JPL Internal Document No. 900-749, Jet Propulsion Laboratory, Pasadena, Calif., July 1976.

3. Lucas, J. W., and Roschke, E. J., "Solar Thermal Power Systems Point-Focusing Distributed Receiver (PFDR) Technology: A Project Description," paper presented at AIAA/ASERC Conference on Solar Energy: Technology Status, in Phoenix, Ariz., Nov. 27-29, 1978.

4. Fujita, T., et al., "Projection of Distributed Collector Solar-Thermal Electric Power Plant Economics to Years 1990-2000," Report No. DOE/JPL-1060-1, JPL Internal Document No. 5102-39, Jet Propulsion Laboratory, Pasadena, Calif., December 1977.

5. Fujita, T., Manvi, R., Roschke, E. J., et al., "Techno-Economic Projections for Advanced Dispersed Solar-Thermal Electric Power Plants to Years 1990-2000, Report No. DOE/JPL-1060-4, JPL Publication No. 79-25, Jet Propulsion Laboratory, Pasadena, Calif., November 1978.

6. Hildebrandt, A. F., and Vant-Hull, L. L., "Power With Heliostats," Science, Vol. 197, pp. 1139-1146, 1977. Also: Holian, S. E., private communication, Jet Propulsion Laboratory, Pasadena, Calif., 1978.

7. Solar Energy Measurements at Selected Sites Throughout Southern California During 1976, by Southern California Edison, The West Associates, June 1977.

8. Randall, C. M., "Barstow Insolation and Meteorological Data Base," Report No. ATR-78(7695-05)-2, Aerospace Corporation, March 13, 1978.

9. Hughes, R. O., "The Sun-Tracking Control of Solar Collector Using High Performance Step Motors," p. 4-25, Proceedings of the ERDA Conference on Concentrating Solar Collectors, Georgia Institute of Technology, Atlanta, Georgia, Sept. 26-28, 1977.

10. Wen, L., "Field Arrangement Analysis for a Solar Thermal Distributed System," Internal Interoffice Memo to L. N. Dumas, 353 GEN-76-360, Jet Propulsion Laboratory, Pasadena, Calif., Feb. 12, 1976.

11. Bailey, M., private communication, NASA Lewis Research Center, Cleveland, Ohio, 1978.

12. Grilikhes, V. A., Grishutin, M. M., and Syrtsov, L. A., "Therma-Hydrolic Calculation of a Coil-Type Solar Receiver and Steam Generator," Geliotekhnika, Vol. 8, No. 1, pp. 8-18, 1972.

13. Heller, J. A., private communication, NASA Lewis Research Center, Cleveland, Ohio, 1978.

14. Little, Arthur D., "Preliminary Design of a 10 kWe Solar Heated Open Brayton-Cycle Engine," Phase 1, Report No. CR 78.003, Naval Civil Engineering Laboratory, Port Hueneme, California, November 1977.

15. Gupta, G., et al., "Technical Feasibility Study of Modular Dish Solar Electric Systems," ERDA/NASA Report No. 19740/76/1, Honeywell, Inc., March 1976.

16. Cameron, H. M., Mueller, L. A., and Namkoung, D., "Preliminary Design of a Solar Heat Receiver for a Brayton-Cycle Space Power System," NASA TM2552, May 1972.

17. McKinnon, R. A., "Lithium Hydride Storage Unit Development For The Sunflower System," pp. 447-460, Power Systems for Space Flight, Edited by M. A. Zipkin, and R. N. Edwards, Progress in Astronautics and Aeronautics, Vol. 11, Academic Press, 1963.

18. Pietsch, A., "Solar Brayton-Cycle Power System Development," pp. 759-793, Space Power Systems Engineering, Edited by G. C. Szego, and J. E. Taylor, Progress in Astronautics and Aeronautics, Vol. 16, Academic Press, 1966.

19. Roschke, J., "Gas Turbine Cycles for Dispersed Power Systems," Internal Trip Report (to AiResearch Mfg. Co., Phoenix, Arizona), Jet Propulsion Laboratory, Pasadena, Calif., February 8, 1978.

20. Roschke, J., "Generator/Gear Box Efficiencies," Internal Interoffice Memo, Jet Propulsion Laboratory, Pasadena, Calif., April 19, 1978.

21. Tarsala, J. A. "Application of Field Modulated Alternator Technology within the Point Focused Distributed Receiver Program," Internal Interoffice Memo, 343-78-370, Jet Propulsion Laboratory, Pasadena, Calif., April 4, 1978.

22. Merrick, W., "Concentrator Prices," Internal Interoffice Memo to J. W. Lucas and H. L. Steele, Jet Propulsion Laboratory, Pasdadena, Calif., April 1978.

23. "Low Cost Point Focus Solar Concentrator, Phase 1," Request for Proposal No. BW-Z-7179-245, Jet Propulsion Laboratory, Pasadena, Calif., April 19, 1978.

24. Doane, J. W., et al., "The Cost of Energy from Utility Owned Solar Electric Systems, a Required Revenue Methodology for ERDA/EPRI Evaluations," ERDA/JPL No. 1012-76/13, Jet Propulsion Laboratory, Pasadena, Calif., June 1976.

25. Pettit, R. B., and Butler, B. L., "Mirror Materials and Selective Optical Coatings," SAND-77-0111, Sandia Laboratory, Albuquerque, February 1977.

26. Frohlich, C., et al., "The Third International Comparison of Pyrheliometers and a Comparison of Radiometric Scales," Solar Energy, Vol. 14, pp. 157-166, 1973.

27. Grether, D. F., Hunt, A., and Wahlig, M., "Circumsolar Radiation: Sensitivity Analysis for Central Receiver Designs," Lawrence Berkeley Laboratory, October 23, 1977.

28. Wen, L., "Thermal Optical Surface Properties and High Temperature Solar Conversion," Paper 78-903, 2nd AIAA/ASME Thermophysics and Heat Transfer Conference, Palo Alto, May 24-26, 1978.

29. Wen, L., "Thermal Performance Trade-Offs for Point Focusing Solar Collectors," Preceedings IECEC Conference, San Diego, Calif., August 20-25, 1978.

APPENDIX A

CONCENTRATORS

A. OPTICAL TRANSMISSION CHARACTERISTICS

The optical performance of a concentrator is governed by its geometrical configuration and critical thermal optical properties, including solar reflectance, specular spreading due to microscopic roughness, surface error, and tracking/pointing accuracy. Solar reflectance and specularity are governed by mirror material selection. Three basic categories of reflector material are generally considered for solar concentrator applications: (1) second surface mirror, (2) metalized plastic films, and (3) polished metal surfaces. Figure A-1 shows the specular reflectance characteristics of some representative materials (Refs. A-1 and A-2). It should be noted that these values are for a cleaned, new surface. Surface degradation and dirt build-up on the reflector surface are very significant factors governing the reflectance properties. The effect of reflectance on the system performance is linear. The specularity, however, plays only a minor role for most reflectance materials (Ref. A-3).

In general, the geometrical center of the collector/receiver does not coincide with the center of the solar image due to the concentrator pointing error. The pointing error includes errors due to inaccurate sun tracking, and misalignment and structural deflections caused by gravity and wind loads. Detailed correlations between pointing error and control logic are discussed in Reference A-4 and will not be repeated here.

Surface slope error has been identified as the most significant parameter governing the optical performance of a solar concentrator (Ref. A-5). An ideal concentrator would have the reflector surface contoured precisely to the shape required by geometrical relationships. However, shape deviations may be caused by macroscopic surface waviness, imperfect alignment, and slope errors due to manufacturing tolerance and structural deflections. The local surface error of a reflector element is defined as the angular deviation of the surface normal from that of a perfect geometry. Theoretically, a detailed mapping of surface error over the entire concentrator body would give the most accurate description of the surface error. The value may vary considerably from hub to rim, and from zone to zone, circumferentially. From a practical point-of-view, the surface errors have to be characterized in a statistical manner. A standard sampling technique must be developed to establish the effective surface error statistics through quantitative measurements. Many approaches have been suggested to characterize surface slope error statistically. These include the method of solar disc scattering (effective enlargement of the apparent solar cone angle, the so-called scatter sun method), and flux scattering functions at the focal plane of the concentrator. According to Schrenk (Ref. A-6), the most desirable approach is to apply a probability function to the reflector surface normals such that the quality of the concentrator can be estimated

$$\rho(\Delta\theta) = \frac{\rho}{R_1 + R_2}\left[\frac{R_1}{2\pi\sigma_{\omega_1}^2}\exp\left(-\frac{\Delta\theta^2}{2\sigma_{\omega_1}^2}\right) + \frac{R_2}{2\sigma_{\omega_1}^2}\exp\left(-\frac{\Delta\theta}{2\sigma_{\omega_2}^2}\right)\right]$$

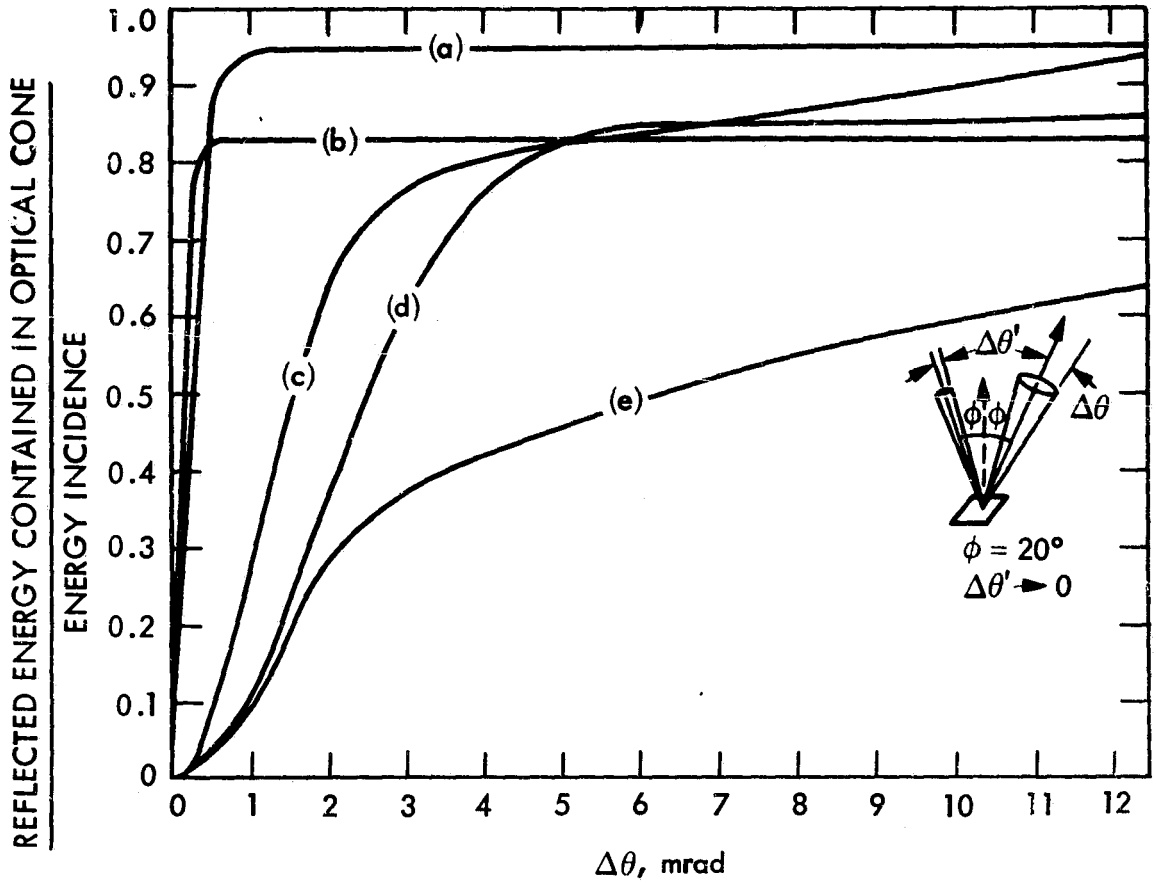

(a) CORNING 0317 GLASS, $\rho = 0.95, \sigma_{\omega_1} = 0.25$ mrad

(b) LAMINATED FLOAT GLASS (CAROLINA MIRROR CO.)
$\rho = 0.83, \sigma_{\omega_1} = 0.15$

(c) CORNING SILVERED MICROSHEET
$R_1 = 0.77, \sigma_{\omega_1} = 1.1$
$\rho = 0.95, R_2 = 0.18, \sigma_{\omega_2} = 6.2$

(d) 3M SCOTCHCAL 5400 PLASTIC FILM
$\rho = 0.85, \sigma_{\omega_1} = 0.19$

(e) TYPE 3002 HIGH PURITY Al-BUFFED AND BRIGHT ANODIZED (METAL FABRICATIONS INC.)
$R_1 = 0.44, \sigma_{\omega_1} = 1.4$
$\rho = 0.84, R_2 = 0.43, \sigma_{\omega_2} = 10.3$

Figure A-1. Specular Reflectance Characteristics

from the design concept and the manufacturing technique. This approach would facilitate an assessment of system cost performance trade-off relationship prior to the construction of concentrators.

Figure A-2 defines the local surface error as described by the directional cosines of the true surface normal $\hat{n}$ in a Cartesian coordinate on the surface element with the ideal surface normal $\hat{n}$ aligned with the Z-axis. In reality different systematic errors are expected from hub to rim, yet, in order to carry out statistical analysis, the distribution of surface error is usually considered to be random. Schrenk (Ref. A-7) suggested that the density function is best represented by a two-dimensional Gaussian (normal) function; he claimed that good correlations have been established between experimental ray-tracing data and the assumed Gaussian distribution function characterized by a circumferential and a radial standard deviation. If it is assumed that cylindrical symmetry exists for the probability density function, i.e., that the circumferential and the radial standard deviations are equal, then the probability that the surface normally falls within a ring bounded by r and r+dr around the ideal normal is given by:

$$dP(r) = \frac{1}{2\pi\sigma_s^2} \exp \frac{-r^2}{2\sigma_s^2} \; 2\pi r \, dr \qquad (A.1)$$

where σ_s is the effective surface slope error (standard deviation).

Equation A.1 can be applied to every element of the concentrator to compute its optical transmission characteristics. It can be seen that the concentrator optical performance is governed by the surface slope error and the geometrical arrangement of the reflecting elements. The geometry of a paraboloidal dish is determined by the rim angle, ψ, which typically varies from 30° to 60° for solar concentrating applications. Individual mirror elements, as well as continuous, monolithic surfaces, may be used. The surface geometry is arranged so that reflected solar image from all individual mirror surface elements converge toward the focal point. However, because of the relative positions of individual mirror elements, elliptical images with different sizes and intensity distributions will be formed at the focal plane by the reflecting cones. The resultant solar image has a high intensity central core surrounded by a fringe area, where the intensity decreases rapidly with distance from the focal axis.

The rim angle determines the concentrator focal length-to-diameter (f/D) ratio as well as the relative size of the high intensity focal spot compared to the fringe area. In the present study, a representative rim angle of 45° was used; however, there exists little practical difference in concentrator optical performance for rim angles between 45° and 60°. The f/D ratio is defined as:

$$\frac{f}{D} = \frac{1}{4} \cot \frac{\psi}{2} \qquad (A.2)$$

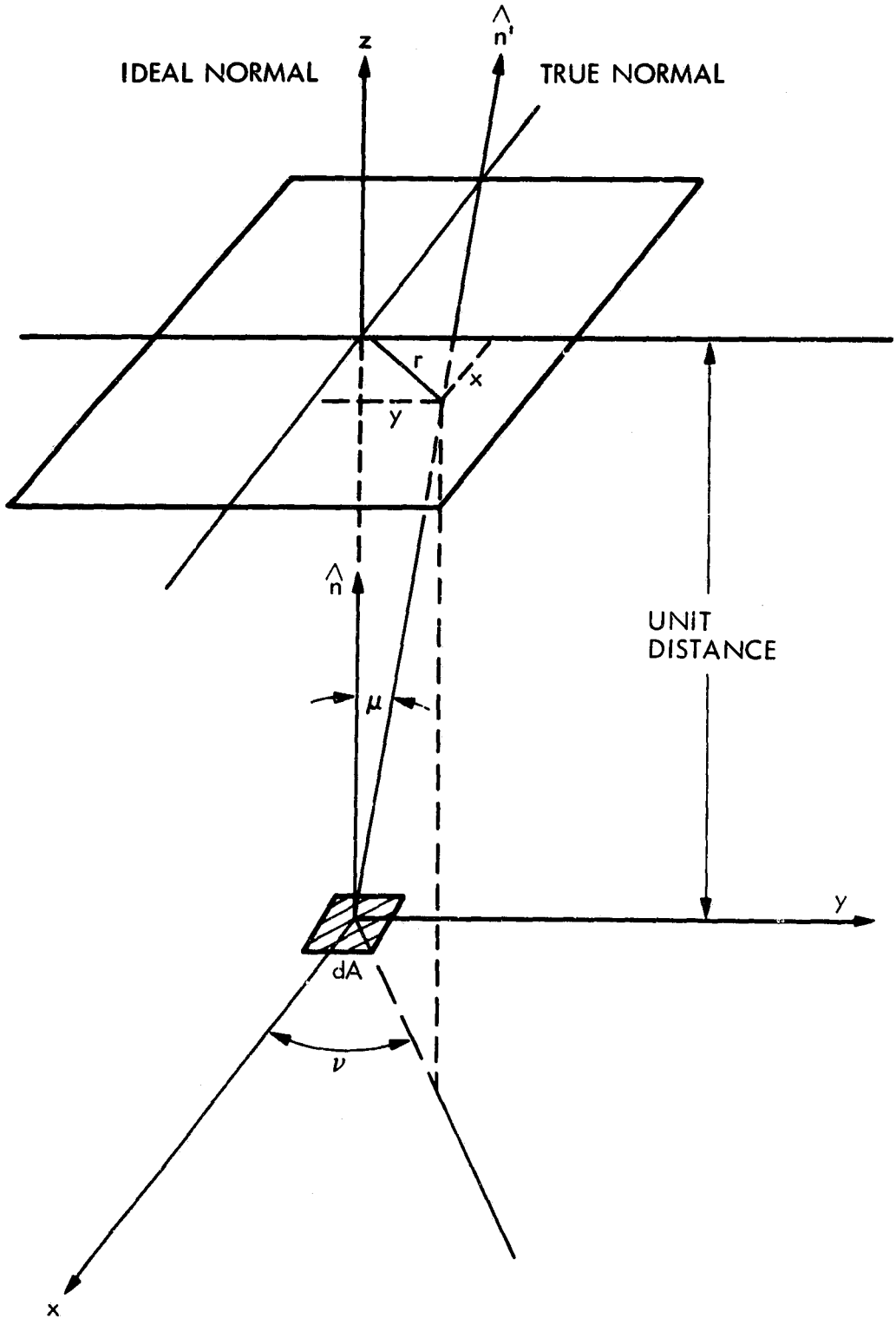

Figure A-2. Definition of Surface Slope Error

Figure A-3 shows the focal plane flux distribution as a function of surface slope error. It can be seen that the intensity at the focal spot may vary by a factor of 50 as the surface error changes from 1 to 10 milliradians (mrad). A slope error of 1 mrad at a given point implies that 68% of the light rays strike the concentrator within 1 mrad of the direction that would be required by a perfect concentrator.

B. CONFIGURATION CONCEPTS

The cost/performance characteristics of concentrators probably are the most important factors that govern the viability of two-axis tracking, point-focusing distributed solar conversion systems. Very few commercial solar concentrators are available at the present time but there have been many conceptual designs/prototypes, as well as experimental models. In the present study, concentrator configurations are limited to those resembling a two-axis, tracking paraboloidal dish. A brief survey of the state-of-the-art is presented herein. Fresnel reflectors are discussed; the following alternative concepts have not been included: Fresnel lenses (Refs. A-8 and A-9); Cassegrainian arrangements (Refs. A-10 and A-11); compound receiver/reflector applications (Ref. A-12); and concepts with a fixed receiver (such as the low-profile design, Ref. A-13), or fixed hemispherical reflector surfaces (Ref. A-14).

1. Monolithic Rigid Paraboloids

High-precision monolithic paraboloidal concentrators have been built primarily for high temperature solar thermionic applications. Several well developed methods have been applied to construct replicas of single-piece concentrators; namely, Electro-forming, cold forming, vacuum deposit of a thick layer of aluminum, and Epoxy casting.

a. Electro-Forming. Small concentrators with qualities approaching theoretical limits have been built by electro-deposition of nickel on activated glass substrates (Refs. A-15 and A-16). Thin-wall nickel concentrators have been obtained from nickel molds. The 9.5 ft diameter dish developed by G.E. for JPL (Ref. A-17) was based on centrifugally cast masters, which were used to make convex nickel molds by electro-forming. The same technique was then employed to obtain the nickel concentrator from the nickel mold. The process of electro-forming aluminum (Ref. A-18) also has been investigated for fabricating light-weight concentrators.

b. Cold-Forming. Thin sheets of electro-polished aluminum can be hydro-formed over suitable paraboloidal molds (Ref. A-19), or sectors can be stretch formed and bonded together. A TRW, 5 ft concentrator with rear-mounted torus was built with 0.016 in. thick aluminum sections stretch formed over a glass search-light mirror. The sections were given an epoxy plastic surface coating and then aluminized before assembled (Ref. A-20).

c. Epoxy Casting. Convex molds can be cast and concentrators then can be obtained directly as replicas (Ref. A-21). Polymer materials have been used at the Physicotechnical Institute of the

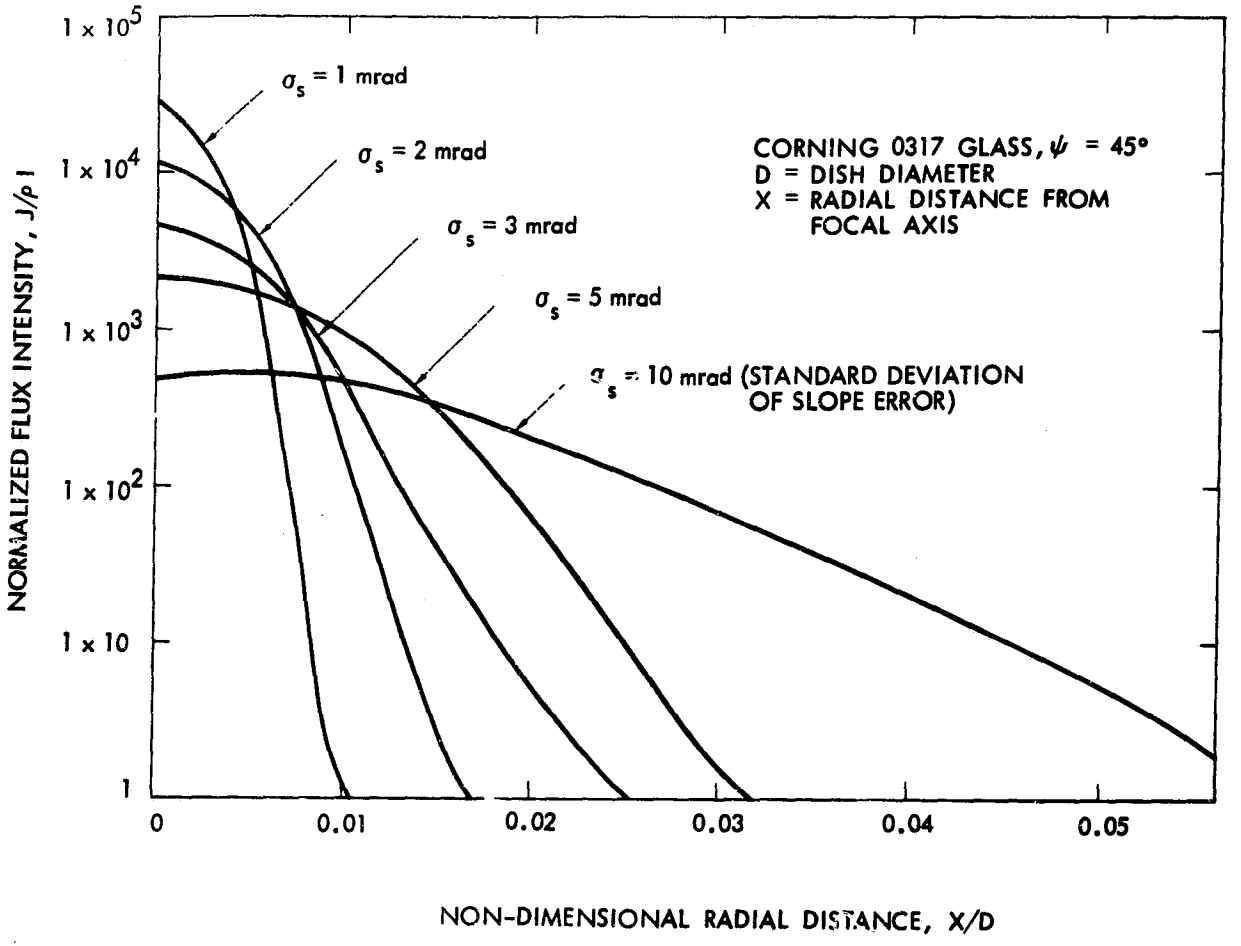

Figure A-3. Focal Plane Flux Distrubution of Concentrated Solar Energy for a Paraboloidal Concentrator

Academy of Science of the Turkmen, USSR to obtain cast duplicates with reflective surface coating, ranging from 0.46 to 1.5 m in diameter (Ref. A-22). A light-weight concentrator constructed at Boeing employed cast epoxy plastic reflecting surfaces bonded to aluminum honey-comb, which in turn was backed up by a plastic Fiberglas panel (Ref. A-23). Spin-casting of plastics also has been investigated (Ref. A-24).

d. Vacuum Deposit. Deposition can be used for thick layers of aluminum as well as for thin reflective coatings. Concentrators have been produced with a shell thickness of up to one inch that reproduce accurately the surface of the mold. The removal of the shell is facilitated by depositing an intermediate layer of silver (Ref. A-25).

2. Panel/Frame Type Concentrators

Large paraboloidal concentrators are difficult and expensive to manufacture in monolithic form. Most large, high quality concentrators, such as solar furnaces, consist of a paraboloidal shell or frame similar to that of a high-gain antenna. Reflecting surfaces are individual panel elements; the surfaces are conformed to the local curvatures of the frame. The panel material may be sagged or pressed second-surface mirrors, or chemically brightened aluminum with deposited aluminum or silver. Clear epoxy or RTV may be used as a protective overcoat.

In 1946 a paraboloidal dish, 10 m in diameter, was made from reinforced concrete at Tashkent (Ref. A-26). Glass reflectors were glued to the shell surface with carbonyl adhesive. The solar furnace at Bouzareah (Ref. A-27) an 8.14 m diameter paraboloidal dish, began operation in 1954. The system utilizes a massive supporting structure for rigidity and has a gross weight of 40 tons. The reflective surface was electro-polished and the reflectance has decreased from 0.83 to 0.7 in 15 years. An experimental solar device for pumping water at Ashkhabad, Central Asia was constructed in 1965 (Ref. A-28). The 4.86 m dish consists of a frame made of thin-wall steel tubing with flat ribs. The reflecting elements, in the form of curved trapezoids, are made by stamping from aluminum sheet, followed by buffing and electro-polishing. The General Electric paraboloidal design for the Shenandoah total energy project (Ref. A-29) is a polar-mount system with 20 panels mounted on a steel frame that is stiffened by supporting ribs (Ref. A-30). The prototype is shown in Figure A-4.

3. Faceted Concentrators

The major difference between a faceted concept and a panel concept is that the facet element does not conform to the curvature of the substructure and has its own individual optical axis. Typical faceted concentrators consist of arrays of small paraboloidal or spherical mirrors; this arrangement provides wind relief. A large variety of material selection and arrangements have been investigated. For example, the Raytheon concentrator (Ref. A-31) is a 6.7 m dish with 228 spherical mirrors, in trapezoidal shape, hand-mounted on an aluminum substructure. Hexagonal and circular

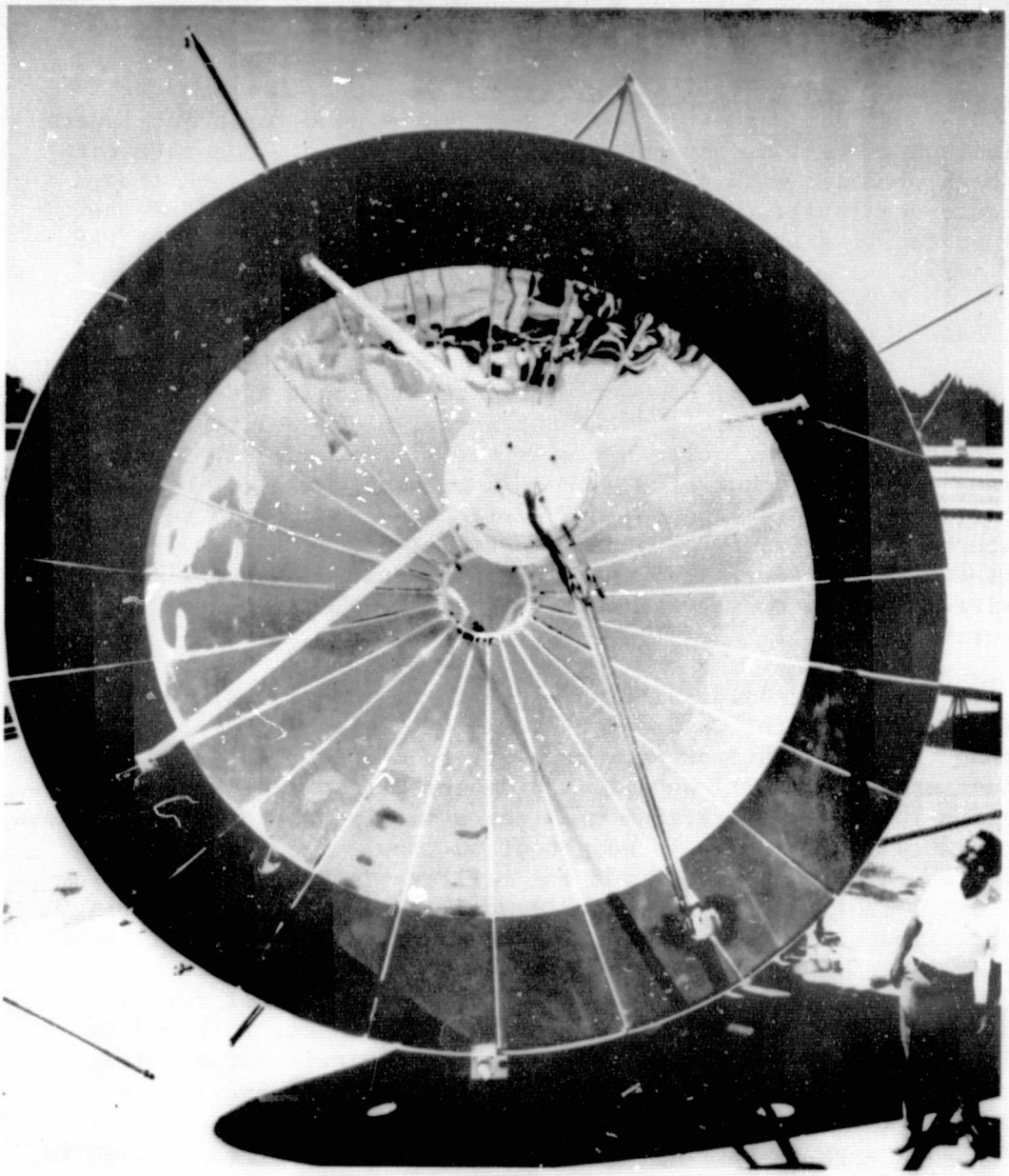

Figure A-4. General Electric 5-Meter Paraboloidal Collector, Prototype for Shenandoah Project

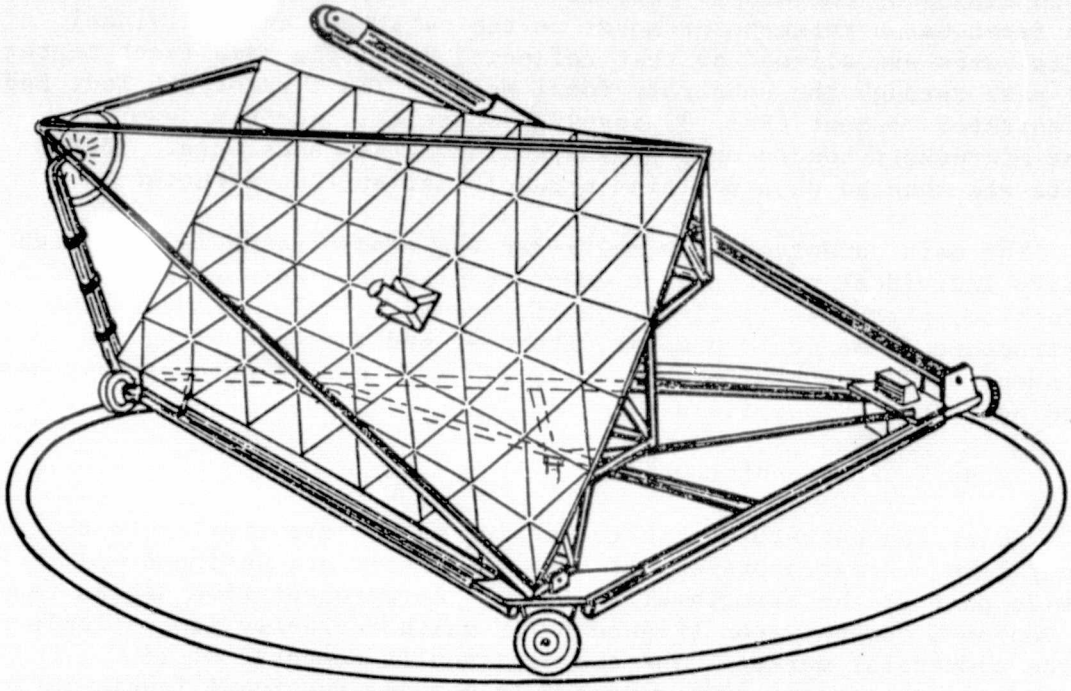

Figure A-5. Concentrator Concept for French THEK System

paraboloidal glass facets have been utilized to form a large concentrator (Refs. A-32 and A-33). The French THEK project has a concentrator design that employs triangular facets (see Figure A-5) to form a rectangular concentrator (Ref. A-27).

Small paraboloidal facets can be manufactured by replication or galvano-plastics processes. However, it was shown (Ref. A-34) that spherical facets have almost the same concentration capability as the paraboloidal ones as long as the ratio of facet area to concentrator area remains small. Because it is generally much easier and less expensive to manufacture high-quality spherical mirrors than paraboloidal ones, it would be more practical to construct faceted concentrators with small spherical mirrors. A representative arrangement is the Gamma-Ray Telescope of the Smithsonian Astrophysical Observatory on Mt. Hopkins, Arizona (Figure A-6). Hexagonal-shaped spherical facets (front surface mirrors with one common radius of curvature) were mounted on a spherical substructure. Each facet has a three-point mount on the substrate and individual optical axes are aligned so that reflected rays from each facet center will pass through the substrate focal point. The current JPL Test Bed Concentrator concept (Ref. 3) involves spherical facets made with glass microsheet bonded on a preshaped foam-glass substrate. The facets are mounted on a modified paraboloidal antenna structure.

The main advantage of a multi-faceted concentrator is that high quality individual reflecting elements can be manufactured in mass production, particularly if all facets are identical. However, the substructure frame could dominate the cost and the assembling and alignment of facets could be a costly labor intensive process that has to be performed in the field.

4. Petal Type Concentrators

Solar concentrators with reflecting petals are similar to the panel/frame concentrators except that the petals are designed to provide part of the structural rigidity. A representative design is the Omnium-G concentrator (Figure A-7), which currently is available in the commercial market. The concentrator is composed of 18 individual petals; the dish diameter is 6 m and the focal length is 4 m. The concentrator is mounted on a light-weight tubular aluminum structure and gimbal. Reflector material is 0.8 mm (32 mils) thick electro-polished and anodized aluminum (Alzak is currently used). Precut segments (in three sections) are placed on a convex plaster surface and forced to shape by application of a vacuum. A special urethane foam (4 to 6 inches thick) is applied to the back surface for structural rigidity (Ref. A-35).

Many petal type concentrators were investigated for space solar conversion applications in the early 1960s. In those cases, all the designs consisted of a hub with attached petals that could fold up to form a compact package for launching. Several prototypes have been built and tested. For example, the TRW "Sunflower" concentrator (Refs. A-36 and A-37) is a 9.9 m (32.2 ft) diameter paraboloidal dish (rim angle of 60°) consisting of 30 laminated aluminum petals. The front surfaces were coated with epoxy and aluminized by vacuum

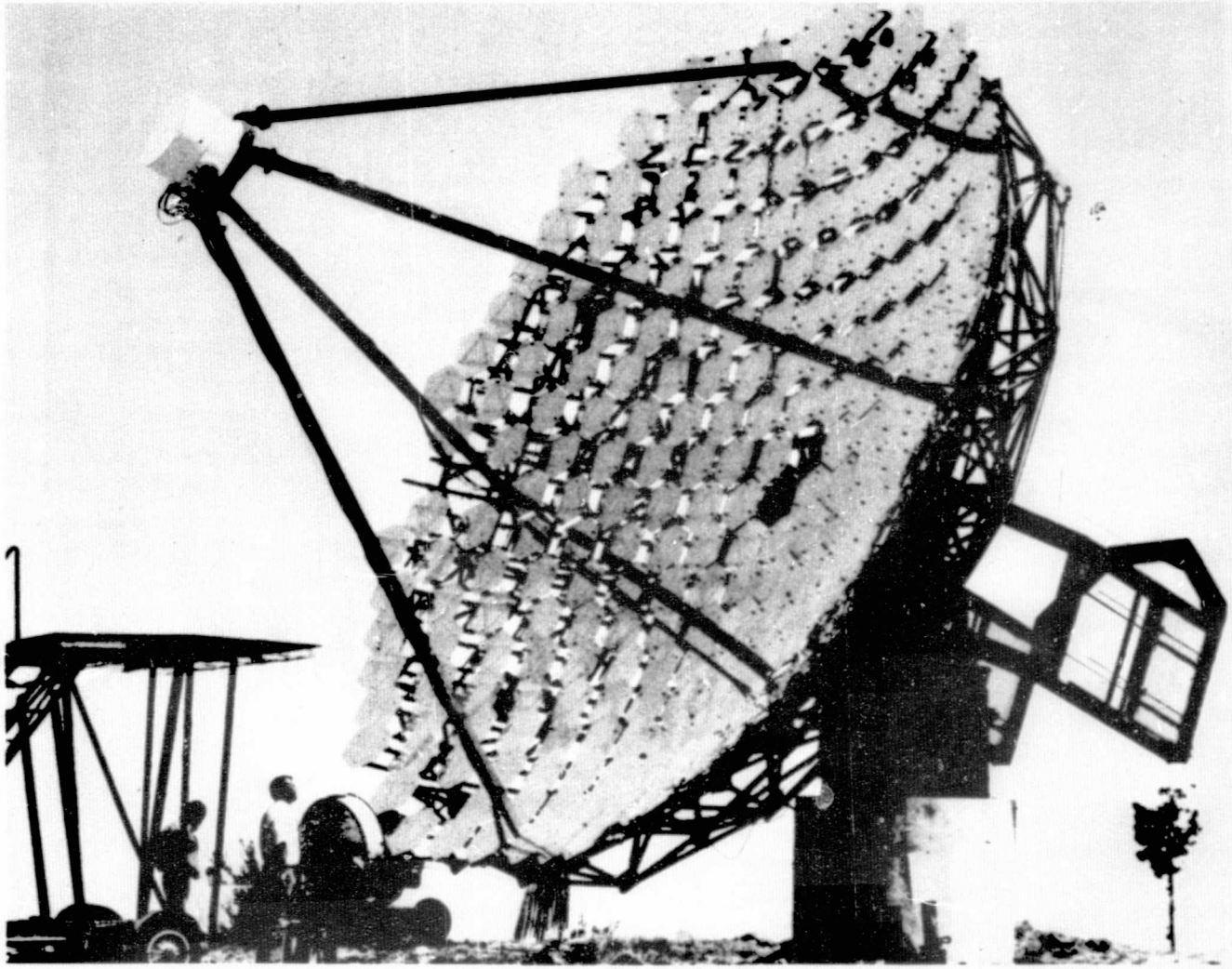

Figure A-6. Gamma-Ray Telescope of Mt. Hopkins, Arizona

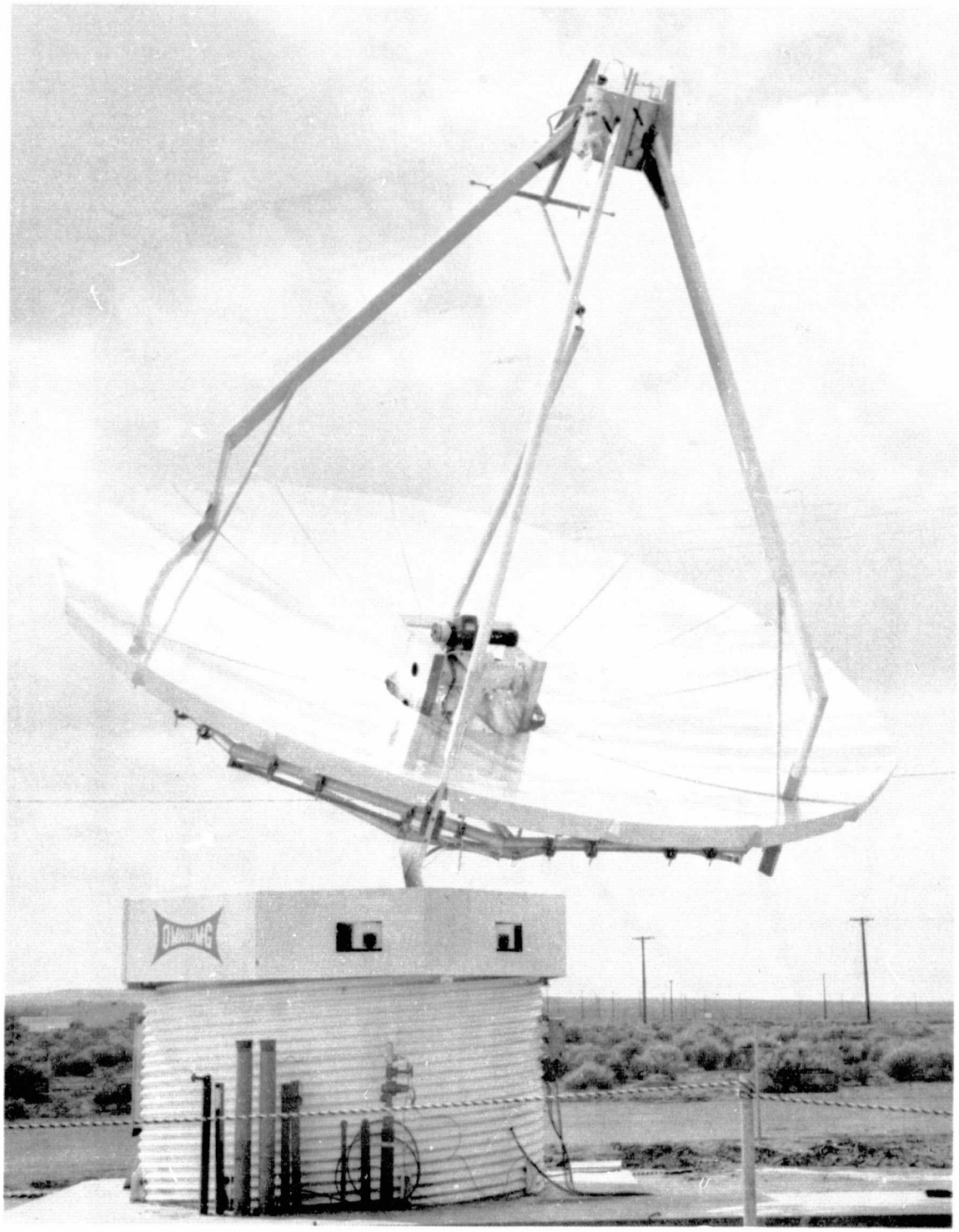

Figure A-7. Omnium-G Concentrator

deposition. A layer of silica protective overcoat was applied. The reflective surfaces were bonded on a honeycomb supporting structure. The standard deviation, σ_s, of the petal slope error was assessed to be 15 minutes (4.36 mrad). The U. S. Air Force developed a 15.75 ft (2.5 m) diameter petal-type concentrator using petals of honeycomb sandwich that consisted of an aluminum reflecting surface, honeycomb, and backing material (Ref. A-38). The model developed by Electro-Optical systems (Ref. A-39) had petals of electro-formed nickel and utilized a monocoque construction. The Ryan design (Ref. A-40) had petals formed of a thin aluminum sheet that was stiffened by a light aluminum lattice truss spot welded to the back. The maximum slope error of the Ryan concentrator was evaluated to be of the order of 2°.

The cost of a petal-type concentrator is determined by the required number of petals and the size of the concentrator, which is governed by the structural support design. The petal construction can be accomplished by various methods, e.g., an aluminum-structure petal with highly reflective metalized film (Ref. A-41). Many low-cost concepts have been investigated for petal-type solar concentrators. Accurate convex molds corresponding to an individual segment of a paraboloid can be obtained. Foam plastic, using phenolformaldehyde resin as a structural material, has been investigated at the Physicotechnical Institute of the Academy of Science, Uzbek, USSR, and was reported to be very promising (Ref. A-42). Other low-cost designs include glass reflectors bonded to a ferroconcrete body (Ref. A-43), and metalized mylar on asbestos cement petals (Ref. A-44). A process of fabricating by softening individual paraboloidal segments has been investigated (Ref. A-45); identical reflecting elements can be fabricated repeatedly in mass production to reduce the cost.

5. Umbrella-Type Concentrators

This type of concentrator is made of single-curvature petals or wedge-shape metalized films stretched over metal ribs in parabolic shape (Refs. A-46 and A-47). A 5-m umbrella-type concentrator with concentration ratio of 500 to 600 has been built at Uzbek, USSR (Ref. A-46). In general, the umbrella-type concentrators have relatively low concentrating capabilities. The performance is proportional approximately to the number of wedge elements.

6. Inflatable - Rigidized Concentrators

Basically, this type of concentrator is an aluminized film paraboloidal mirror that is rigidized by the application of a foamed plastic epoxy (Refs. A-48 and A-49) or a plastic-impregnated fiberglass backing to the back surface of the collector (Ref. A-50). For example, a layer of epoxy approximately 0.02 in. thick is sufficient to hold the concentrator shape. However, additional strength is required to withstand wind and handling loads. The additional rigidity can be provided by a variety of methods. The Goodyear 5 ft inflatable rigidized concentrator consists of three sections of fiberglass-reinforced plastic and a rim-ring for support. The 13.6 m (44.5 ft) diameter concentrator was rigidized by spray-coating the film with 0.025 in. epoxy, 1.7 in. polyurethane foam, and

then 0.025 in. epoxy. An aluminum truss structure was attached for support. Optical measurement of slope error indicated that maximum surface error is less than 0.5°, which is approximately the same as the petal-type concentrators.

7. Pressure-Stabilized Film Concentrators

The deformation of film surface under the action of gas pressure has been applied to form concave reflecting surfaces for solar energy concentration. Inflatable concentrators have been constructed with two layers of plastic films. The lower surface is metalized. The upper surface is transparent and has an anti-reflective coating. The curvature is created by inflating the space between the two surfaces, which are constrained by a ring at the periphery. For large-size concentrators, the skin of the concentrator may consist of wedge-shape strips of metalized films. An inflatable mirror of 13 ft^2 was built by Electro-Optical Systems (EOS)(Ref. A-51). The general configuration is that of a torus surrounding a ballon consisting of a front window and a rear reflector surface.

The concentrator contour also can be created by a partial vacuum. A 15.2 m (50 ft) diameter concentrator concept consisting of a tube-constructed, conical frustum, a thin film, aluminized polyester film, fabric bag and a pressure maintenance subsystem, was proposed at Marshall Space Flight Center (Ref. A-52). A 3.9 m (12.75 ft) diameter concept verification model has been constructed and tested.

Pressure stabilized concentrators have been shown to resist wind loads up to 5-6 m/s airspeed. A vacuum-type film-concentrator enclosed in a transparent bubble was proposed by Boeing to Sandia (Ref. A-53) to minimize the wind effect. A 2 m diameter proof-of-concept model is being constructed.

The concentrating capability of a pressure-stabilized concentrator is moderate because of the inaccuracy of the concave-film surface relative to a corresponding (perfect) paraboloid. The surface curvature is affected by many factors: the pressure difference, seam arrangements and gravity effect of its own mass. For small pressure differences the deflection depends linearly on the applied pressure and the shape of the deformed surface of a vacuum-shaped or an inflated concentrator, resembling a paraboloid. However, at large deflections the slope approaches that of a spherical segment, that would result in spherical aberration. The radial deformation at the edge of an existing concentrator was assessed to be approximately 20% greater than that at the center (Ref. A-54).

The mean concentration ratio of an experimental 2.7 m diameter, vacuum-film concentrator has been evaluated to be in the range of 400 to 600 (Ref. A-55). However, for larger concentrator sizes the film strips must be seamed together, and this affects the surface contour as well as optical transmission. Furthermore, the stiffness of the film surface decreases with the diameter, and thus the concave shape and the concentrating capability will probably be degraded as the diameter is increased.

8. Film-Faceted Concentrators

The film-faceted concentrator is a special case of faceted systems; in this case all the facets are made of inflated or vacuum films. A patented scheme for flat, stretched metalized film, under the influence of an electrostatic field to form a concave facet, has also been investigated (Ref. A-48). Circular, and hexagonal, vacuum-film facets have been made by stretching metalized film across a rigid frame with epoxy glue applied to the edge. Once the resin has cured, the facet may be removed from the frame and a concave surface can be maintained by partial evacuation. Concentrators with diameters ranging from 1.5 to 5 m have been constructed with 7 to 60 facets on paraboloidal frames made of steel angles and metal strip. The mean concentration ratio was assessed to be around 1700 to 2000 with maximum concentration ratio at the focal spot being 3000 to 3500 (Refs. A-56 and A-57). The major advantages of the film-facet approach are its light weight, that requires less stringent structural support, and low cost. The chief disadvantage is the durability of the facets. Polymer film may become brittle, loses its elasticity in a few years, and thus requires replacement.

9. Fresnel Reflectors

The Fresnel-type concentrator consists of a number of concentric reflecting elements which usually are sections of a paraboloid. These elements also may be spherical or conical, and the concentrator may be of monolithic form (Refs. A-58 and A-59), or faceted arrangements. The reflecting elements can be made of polished metal, sagged second-surface mirror, metalized film or foam plastics. Vacuum-film type Fresnel arrangements have been investigated as well.

The advantage of a Fresnel arrangement is its relative flatness, which facilitates less complicated structural support designs. However, for the same reason, it may suffer significant shading between reflecting elements unless very large focal lengths are utilized. For solar collector applications, a long focal length implies a more stringent requirement on the supporting structure for the receiver. Typical concentrator designs would have the f/D ratio limited to 0.6 or less.

C. CONCENTRATOR QUALITY

Concentrator quality is dictated by surface reflectance and geometrical accuracy. Surface reflectance characteristics have been well investigated, and their effect on solar concentrator performance is nearly linear. Geometrical accuracy of a concentrator depends upon the configuration, construction material, and tooling tolerance. Typically, the concentrator quality cannot be assessed until the surface error distribution is reasonably well determined; this requires at least partial fabrication of the hardware and initial, but accurate optical measurements. There are three types of conventional measurements used to determine the surface accuracy and concentrator quality: (1) slope error measurements, (2) focal plane flux mapping, and (3) calorimetric efficiency measurements.

1. Slope Error Measurements

Surface accuracy is the most direct and fundamental quantity that governs the optical transmission characteristics of a concentrator. Slope error, in linear or angular quantities, is the degree to which an individual surface element deviates from the ideal shape at the corresponding surface position. Slope error measurements have been performed either by contact or optical methods. Contact probe methods have been widely used in measuring the roughness of high-gain antenna surfaces. A hard-tipped probe, moving over the entire surface, can reproduce the surface irregularity in a profilograph. Most concentrator surface slope error measurements have been performed with optical methods, which rely on the fact that rays parallel to the optical axis of a paraboloid converge ideally to a small focal spot, and vice versa.

In the operation of an aberrograph (Ref. A-60), a narrow light beam from a collimating device is directed to pass through a prism and a pentaprism so that the ray follows a path parallel to the concentrator axis. The reflection from the surface produces a trace on the photographic plate at the focal plane. The record, which indicates the deviation from the ideal focal position, can be related to local surface error. A similar method is the modified Hartman test, which is a modification of a test developed by astronomers for evaluating telescope mirrors. Surface irregularities are detected by tracing the rays which strike the concentrator after passing through a perforated mask. The Hartman test of the 9.5-ft JPL/GE concentrator (Refs. A-61 and A-62) employed an opaque, perforated, aluminum screen that had 200 small holes. An individaul hole, or a group of holes, were uncovered successively to record the image patterns at the target. The para-axial ray intercept-points at the focal plane were established by the intersection of the major and minor elliptical axes. The local surface slope error can be determined analytically with an appropriate geometrical relationship. In addition to the local slope error distribution, the test data can be evaluated to establish the so called "Hartman factor", or "geometrical efficiency", which is the interception factor at a specified aperture size.

A different type of optical instrument developed at NASA Lewis Research Center (Ref. A-63) employs the reciprocal principle. A small xenon arc lamp is placed at the focus to approximate a point-light source. Reflected rays would be parallel to the concentrator axis if the surface were ideal. The viewing instrument is a telescope, focused at infinity with its optical axis aligned parallel to the concentrator axis. The position of the center of the image with respect to the telescope cross-hair can be calibrated in terms of local surface slope error and can be displayed to indicate both the tangential and radial components. The instrument can be used for concentrators with diameters ranging up to 6.1 m (20 ft).

Recent development in laser ray tracing technology enables faster and more accurate scanning of concentrator surface (Refs. A-64, A-65, and A-66). Laser scanning systems used both in laboratory and field situations have been developed.

The surface slope error characteristic is the most significant factor that governs the optical performance of a concentrator. Measurement data typically are presented in the form of histograms such as the one shown in Figure A-8 (Ref. A-67). Best-fit normal distributions are used to approximate the histograms.

2. Flux Mapping

In practice, it is difficult and expensive to obtain slope error information for large-diameter concentrators. This is due to difficulty in accurately aligning the measurement instrument with the concentrator axis. An alternative method for characterizing the surface accuracy is to measure the solar flux distribution near the focal plane. Qualitative flux mapping may employ photographic or transient calorimetric techniques (Ref. A-68). Accurate flux mapping relies on radiometric or photometric methods. Radiometric methods are based on the thermal-emf response of a sensor. Usually, light filters and other devices are required to attenuate the flux intensity at the focal plane. Photometric methods are based on the response of photo cells (Refs. A-22 and A-69) or photomultipliers. Fiberoptic microphotometers (as small as 10 to 15μ in diameter) have been used to limit the probe aperture. Scanning of the flux distribution at the focal plane is usually performed with very short camera exposure.

Current JPL activity in flux mapping involves a photometric flux scanner. Intensity values up to 10,000 times the nominal solar irradiance (around 1 kW/cm^2) can be measured with the device. P.I.N. Diodes or thermoelectric sensors are placed at the end of a probe connector (Figure A-9). Typical scanning periods are around 5 seconds (Ref. A-70).

Accurate flux mapping can be computed from a detailed surface error distribution. On the other hand, a measured flux distribution provides only integrated surface accuracy information, and does not contain sufficient detail to reconstruct the slope error distribution. If the slope error distribution truly is a random Gaussian function, then there exists a one-to-one correlation between the flux distribution and the slope error standard deviation, σ_s.

Figures A-10 and A-11 display the flux distributions on planes parallel to the focal plane that were calculated for a concentrator composed of spherical facets in trapezoidal shape. The diameter of the concentrator is 11 m; the f/D ratio of the paraboloidal substructure, as well as the composite concentrator, is 0.6. A single radius of curvature of 612 in. is being considered for all faceted spherical mirrors. Two levels of slope errors were considered in the flux distribution computation, namely, σ_s = 1 mrad and σ_s = 2 mrad.

3. Calorimetric Measurements

The major drawback of a flux mapping measurement is that the numerical data are relative, not absolute, and the sensor may have different sensitivities at different wavelengths and different intensities. The thermal performance assessment of an existing

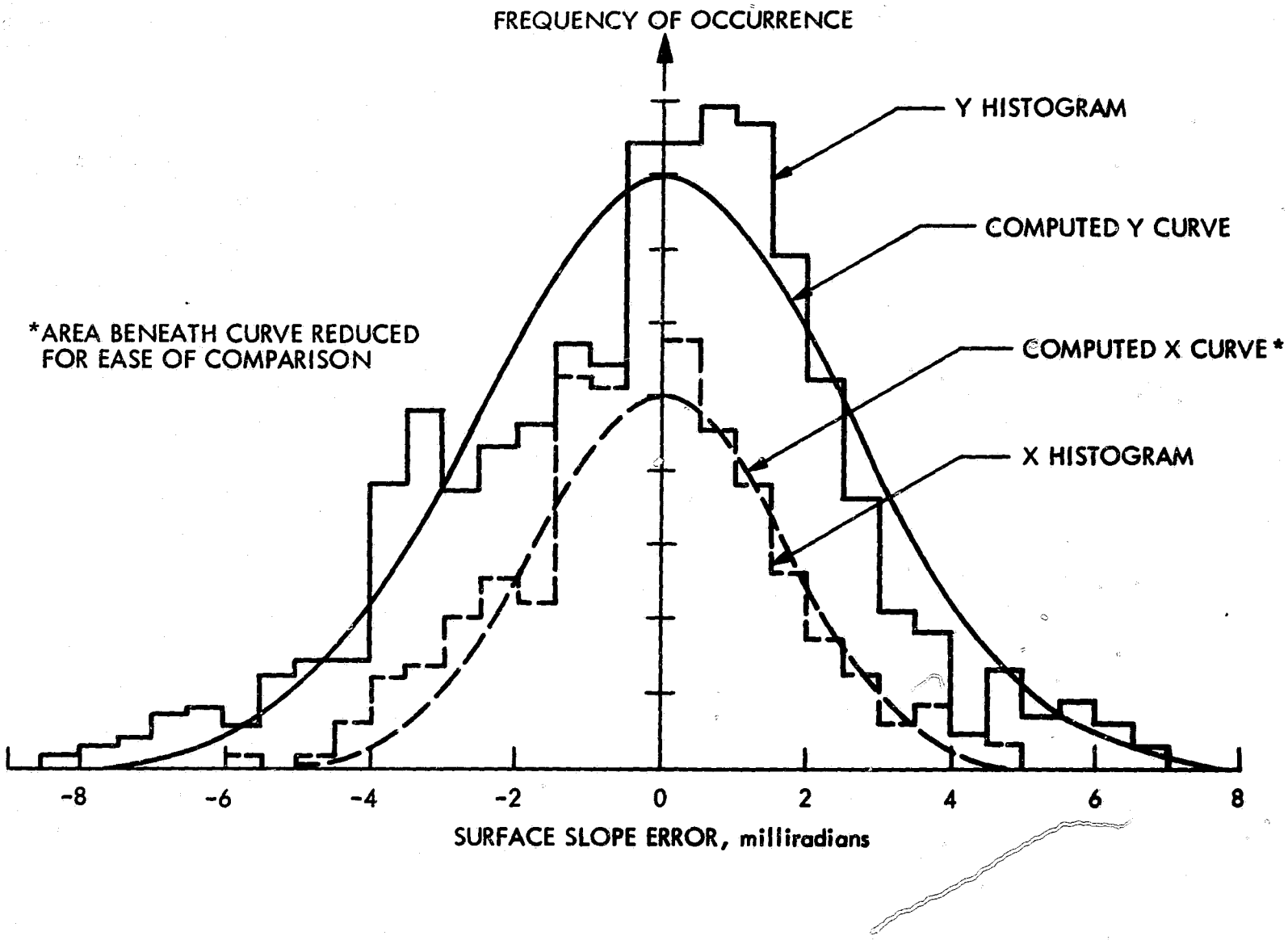

Figure A-8. Representative Slope Error Histograms

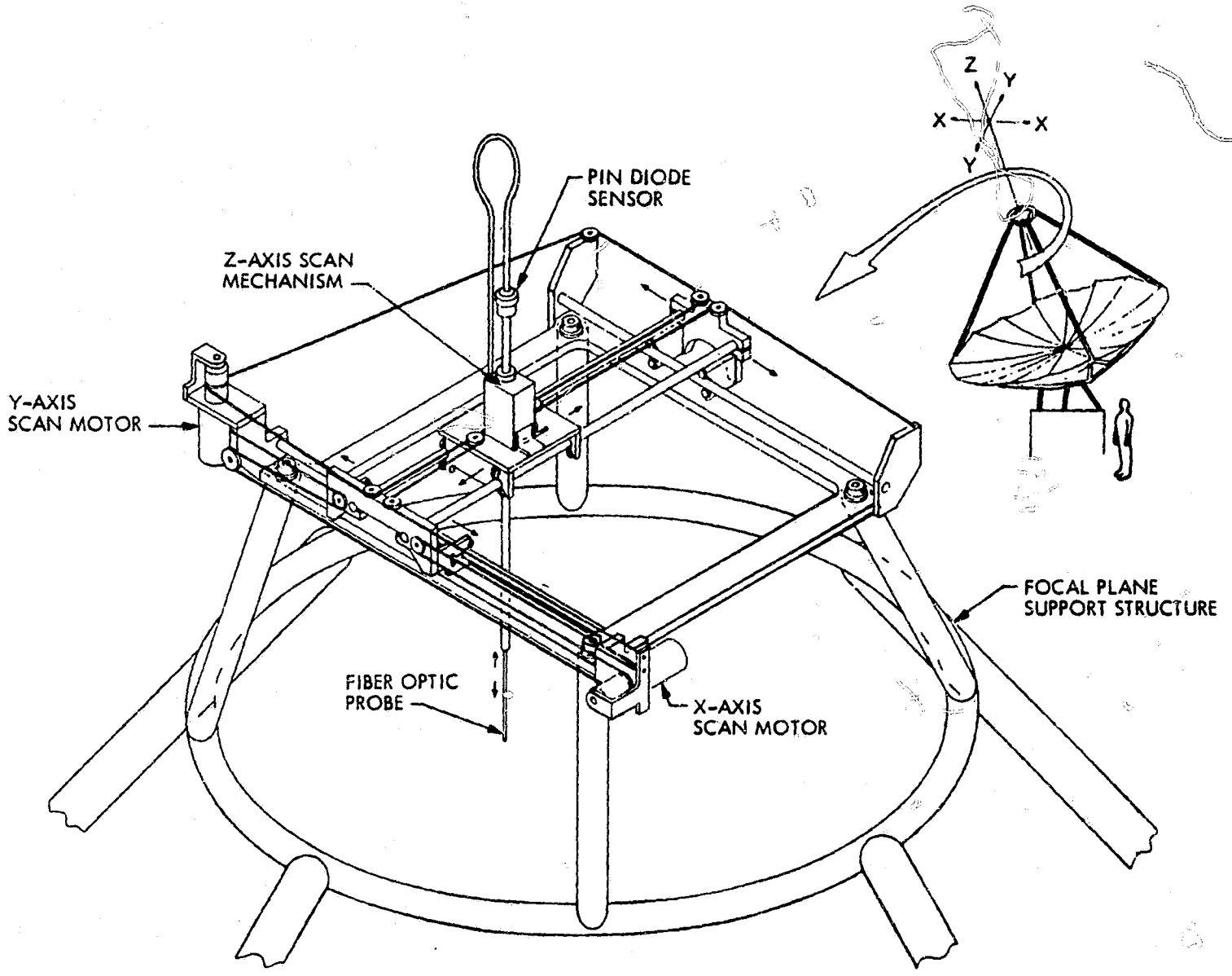

Figure A-9. JPL Solar Flux Mapper

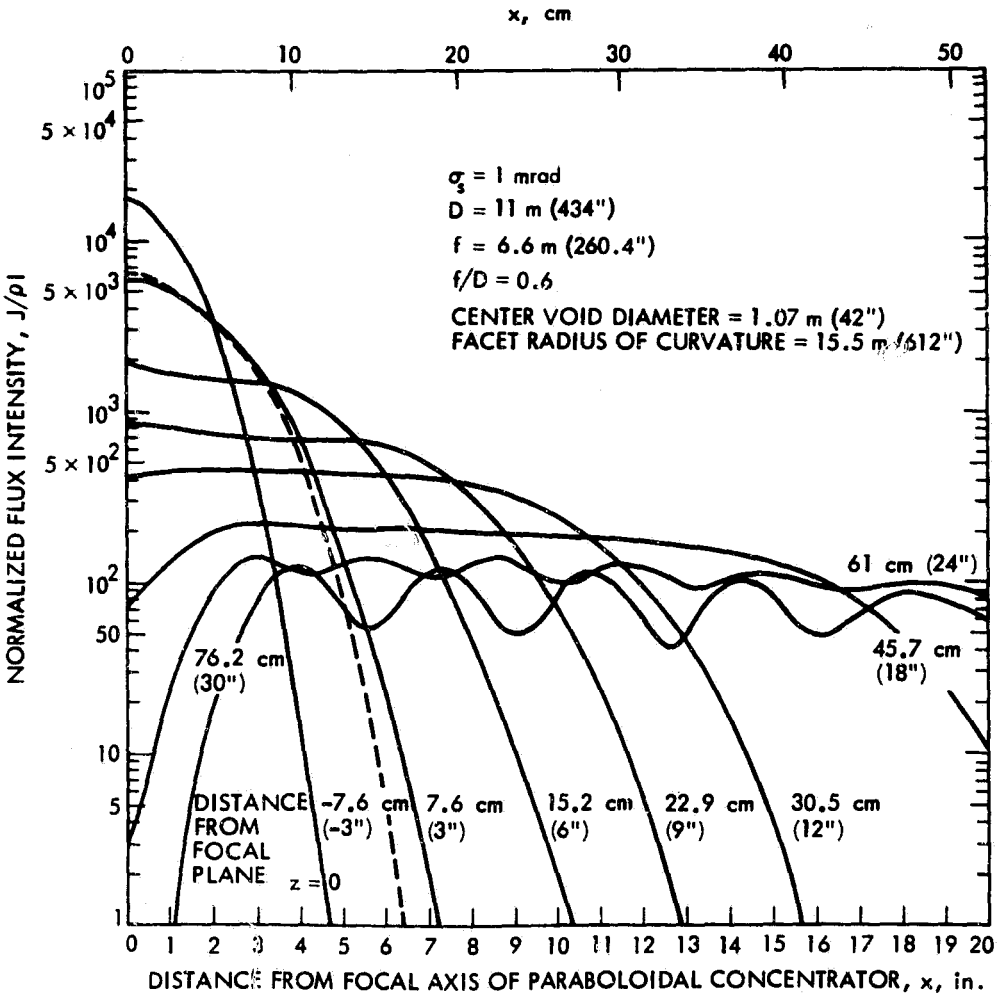

Figure A-10. Representative Flux Mapping with 1 mrad Slope Error

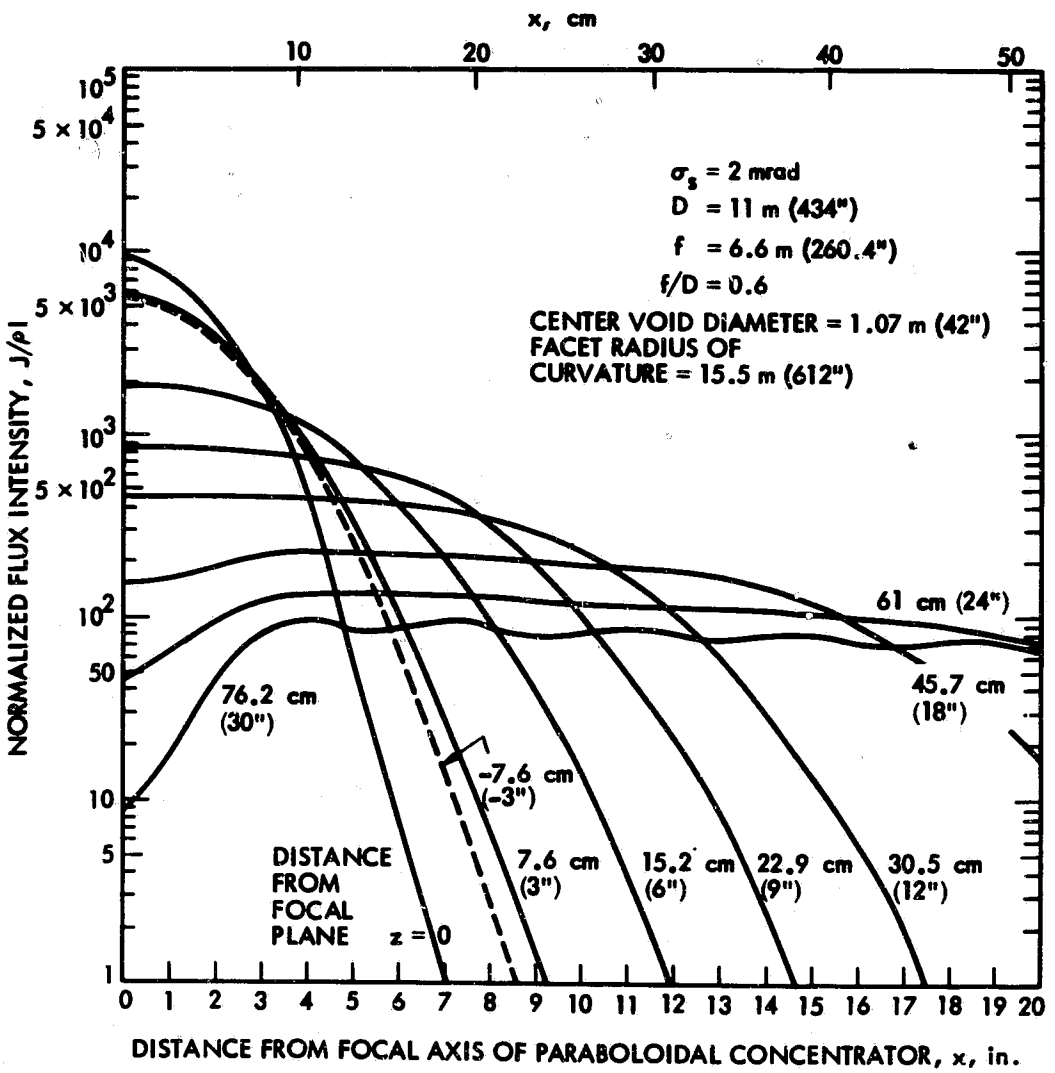

Figure A-11. Representative Flux Mapping with 2 mrad Slope Error

concentrator is accomplished best by calorimetric measurements. The calorimeter may be equipped with apertures of different sizes (e.g., interchangeable orifice plates, with apertures of various diameters: then the calorimetric results can be correlated with the flux mapping data. Different types of calorimeters for solar investigations have been constructed (Ref. A-71); basically, they resemble the shape of a cavity receiver. The cavity wall is surrounded by tubes to convey coolant water flow during a test. Test data are obtained by simultaneous recordings of fluid flow rates and the temperature rise in the fluid. Flow rate is adjusted so that the water temperature rise is sufficiently small and radiative (aperture) heat loss to ambient is negligible. The orifice plates are water cooled to prevent heat radiation internally to the cavity. "Universal Calorimeters" are designed to have a diaphragm with multiple apertures on a common water cooled disc. Turning the disc about its axis would yield different orifice plate openings without interrupting the experiment.

A typical series of calorimetric tests consists of measurements for various aperture diameters. Calorimetric efficiency, which is defined as the ratio of the energy collected, by a cavity-type cold-wall calorimeter, to the total energy incident in the concentrator, can then be established as a function of the aperture diameter. Many of the published data are presented in terms of the so-called "Concentration Ratio", which is the ratio of the net projected reflector area of the concentrator to the area of the calorimeter aperture. Figure A-12 shows the performance of various concentrator models constructed in the 1960s. The data are based on those published in References A-72 and A-73. It can be seen that large variations existed in surface reflectance, as well as in the geometrical accuracy of the different concepts.

It should be pointed out that the energy balance relationship is similar to that of a solar receiver, see Eq. 2.1, except that the heat loss from a cold wall calorimeter is negligible. The energy equation would take the following form:

$$Q_c = \rho I A_c G \Phi \alpha_{eff} \qquad (A.3)$$

the calorimetric efficiency would be

$$\zeta_{cal} = Q_c / A_c I = \rho G \Phi \alpha_{eff} \qquad (A.4)$$

There is a constant relationship between the calorimetric efficiency, ζ_{cal} and the interception factor; in fact, the interception factor, Φ, can be viewed as a normalized calorimetric efficiency. Figure A-13 shows the variation of interception factor as a function of receiver aperture size; note estimates for the Omnium-G module. The same relationship is presented in Figure A-14, (solid curves) in terms of the concentration ratio, $CR = (D/2R)^2$; calorimetric efficiency data (shown in Figure A-12) were normalized and presented for comparison.

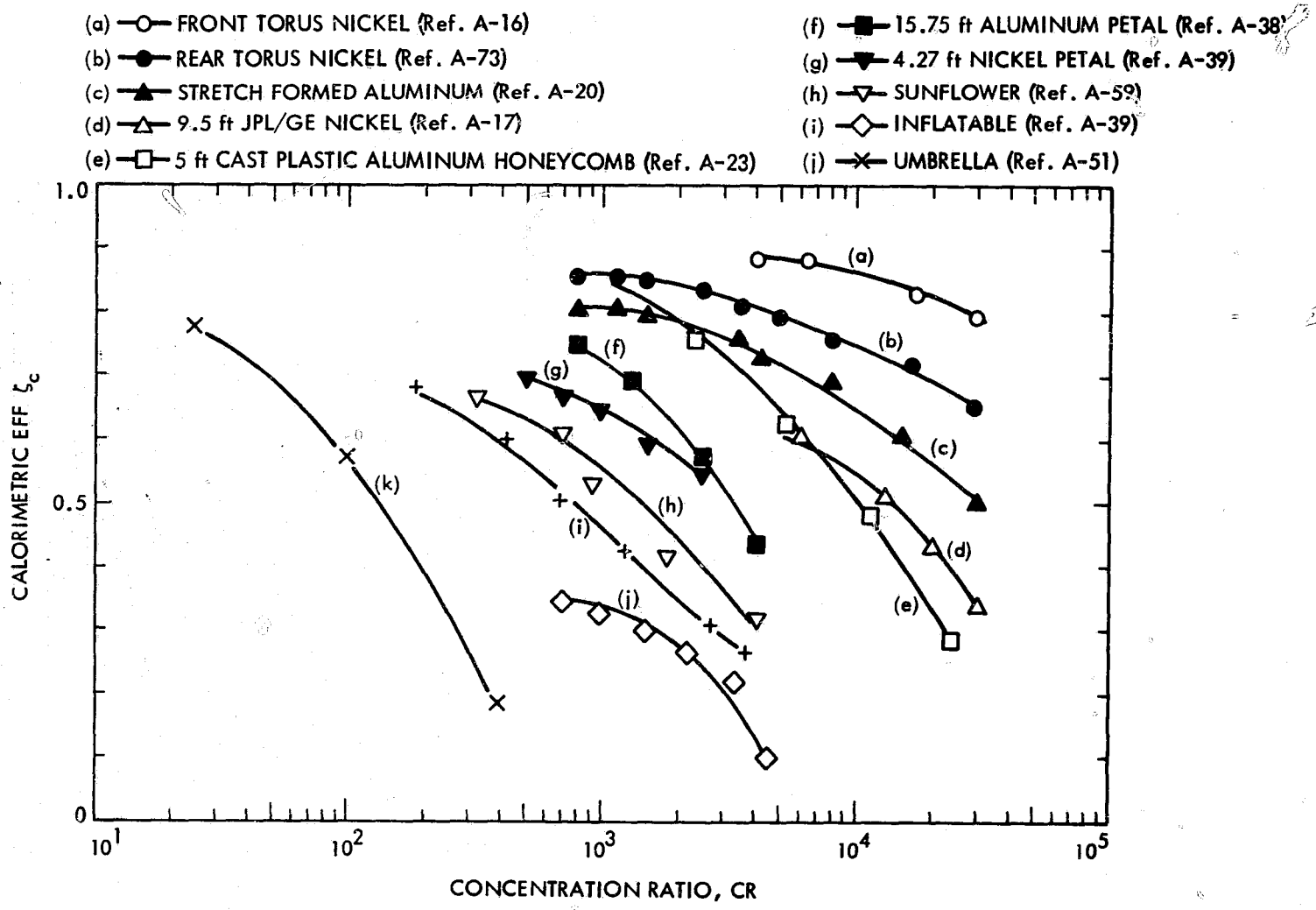

Figure A-12. Experimental Calorimetric Efficiency Data for Various Existing Concentrators

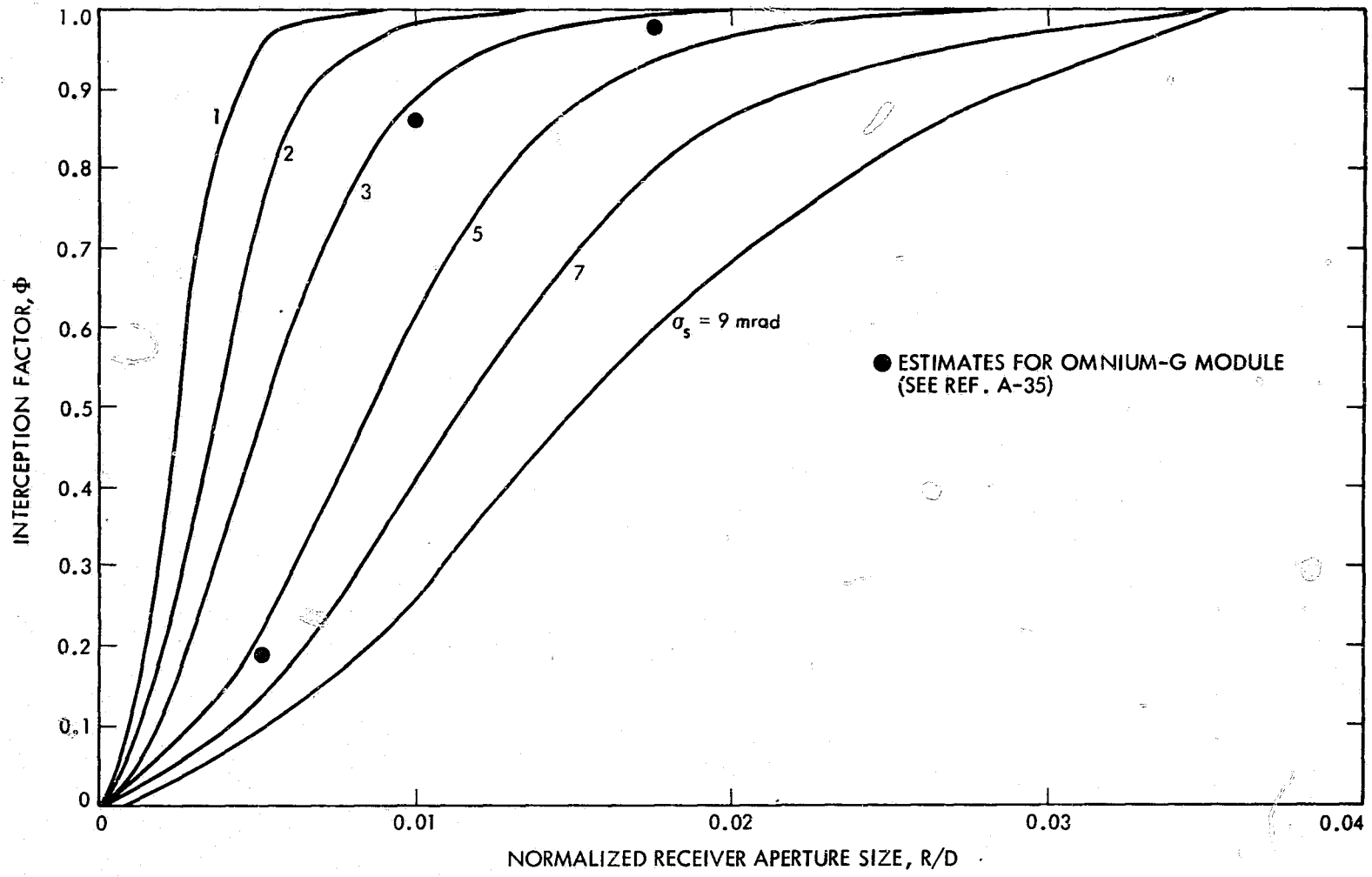

Figure A-13. Theoretical Interception Factor versus Receiver Aperture Size

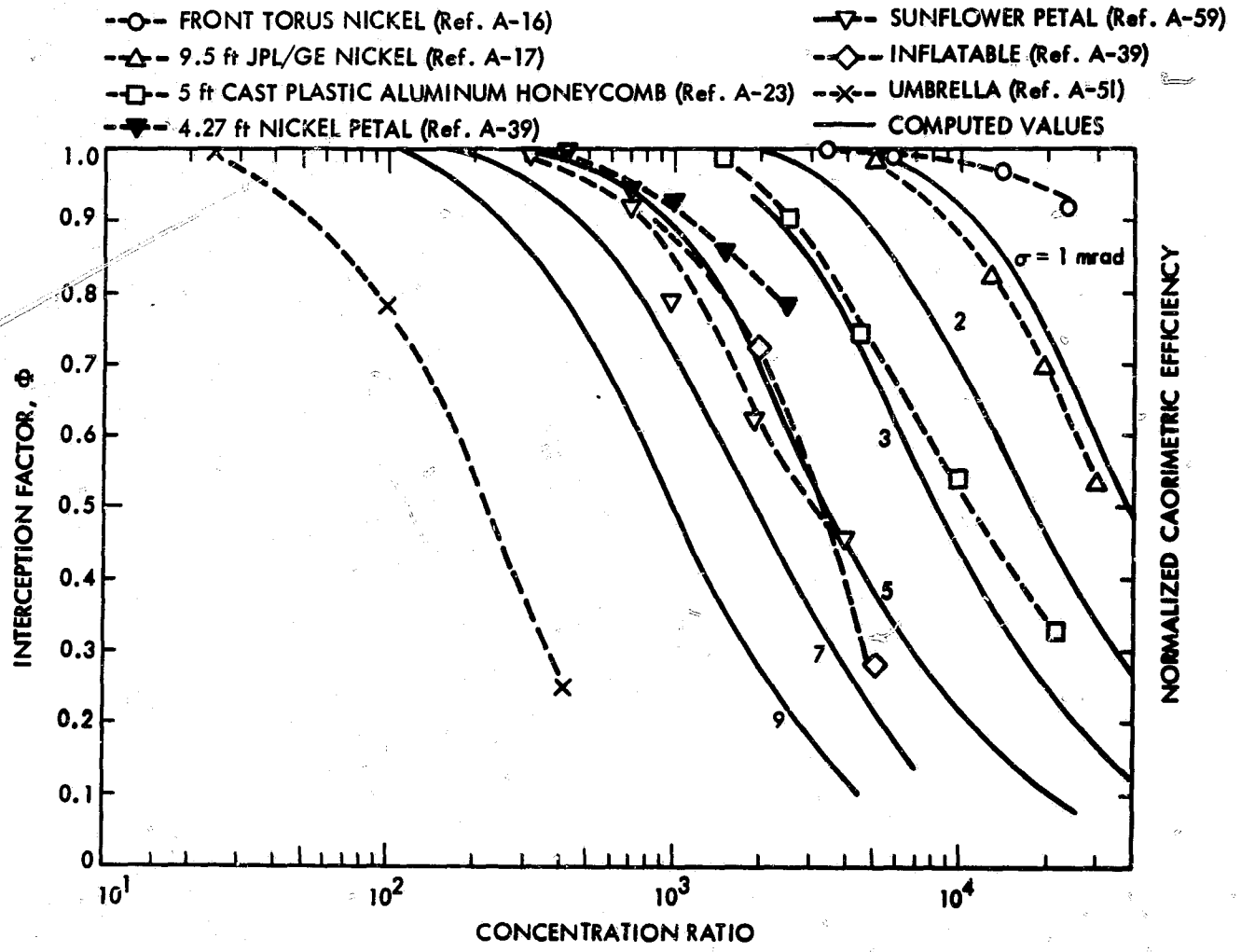

Figure A-14. Enterception Factor versus Concentration Ratio, Theoretical Prediction and Experimental Results for Various Models

The monolithic electro-formed nickel concentrators (Ref. A-17) had a surface slope error less than 1 mrad. The stretch-formed aluminum 1.5 m (5 ft) diameter concentrator (Ref. A-20) had lower surface reflectance and less accurate geometry, corresponding to a slope error σ_s around 1 to 1.5 mrad. The 9.5 ft JPL/GE electro-formed nickel concentrator (Ref. A-17), currently at Table Mountain, Calif., had a low surface reflectance because the master had a slightly etched surface. The annular area near the rim was found to have a shorter focal length than the remainder of the concentrator. The corresponding slope error also was in the range of 1 to 1.5 mrad. The cast-plastic aluminum honeycomb model constructed at Boeing (Ref. A-23) was not as good as that of the electro-formed concentrators. The corresponding slope error was around 2.5 mrad. The three petal type concentrators built in the 1960s had performance characteristics in the same general range. The 15.75 ft diameter aluminum honeycomb petal-model (Ref. A-38) and the 4.27-m diameter electro-formed nickel petal concentrator (Ref. A-39) had very similar surface accuracy. The calorimetric data for the 32.2 ft diameter "Sunflower" concentrator was for just a single petal, and did not include the alignment errors. All three petal-type concentrators are in the 3.5 to 5 mrad slope error range. It is interesting to observe that the estimated Omnium-G interception factor relationship (Figure A-13) also indicates that the effective surface slope error* is between 3 mrad and 5 mrad.

The inflatable rigidized 10 ft model (Ref. A-48) and Fresnel concentrator had about the same calorimetric efficiency. The 4.72 ft diameter inflatable paraboloidal concentrator (Ref. A-39) had relatively low performance because of front-surface transmission/reflectance loss, as well as poor surface accuracy. The concentrating ability of the umbrella-type concentrator (Ref. A-5) was quite poor, due mainly to the poor accuracy of the surface gores between ribs. The corresponding effective surface slope error would be greater than 10 mrad.

---

*Twenty percent of the concentrated solar image was within a 3-cm diameter circle (core), 87% was within a 6-cm circle, and 97% was within a 10-cm circle (Ref. A-35).

APPENDIX A

REFERENCES

A-1. Butler, B. L., and Pettit, R. B., "Optical Evaluation Techniques for Reflecting Solar Concentrators," SAND 77-1356, paper presented at Society of Photo-Optical Instrumentation Engineering 21st International Symposium, San Diego, California, Aug. 22-26, 1977.

A-2. Pettit, R. B., "Characterization of the Reflected Beam Profile of Solar Mirror Materials," Journal of Solar Energy, Vol. 19, pp. 733-741, Dec. 1977.

A-3. Truscello, V. C., "The Parabolic Concentrating Collector," paper presented at the Solar Thermal Concentrating Collector Technology Symposium, Denver, Colorado, June 14 and 15, 1978, JPL Publication No. 79-7, Jet Propulsion Laboratory, Pasadena, Calif., February 1979.

A-4. Hughes, R. O., "Effects of Pointing Errors on Receiver Performance for Parabolic Dish Concentrators," Paper No. 789264, IECEC Conference, San Diego, California, Aug. 20-25, 1978.

A-5. Wen, L., "Thermal Optical Surface Properties and High Temperature Solar Conversion," AIAA Paper 78-903, 2nd AIAA/ASME Thermophysics and Heat Transfer Conference, Palc Alto, May 24-26, 1978.

A-6. Schrenk, G. L., "Final Report, Analysis of Solar Reflectors - Mathematical Theory and Methodology for Simulation of Real Reflectors," EDR 3693, General Motors Corporation, Allison Division, Dec. 1963.

A-7. Schrenk, G. L., "The Role of Simulation in the Development of Solar Thermal Energy Conversion Systems," Preceedings of the 11th IECEC Conference, Vol. II, pp. 1256-1263, Sept. 1976.

A-8. Cosby, R. M., "Solar Concentrator by Curved Based Fresnel Lenses," Preceedings of ERDA Conference on Concentrating Solar Collectors, p. 2-61, Georgia Institute of Technology, Atlanta, Georgia, Sept. 26-28, 1977.

A-9. Hastings, L. J., and Allums, S. L., "Performance Characteristics of a 1.8 by 3.8 meter Fresnel Lens Solar Concentrator," Preceedings of ERDA Conference on Concentrating Solar Collectors, Georgia Institute of Technology, Atlanta, Georgia, Sept. 26-28, 1977.

A-10. Umarov, G. Ya,. Alimov, A. K., and Alavutdinov, Dzh N., "A Cassegrainian System for Solar Radiation," Geliotekhnika, Vol. 12, No. 2, pp. 68-69, 1976.

A-11. Zakhidov, R. A., and Vainer, A. A. "Paraboloid-Hyperboloid Concentrating Systems and Their Accuracy," Geliotekhnika, Vol. 13, No. 1, pp. 42-49, 1977.

A-12. Baranov, R., "Method for Calculating the Profiles of Focones and Foclines," Gelioteckhnika, Vol. 12, No. 6, pp. 24-28, 1976.

A-13. Perkins, G. S., "A Low Cost High Temperature Sun Tracking Solar Energy Collector," 11th Aerospace Mechanism Symposium, Greenbelt, Maryland, April 1977.

A-14. Steward, F. W., and Kreith, F., "Stationary Concentrating Reflector Cum Tracking Absorber Solar Energy Collector," Applied Optics, Vol. 14, No. 7, pp. 1509-1512, 1975.

A-15. Nibiullin, F., Sladkov, M. S., et al., "Manufacture of Parabolic Concentrators by the Electro-formed Replica Method," Geliotekhnika, Vol. 2, No. 3, pp. 28-33, 1966.

A-16. Menetrey, W. R., "Solar Energy Thermionic Conversion Systems," Final Rept. No. 1850, Electro-Optical Systems Inc., Jan. 1962.

A-17. Guy, J. J., et al., "9-1/2 Foot Diameter Master and Mirror," Final Report No. 64 SD 340, General Electric, March 1964.

A-18. Schmidt, F. J., and Hess, I. J., "Forming Aluminum for Solar Energy Concentrators," NASA CR 56022, General Electric, April 1964.

A-19. Ferrara, J. R., "A Solar Thermoelectric Generator System Study," Aeronautics Systems Div, U. S. Air Force, TR 61-315, Nov. 1961.

A-20. "60-Inch Stretch-Formed Aluminum Solar Concentrator," TRW NASA CR-47, June 1964.

A-21. Umarov, G. Ya., et al., "Rotation Method of Manufacturing Paraboloidal Collectors," Geliotekhnika, Vol. 2, No. 6, pp. 53-55, 1966.

A-22. Bazarov, B. A., Kapelyushnikov, U. M., and Kalinin, B. A., "Investigating the Geometric Quality of Cast Polyurethane Foam Duplicates for Solar Energy Concentrators," Geliotekhnika, Vol. 14, No. 2, pp. 25-29, 1976.

A-23. Steele, H. L., Gillette, R., and Snyder, H. E., "Development and Testing of Light Weight Solar Concentrators," D2-10107, Boeing Airplane Company, 1961. Also: Steele, H. L., "Results of Tests on 5 Foot Diameter Light Weight Concentrators," Proceedings of Round Table Discussion, Interagency Advanced Power Group, 1961.

A-24. Castle, C. H., "Solar Concentrator Development Status at TRW," Technical Memo 3345-68, TRW Inc., TAPCO Div., Feb. 1962.

A-25. Grilikhes, V. A., "New Methods of Manufacturing Solar Concentrators," Geliotekhnika, Vol. 4, No. 3, pp. 44-53, 1968.

A-26. Umarov, G. Ya, "Problems of Solar Energy Concentration," Geloitekhnika, Vol. 3, No. 5, pp. 32-51, 1967.

A-27. Walton, J. D., "International Developments in Concentrators," presented at the Solar Thermal Concentrating Collector Technology Symposium, Denver, Colorado, June 14-15, 1978.

A-28. Vladimirova, L. N. and Garf, B. A., "The Optico-Mechanical Part of the SV-1 Solar Water-Raising Unit," Geliotekhnika, Vol. 2, No. 2, pp. 45-49, 1966.

A-29. Solar Total Energy System Preliminary Design Review, No. 2, Solar Total Energy -- Large Scale Experiment at Shenadoah, Georgia, Sandia Lab., Albuquerque, May 1 and 2, 1978.

A-30. Poche, A. J., Han, S. A., and Hanke, R. W., "Preliminary Design of the Solar Total Energy -- Large Scale Experiment at Shenandoah, Georgia," Proceedings of the 13th IECEC, pp. 1508-1513, San Diego, CA, Vol. 11, Aug. 20-25, 1978.

A-31. Levine, A. L., Raradis, L. R., and Truesdale, K. L., "Parabolic Collector for Total Energy System Applications," Proceedings of the ERDA Conference on Concentrating Solar Collectors, pp. 4-33, Georgia Institute of Technology, Atlanta, Georgia, Sept. 26-28, 1977.

A-32. Alimov, A. K., Alavutdinov, J. N., and Abduazizov, A., "Properties of a Solar Concentrator with Hexagonal Glass Facets," Geliotekhnika, Vol. 11, No. 3/4, pp. 20-22, 1975.

A-33. Alimov, A. K., Alavutdinov, Dzh. N., and Abdurakhmanou, A., "Energy Concentrator Assembled from Circular Glass Facets," Geliotekhnika, Vol. 9, No. 5, pp. 58-60, 1973.

A-34. Zakhidov, R. A. and Khodzhaev, A. Sh., "Concentrating Capability of Spherical Facet," Geliotekhnika, Vol. 12, No. 6, pp. 35-37, 1976.

A-35. Roschke, J., "Addendum to Pending JPL Purchase of Omnium-G System Module," Internal Interoffice Memo 341-78-1017, Jet Propulsion Laboratory, Pasadena, Calif., June 26, 1978.

A-36. Castle, C. H., "Solar Concentrator Development Status at TRW," Technical Memo 3345-68, TRW, Inc., TAPCO Div., Feb. 1962.

A-37. Kovalcik, E. S., et al., "Sunflower Solar Collector," NASA-CR-46, TRW, Inc., May 1964.

A-38. Cuthbert, D. J., et al., "Solar Thermionic Electrical Power System," Technical Document Report ASD-TDR-62-94, U. S. Air Force, March 1962.

A-39. Springer, L. M., "Study, Design and Fabrication of Solar Energy Concentrator Models," EOS Rept. 1577-Final, Electro-Optical System, Inc., Sept. 1961.

A-40. Sandborn, D. S., "The Development of Deployable Solar Concentrators for Space Power," SAE paper 425D, Ryan Aerospace, 1961.

A-41. Peterson, R. C., and Evans, R. A., "Modular Electrical Generation Using Parabolic Dish Solar Concentrator," Proceedings of the ERDA Conference on Concentrating Solar Collectors, p. 4-1, Georgia Institute of Technology, Atlanta, Georgia, Sept. 26-28, 1977.

A-42. Umarov, G. Ya., and Zakhidov, R. A., "Development of Solar Engineering in Uzbekistan," Geliotekhnika, Vol. 8, No. 6, pp. 9-15, 1972.

A-43. Umarov, G. Ya., et al., "Long Focal Length Concentrator made from Wedge-Shape Window Glass Element," Geliotekhnika, Vol. 10, No. 4, pp. 20-22, 1974.

A-44. Umarov, G. A. and Abduazizov, A., "Asbesto-Cement Film Concentrator Fabrication Technology," Geliotekhnika, Vol. 4, No. 4, pp. 56-57, 1968.

A-45. Umarov, G. Ya., et al., "Fabricating Paraboloidal High Temperature Solar Concentrators from Mollified Sectors," Geliotekhnika, Vol. 10, No. 6, pp. 31-36, 1974.

A-46. Nowlin, W. D., and Bensor, H. E., "Study of an Erectable Paraboloidal Solar Concentrator for Generation of Spacecraft Auxiliary Power," NASA TN D-1368, 1962.

A-47. Henderson, R. F., and Dresser, D. L., "Solar Concentration Associated with the Stirling Engine," Paper No. 1312-60, American Rocket Society (ARS) Space Power System Conference, Santa Monica, Calif., Sept. 1960.

A-48. Lyman, R., and Houmard, J. E., "Inflatable Foam Rigidized Approach to Solar Concentrators," presented at the ARS Space Power System Conference, Santa Monica, Calif., Sept. 25-28, 1962.

A-49. McCusker, T. J., "Solar Concentrator Design and Construction," AIAA paper 64-733, also, pp. 687-700, Space Power System Engineering, Edited by G. C. Szego and J. E. Taylor, Progress in Astronautics and Aeronautics, Vol. 16, Academic Press, 1966.

A-50. Schwartz, S., "Rigidized Inflatable Solar Energy Concentrator," Hughes Aircraft Corp., NASA CR-56457, May 1964.

A-51. Nowlin, W. D., and Bensor, H. E., "Study of an Erectable Paraboloidal Solar Concentrator for Generation of Spacecraft Auxiliary Power," NASA TN D-1368, 1962.

A-52. Brantley, L. W., "Pressure Stabilized Solar Collector (PSSC)," Proceedings of the ERDA Conference on Concentrating Solar Collectors, Georgia Institute of Technology, Atlanta, Georgia, Sept. 26-28, 1977.

A-53. Plastic Parabolic Concentrator Feasibility Study, Sandia Lab.-Albuquerque Contract 05-4467, 1978.

A-54. Umarov, G. Ya, Zhadraev, U. Zh., Dzhalalov, Z., "Investigation of the Deformation Field of Film Concentrators under Air Pressure," Geliotekhnika, Vol. 3, No. 4, pp. 71-76, 1967.

A-55. Umarov, G. Ya, and Gafurov, A. M., "Test Results for Suction Type Film Concentrator," Geliotekhnika, Vol. 5, No. 2, pp. 70-72, 1969.

A-56. Umarov, G. Ya, Alimov, A. K., et al., "Study of Circular and Hexagonal Vacuum Film Facets for Solar Concentrators," Geliotekhnika, Vol. 3, No. 1, pp. 17-20, 1967.

A-57. Alavutdinov, Dzh N., Alimov, A. K., and Umarov, G. Ya, "Investigation of Solar Concentrators Composed on Doubly Curved Facets," Geliotekhnika, Vol. 3, No. 3, pp. 20-23, 1967.

A-58. Tyler, R. D., and McClure, R. B., "Material and Construction Techniques for Space Solar Reflectors," p. 713-732, Power Systems for Space Flight, Edited by M. A. Zipkin and R. N. Edwards, Progress in Astronautics and Aeronautics, Vol. 11, Academic Press, 1963.

A-59. "Experimental Reflector Orbital Shot (EROS)," Technical Report -TDR-63-266, Vol. I, Part 1, Aeronautics System Div., U.S. Air Force, April 1963.

A-60. Tveryanovich, E. V., and Madaev, V. V., "Tests on Paraboloidal Concentrator Using the Leonov Aberrograph," Geliotekhnika, Vol. 10, No. 3, pp. 28-33, 1974.

A-61. Blake, F. A., "Solar Performance Evaluation Test Program of the 9.5 ft Diameter Electroformed Nickel Concentrator S/N1 at Table Mountain, Calif.," NASA TM33-206, Jet Propulsion Laboratory, Pasadena, Calif., June 15, 1967.

A-62. Rouklove, P., "Solar Energy Thermionic Electrical Power Supply Development," JPL Space Programs Summary No. 37-26, Vol. IV, pp. 31-39, Jet Propulsion Laboratory, Pasadena, Calif., 1966.

A-63. Cameron, H. M., private communication, NASA Lewis Research Center, Cleveland, Ohio, 1978.

A-64. Zentner, R. C., "Performance of Low Cost Solar Reflectors for Transferring Sunlight to a Distance Collector," Journal of Solar Energy, Vol. 19, pp. 15-21, 1977.

A-65. Pettit, R. B., and Butler, B. L., "Laser Ray Trace and Bi-directional Reflectometry Measurements of Various Solar Concentrators," paper 6.5, Proceedings of ERDA Conference on Concentrating Solar Collector, Georgia Institute of Technology, Atlanta, Georgia, Sept. 26-28, 1977.

A-66. Orear, L., "Sensitivity of Slope Measurements on Parabolic Solar Mirrors to Positioning and Alignment of the Laser Scanner," SAND 78-0700, Sandia Lab.-Albuquerque, May 1978.

A-67. Castle, C. H., and Kovalcik, E. S., "Development Status of Aluminum Solar Concentrators," AIAA paper 64-731, also, pp. 821-847, Space Power System Engineering, Edited by G. C. Szego and J. E. Taylor, Academic Press, 1966.

A-68. Grilikhes, V. A., "Methods for Monitoring the Quality of Reflecting Surface of Solar Energy Concentrators," Geliotekhnika, Vol. 8, No. 4, pp. 3-15, 1972.

A-69. Veinberg, V. B., Konaeva, G. Ya, and Stattarov, D. K., "Measurement of the Distribution of Light at the Focal Point of Solar Energy Collectors," Geliotekhnika, Vol. 1, No. 2, pp. 9-14, 1965.

A-70. Berdahl, M., private communication, Jet Propulsion Laboratory, Pasadena, Calif., 1978.

A-71. Aparisi, R. R., Kolos, Ya G., and Teplyakov, D. I., "Calorimetric Investigation of High Temperature Solar Device," Geliotekhnika, Vol. 1, No. 6, pp. 25-31, 1966.

A-72. Heath, A. R., "Status of Solar Energy Collector Technology," pp 655-668, "Power Systems for Space Flight," Edited by M. A. Zipkin and R. N. Edwards, Progress in Astronautics and Aeronautics, Vol. 11, Academic Press, 1963.

A-73. Heath, A. R., and Hoffman, E. L., "NASA Solar Concentrator Development," AIAA paper 64-730, also in pp 897-908, "Space Power Systems Engineering," Edited by G. C. Szego and J. E. Taylor, Progress in Astronautics and Aeronautics, Vol. 16, Academic Press, 1966.

APPENDIX B

RECEIVERS

The function of a receiver is to capture solar energy reflected from the concentrator and to transfer it to a working fluid at the state conditions required by the power conversion unit. Basically, the receiver is merely a heat exchanger. Solar receivers fall into two categories: (1) the exposed-tube (or external) type, and (2) the cavity type. Exposed-tube designs usually are associated with special types of collector systems such as the Crosbyton/PERICLE concept, where the concentrator is stationary, or with a stationary receiver design. For two-axis, tracking point-focusing concentrators with receivers mounted near the concentrator focal plane, the exposed-tube receiver designs were considered to have significantly poorer thermal performance in comparison to a cavity type (Ref. B-1). In the present study, only the cavity-type receiver is considered. The general configuration of a cylindrical cavity receiver is shown in Figure B-1, and consists of an orifice plate (which forms the aperture), the cavity body/supporting structure, an absorber/heat exchanger, and appropriate insulation.

A. CAVITY RADIATIVE CHARACTERISTICS

Thermal radiation in an enclosure is strongly affected by the temperature level and distribution, the surface optical properties, and the geometrical configuration. Accurate heat transfer analysis is complex due to multiple specular reflections and non-uniform thermal emission. Ideal cavities are isothermal but this condition is achieved rarely in practice. However, many approximate approaches have been developed, and reasonably accurate heat transfer assessments can be obtained for most practical situations. Conventionally, cavity radiative characteristics are expressed in terms of "apparent" or "effective" emittance, ϵ_{eff}, and absorptance, α_{eff}. The effective emittance is defined as the ratio of radiative efflux from the aperture at the effective temperature, to the rate of emission by a black body at the same temperature. The effective absorptance is defined as the ratio of absorption of radiant energy in the cavity to the rate of incoming radiant energy. A closed-form expression by Gouffe (Ref. B-2), shown in Equations B.1 and B.2 has been used as the basis of a shallow-hole method for measuring the emittance of non-metals at high temperature.

$$\epsilon_{eff} = \frac{\epsilon_s \; 1 + (1 - \epsilon_s)\left(\frac{A_o}{A_w} - f_g\right)}{\epsilon_s \left(1 - \frac{A_o}{A_w}\right) + \frac{A_o}{A_w}} \qquad \text{(B.1)}$$

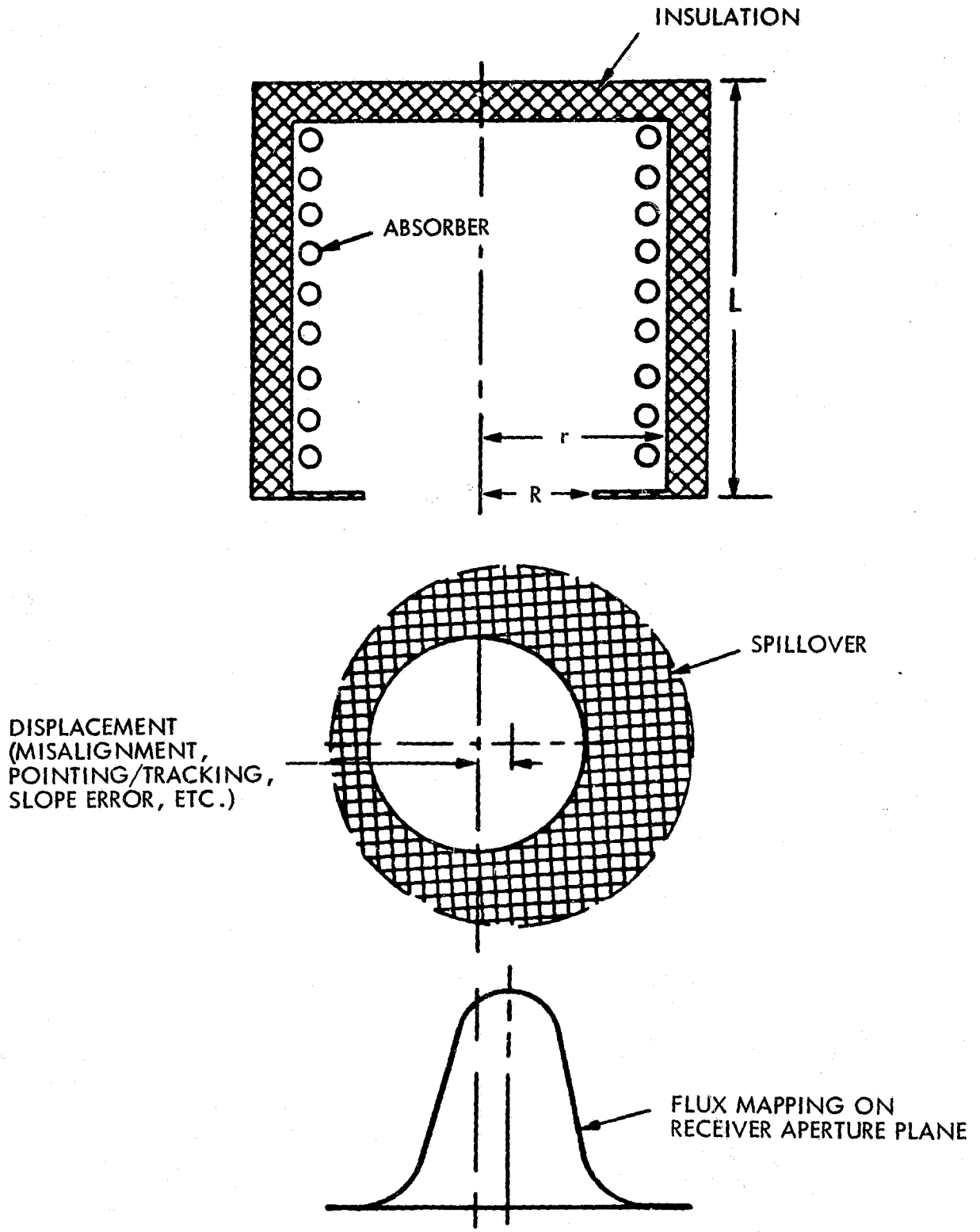

Figure B-1. Representative Cylindrical Cavity Receiver

$$\alpha_{eff} = \frac{\alpha_s \left[1 + (1 - \alpha_s)\left(\frac{A_o}{A_w} - f_g\right)\right]}{\alpha_s \left(1 - \frac{A_o}{A_w}\right) + \frac{A_o}{A_w}} \qquad \text{(B.2)}$$

where

A_o/A_w = the ratio of area of cavity aperture to total wall area (including the opening)

For a cylindrical cavity with radius, R, and length, L:

$$\frac{A_o}{A_w} = \frac{1}{2\left[1 + (L/R)\right]}$$

f_g = Gouffe's view factor, which is the fraction of the reflected flux that is returned through the opening without considering a second reflection.

For a diffuse cylindrical cavity (Ref. B-3),

$$f_g = \frac{1}{\left[1 + (L/R)^2\right]}$$

The expressions were derived assuming that the surfaces are diffuse and gray, and that the radiosity is uniform in all directions. In recent years, more rigorous expressions have been derived based on an energy balance integral equation. Solutions for general configurations were evaluated through numerical computation (Refs. B-4 and B-5). A closed-form solution was derived for spherical cavities (Ref. B-3) and is shown in Equations B.3 and B.4.

$$\epsilon_{eff} = \frac{\epsilon_s}{1 - 0.5\,(1 - \epsilon_s)(1 + \cos\phi^*)} \qquad \text{(B.3)}$$

$$\alpha_{eff} = \frac{\alpha_s}{1 - 0.5\,(1 - \alpha_s)(1 + \cos\phi^*)} \qquad \text{(B.4)}$$

where ϕ^* is the opening angle of a spherical cavity (inset of Figure B-2). Numerical results of a computation are shown in Figure B-2.

Comparisons of the analytical expression with experimental data at NBS (Ref. B-6) led to the conclusion that the Gouffe's expression and the more rigorous numerical results predict cavity effective emittance to within 0.01 when the wall material is a good diffuse reflector. If the cavity material has a relatively large specular component, at large angle of incidence, the analytical expressions still agree with the experimental data for a cylindrical cavity with L/r = 0.5. However, agreement becomes progressively poorer as the L/r ratio increases. The difference observed at L/r = 2.0 was 3.5%. Numerical evaluation also has confirmed that a specular reflecting cavity is a more effective emitter and absorber than the diffusely reflecting cavity (Ref. B-7). This is true especially for cavities having large A_w/A_o ratio and walls with low surface emissivity, ϵ_s, or solar absorptivity, α_s.

In practical engineering computations, the effective cavity characteristics may be expressed by simple textbook expressions (Ref. B-8) as shown in Eqs. B.5 and B.6.

$$\epsilon_{eff} = \frac{\epsilon_s}{1 - (1 - \epsilon_s)\left[1 - \left(\frac{A_o}{A_w}\right)\right]} \qquad (B.5)$$

$$\alpha_{eff} = \frac{\alpha_s}{1 - (1 - \alpha_s)\left[1 - \left(\frac{A_o}{A_w}\right)\right]} \qquad (B.6)$$

The derivation assumes that, in addition to having gray diffuse surfaces, the view factors between surface elements and the aperture are constant everywhere, and the interior surfaces are gray and diffuse. The expressions are simple to use and yield reasonably accurate results. Figure B-3 shows the numerical value of cavity emittance (or absorptance) in terms of the surface optical properties and the geometrical area ratio. Excellent agreement between Figures B-2 and B-3 confirms the validity of the simplified expressions for a cavity similar to that of a spherical cavity.

B. ABSORBER ARRANGEMENTS

The absorber/heat exchanger design is the most critical element of the receiver. The absorber requirements are governed strongly by the type of working fluid, the operating temperature, the material selection, and the solar flux distribution on the absorber, and the cavity configuration. Figure B-4 shows the variation of solar flux distribution along a cylindrical cavity wall, for various cavity

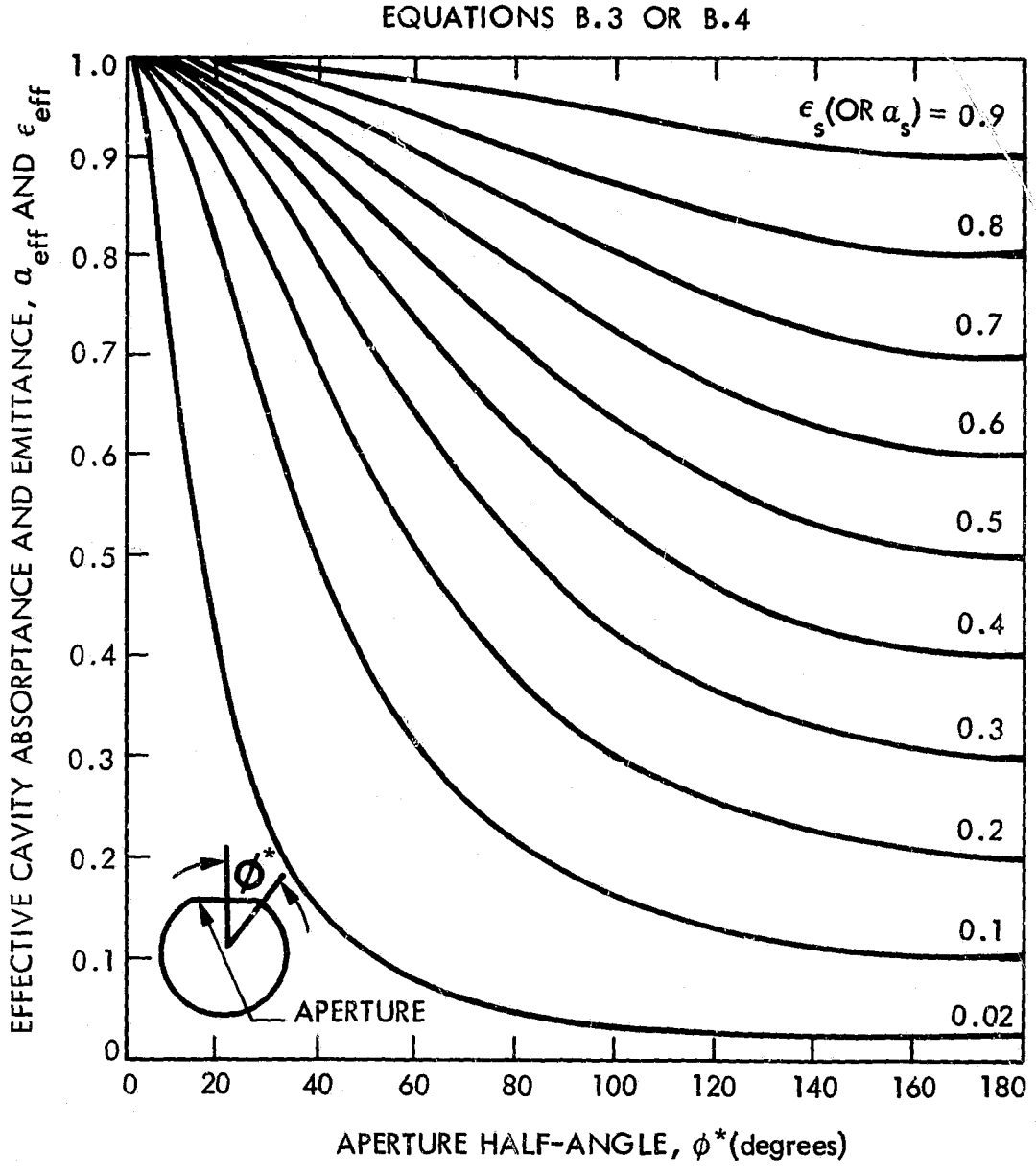

Figure B-2. Effective Radiative Properties of a Spherical Cavity

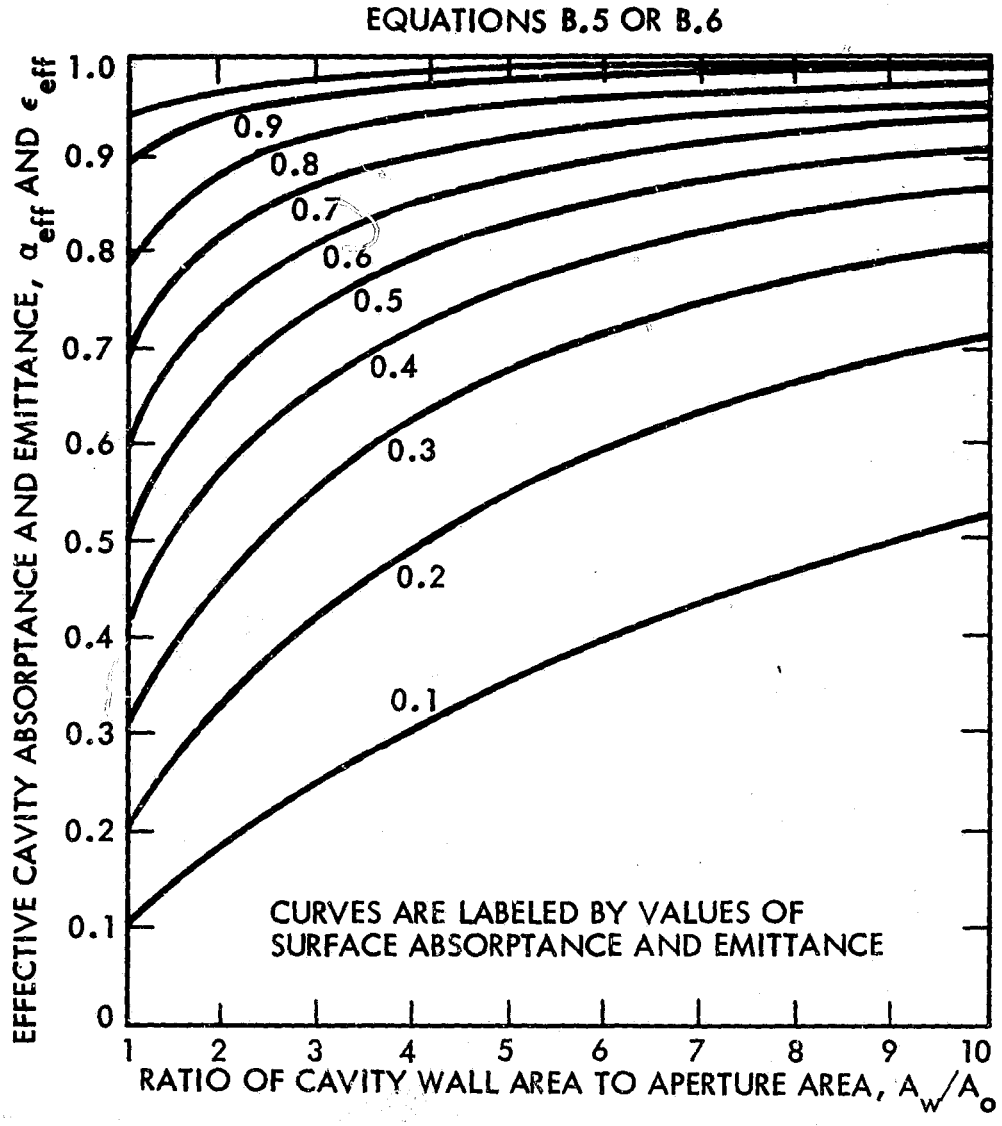

Figure B-3. Effective Cavity Absorptance and Emittance as a Function of A_w/A_o

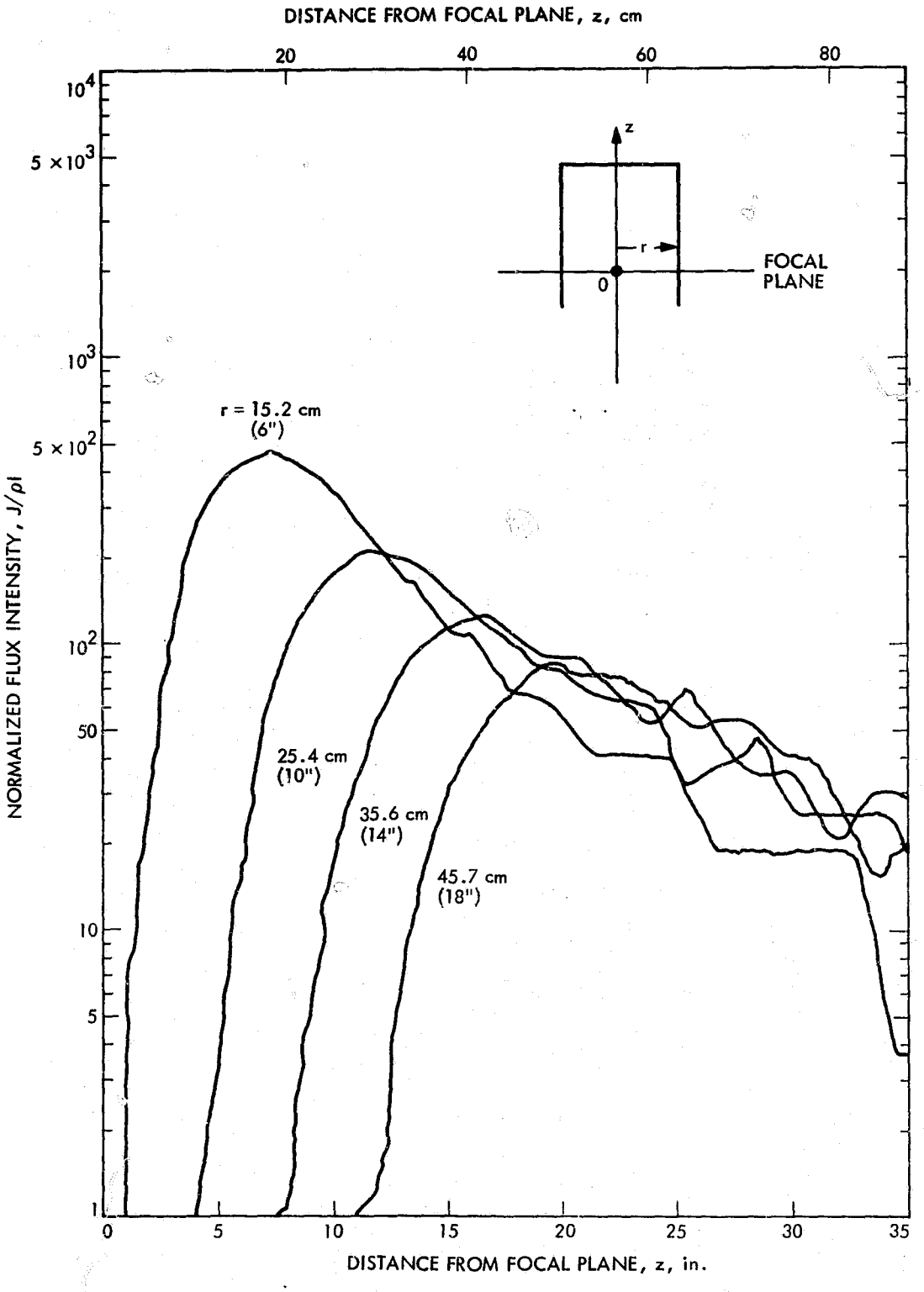

Figure B-4. Solar Flux Distribution along a Cylindrical Receiver Wall

radii. The local heat transfer between the absorber and the working fluid is governed by the heat transfer coefficient and the wall-to-fluid temperature difference:

$$J = h_w (T_w - T_{fl}) \qquad (B.7)$$

The local coefficient of heat transfer, h_w, is determined by the thermophysical properties of the fluid and flow characteristics such as flow velocity and pressure. It is necessary to have a sufficiently high coefficient of heat transfer to limit the temperature differentials and to prevent possible burnout. Figure B-5 (Ref. B-9) shows several typical flow arrangements. One of the critical dimensions is the diameter of the heat exchanger tubes, which affects both the heat transfer coefficient, h_w, and the fluid friction pressure loss. Total heat exchanger area requirements are governed by the total thermal energy input to the receiver, the thermophysical properties of the working fluid, and the flow arrangement. An undersized absorber could result in an excessive mean temperature difference between the fluid and the receiver, resulting in high-temperature heat losses. On the other hand, an oversized receiver might lead to an unacceptable weight increase and large conductive heat loss. Figure B-6 shows the heat transfer area and the mean absorber temperature differential relationship for typical receivers with 60 kWth output and different types of engine/working-fluid arrangements (Ref. B-10).

C. RECEIVER HEAT LOSSES

Thermal energy losses from the receiver include three contributions: (1) radiative heat loss through the aperture, (2) convective heat transfer to the ambient air through the aperture, and (3) conductive/convective heat loss through the receiver insulation.

1. Radiative Losses

Thermal emission from the cavity receiver is governed by the effective receiver temperature, T_r, and the effective cavity emittance, ϵ_{eff}.

$$Q_{rad} = \epsilon_{eff} A_o \sigma (T_r^4 - T_a^4) \qquad (B.8)$$

where

Q_{rad} = radiative heat loss
ϵ_{eff} = effective cavity emittance
σ = Stefan-Boltzmann constant
T_r = effective cavity radiation temperature
T_a = ambient temperature
A_o = receiver cavity aperture area

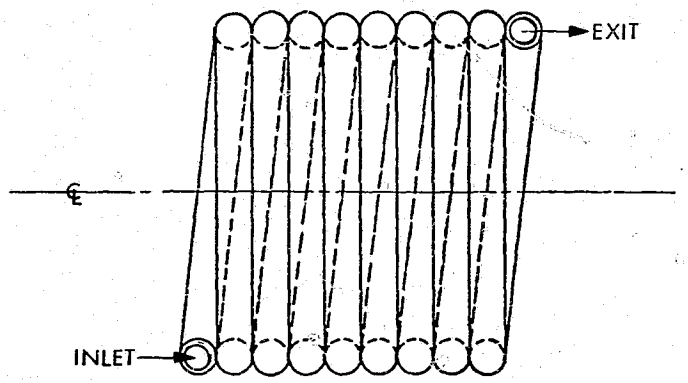

(a) HEAT RECEIVER ONE-PASS TUBE HELIX

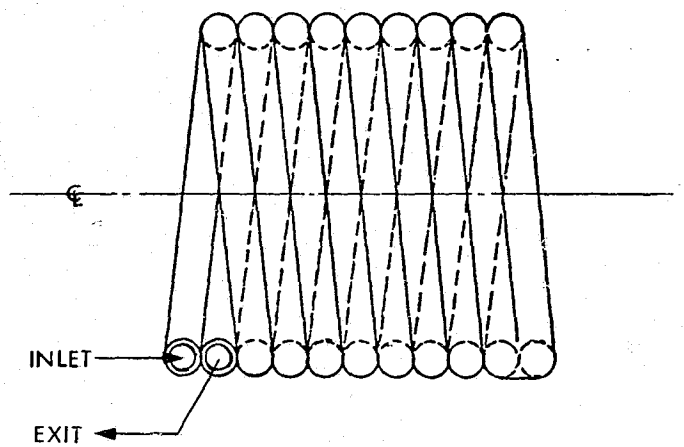

(b) HEAT RECEIVER TWO-PASS TUBE HELIX

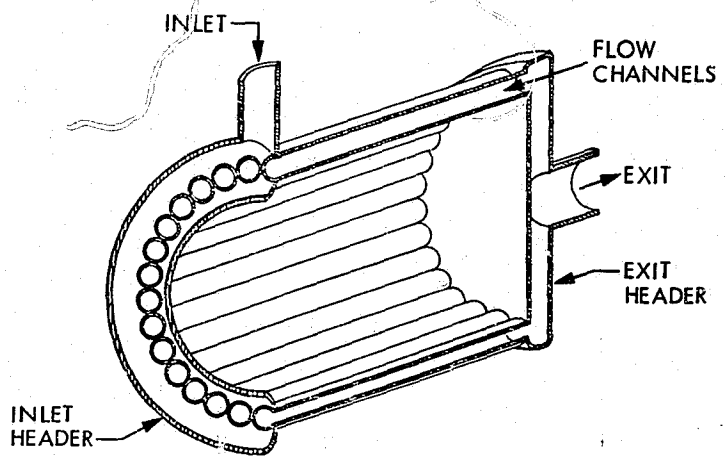

(c) HEAT RECEIVER ONE-PASS AXIAL FLOW TUBE BUNDLE

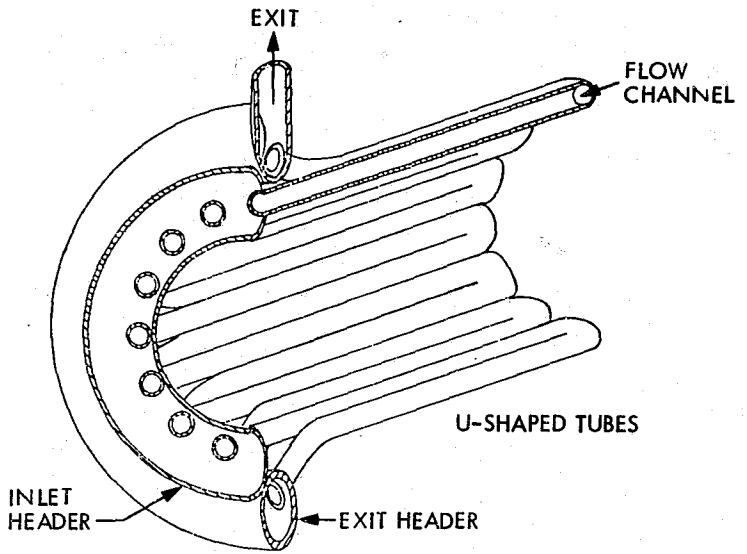

(d) HEAT RECEIVER MULTI-PASS AXIAL FLOW TUBE BUNDLE

Figure B-5. Typical Solar Absorber Arrangements

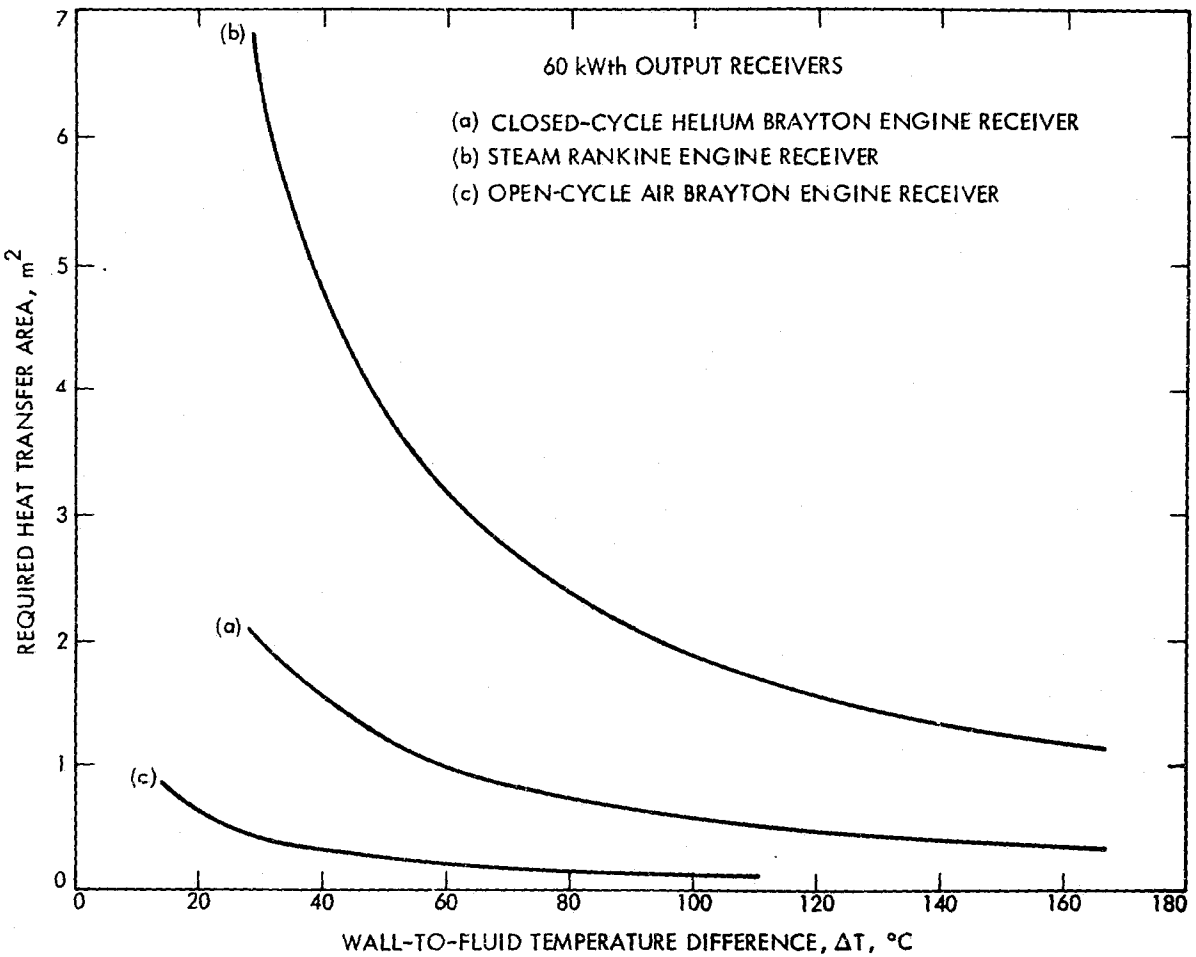

Figure B-6. Heat Transfer Area and Temperature Difference Relationship for Typical Receivers

The effective emittance is a direct function of surface emissivity and the cavity geometrical configuration. The application of selective coatings may improve the receiver effectiveness (Ref. B-11). However, very little research has been devoted to high-temperature selective coatings due to a lack of suitable materials and a significant mismatch between the solar spectrum and the high-temperature infrared emission spectrum. The effect of selective coatings is not included in the present investigation. Flat-black absorbers with a surface absorptance and emittance of 0.8 are assumed.

2. Convective Losses

Convective heat transfer relationships between the cavity and the ambient air are complex (Ref. B-12) because both natural (free) and forced convection components are involved.

a) Free Convection. Without bulk air movement, the convective heat transfer of a surface involves air motion induced by a fluid density gradient, a result of a temperature difference between the absorber and the ambient air, and the action of gravity. This is referred to as free (natural) convection. Generalized heat transfer relationships for free convection of surfaces are expressed in terms of dimensionless parameters (Ref. B-13).

$$Nu = 0.736\ (Gr \cdot Pr)^{1/4}; \quad \text{Laminar Range Gr. Pr} < 10^8$$
$$Nu = 0.3\ (Gr \cdot Pr)^{1/3}; \quad \text{Turbulent Range } 10^8 < Gr \cdot Pr < 10^{12}$$

where

Nu	=	Nusselt number = $\frac{hL}{K}$
Gr	=	Grashof number = $Bg\ (\Delta T)\ L^3/\nu^2$
Pr	=	Prandtl number = $\rho_d\ C_p\ \nu/K$, for air Pr $\sim$ 0.72
h	=	Convective coefficient of heat transfer
K	=	Thermal conductivity of air
L	=	Receiver length
B	=	Coefficient of thermal expansion (air)
g	=	Gravitational constant
ΔT	=	Temperature difference between a surface and the ambient air
ν	=	Kinematic fluid viscosity

For a flat plate tilted at an angle, τ, with respect to horizontal, an approximate relationship is $h_{fr} = 0.71\ h_h\ (\sin\tau)^{1/3}$, (Ref. B-14), where h_{fr} is the coefficient of heat transfer at the front surface, and h_h is the coefficient of heat transfer for a horizontal plate. No accurate correlation is available for the back surface of a flat plate. An approximate expression was suggested (Ref. B-15), and a reasonably good agreement with test-data correlations was observed as based on the heat transfer coefficient for a vertical plate, h_v.

$$h_{back} = h_v\ (\sin\tau)^{1/3} \qquad (B.9)$$

For a tilted cavity, the cavity wall-temperature is not uniform and the tilt angle is a function of the sun position. As a first approximation, it is reasonable to utilize the average effects of wall temperature and tilt angle. The corresponding average, free convection coefficient is:

$$h_f \simeq 6 \times 10^{-4} (T_e - T_a)^{1/3} \quad kW/m^2\text{-}^oC \qquad (B.10)$$

where

h_f = average coefficient of free convective heat transfer
T_e = average cavity temperature

b) Forced Convection. Forced convection (wind) over the cavity aperture involves a large number of variables such as wind speed, wind direction, cavity configuration, etc. A generalized correlation is too complex to handle. An approximate approach is to treat the cavity opening as a flat plate with effective temperature, T_e. The classical heat transfer relationship for a flat plate geometry is

$$Nu = 0.664\ Re^{1/2}\ Pr^{1/3}$$

where

Re = Reynold's number = VD/ν
V = free stream fluid velocity
ν = Kinematic fluid viscosity

Field test data (Refs. B-13 and B-16) indicate that an assumed linear relationship between the forced convection heat transfer coefficient and the wind speed yield reasonably good heat transfer results; a satisfactory correlation is:

$$H \sim 0.002\ V \qquad (B.11)$$

where

H = forced convection heat transfer coefficient
V = wind speed m/sec

In engineering practice it has been an accepted approximation to superimpose the effects of free and forced convections.

$$Q_{conv} = A_o\ (h_f + H)(T_e - T_a) \qquad (B.12)$$

3. Conductive Losses

Conductive heat loss through the receiver insulation is dominated by the insulation thickness and thermal conductivity.*

$$Q_{cond} = A_w h_c (T_e - T_a) \qquad (B.13)$$

where

Q_L = conductive heat loss through insulating walls
A_w = effective cavity wall area
h_c = effective conductive heat loss coefficient.

Representative values of the heat loss coefficient, h_c, are shown in Figure B-7 for a spherical receiver (Ref. B-10). The insulation material is considered to be a typical type of flexible Min-K insulator from Johns-Manville (Ref. B-17) with an average thermal conductivity of K = 0.052 W/m-^{o}C.

*Thermal resistance in the insulation layer (conduction) is usually much more significant than the convective heat transfer at the outer surface.

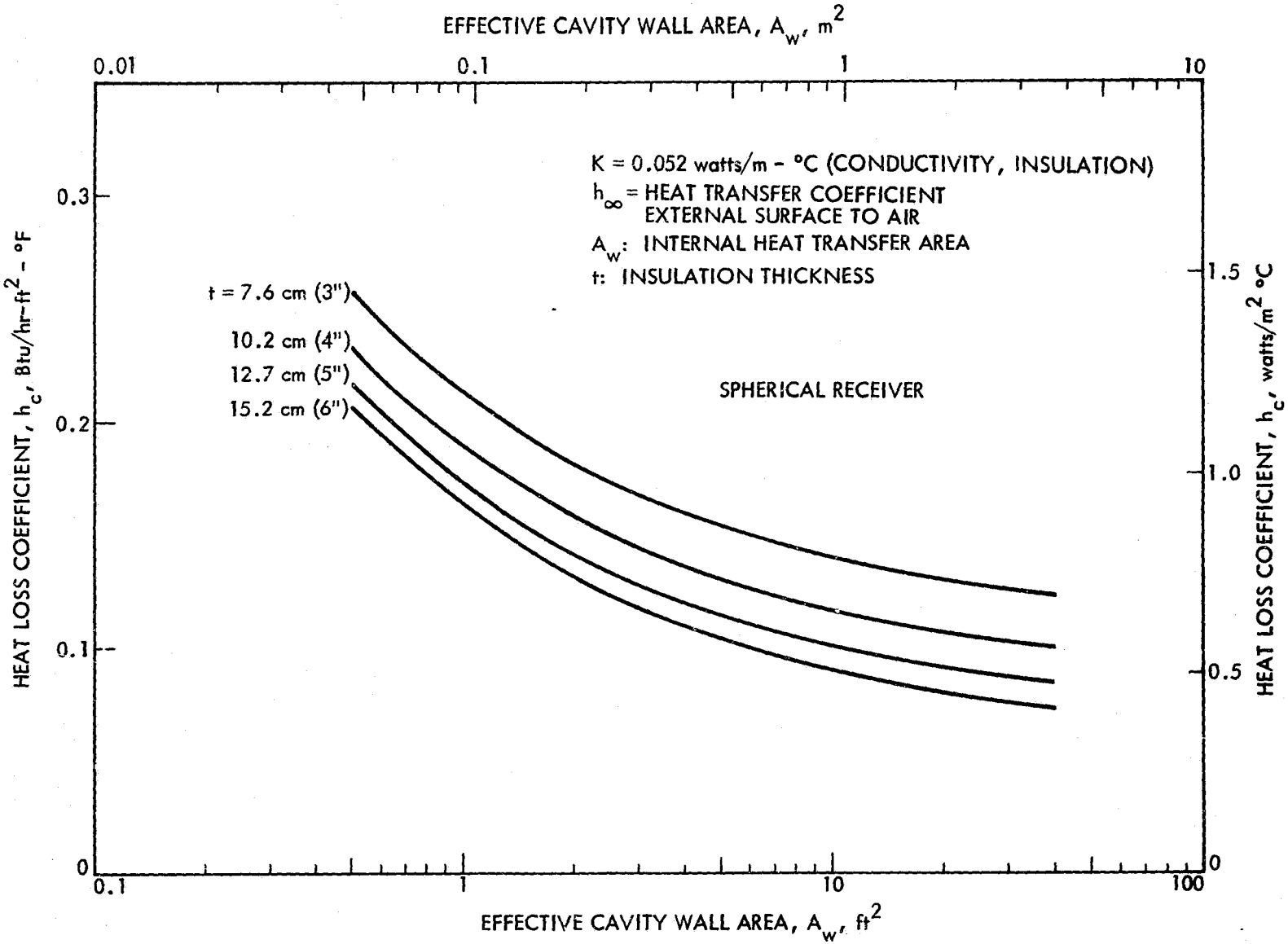

Figure B-7. Representative Receiver Conductive Heat Loss Coefficient

APPENDIX B

REFERENCES

B-1. Wu, Y. C., and Wen, L., "Solar Receiver Performance of Point Focusing Collector System," paper presented at ASME Annual Winter Meeting, San Fransico, Dec. 1978.

B-2. Gouffe, A., Rev. d'Optique, Vol. 24, No. 1-3, pp. 1-10, 1945.

B-3. Sparrow, E. M., Albers, L. U., and Eckert, E. R. G., "Thermal Radiation Characteristics of Cylindrical Enclosure," pp. 73-81, Journal of Heat Transfer, Trans. ASME, Series C, Feb., 1962.

B-4. Sparrow, E. M., and Jonsson, V. K., "Absorption and Emission Characteristics of Diffuse Spherical Enclosures," pp. 188-189, Journal of Heat Transfer, Trans. ASME, Series C, May, 1962.

B-5. Sparrow, E. M., and Albers, L. V., "Apparent Emissivity and Heat Transfer in a Long Cylinder Hole," pp. 253-255, Journal of Heat Transfer, Trans. ASME, Series C, Aug., 1960.

B-6. Kelley, F. T., and Moore, D. G., "A Test of Analytical Expressions for the Thermal Emittance of Shallow Cylindrical Cavities," NASA SP-55, pp. 117-131, Symposium on Thermal Radiation of Solids, 1964.

B-7. Sparrow, E. M., "Radiant Emission, Absorption and Transmission Characteristics of Cavities and Passages," NASA SP-55, pp. 103-115, Symposium on Thermal Radiation of Solids, 1964.

B-8. Kreith, F., Radiation Heat Transfer - for Spacecraft and Solar Power Plant Design, International Textbook Company, Stranton, Penn., 1962.

B-9. Hedgepeth, L. M., Huffman, G. D.,. and Ostdiek, F. R., "Comparisons of Weights and Performances of Solar Dynamic Energy Conversion Systems," Technical Report AFAPL-TR-65-44, U.S. Air Force, Sept., 1965.

B-10. Wu, Y. C., "Solar Receiver Performance in the Temperature Range of 300 to 1300°C," (also Internal Interoffice Memo 353-78-196), JPL Internal Doc. No. 5102-82 (Preliminary Issue), Jet Propulsion Laboratory, Pasadena, Calif., October 1978.

B-11. Wen, L., and Caputo, R., "Effects of Surface Optical Characteristics on Point Focusing Solar Collectors," paper presented at Selective Absorber Coating Workshop, sponsored by SERI, Golden, Colorado, Dec. 6-7, 1977.

B-12. Yin, S. H., Wung, T. Y., and Chen, K., "Natural Convection in an Air Layer Enclosed Within Rectangular Cavities," International Journal of Heat Mass Transfer, Vol. 21, pp. 307-315, 1978.

B-13. Am. Soc. Heating, Refrigerating, Air Conditioning Engineers (ASHRAE), Handbook of Fundamentals, New York, 1967.

B-14. Raithby, G. D., and Hollands, K. G., "A General Method of Obtaining Approximate Solution to Laminar and Turbulent Free Convection Problems," Advances in Heat Transfer, pp. 265-316, Vol. 11, Edited by T. F. Irvine and J. P. Hartness, Academic Press, 1975.

B-15. Wen, L., "Interim Report on LSSA Thermal Investigation," Internal Interoffice Memo to R. G. Ross, 353-GEN-76-487, Jet Propulsion Laboratory, Pasadena, Calif., Sept. 28, 1976.

B-16. Stultz, J. W. and Wen, L., "Thermal Performance Testing and Analysis of Photovoltaic Modules in Natural Sunlight," LSA Project Task Report, Internal Document No. 5101-31, Jet Propulsion Laboratory, Pasadena, Calif., July 29, 1977.

B-17. Min-K Thermal Insulation Data Sheet, IND-3263-9-76 Johns-Manville Insulation Center, Denver, Colorado, Sept. 1976.

APPENDIX C

POWER CONVERSION UNITS

A wide variety of thermodynamic cycles and a large range of engine power capacities have been considered for solar thermal applications. The engine efficiency is governed by the cycle characteristics, the working fluid properties, operating temperatures, and capacity/load conditions. The efficiency of the generator/alternator assembly increases, to some extent, with increasing system size. Detailed surveys of power conversion subsystems for solar thermal applications are available for state-of-the-art as well as advanced power conversion systems (Refs. C-1, C-2, and Appendix A of C-3).

In the present study simple Rankine and Brayton engine subsystems were considered (Section II, Part B); only relevant efficiency characteristics are reviewed briefly herein for illustrative purposes.

A. STEAM RANKINE UNITS

The basic steam Rankine cycle operates as follows: water is pumped under pressure into a boiler (receiver in the case of solar applications) where it is heated to a vapor or superheated state. The steam is then expanded through turbine blades (or pistons) to produce mechanical energy. The low pressure steam emerging from this expansion process is condensed to water and then pumped under pressure back to the boiler to complete a cycle.

Steam Rankine turbines have been used widely in electric utilities for conventional fossil-fueled and nuclear power generation stations. Rankine-cycle thermal efficiencies are in the 37 to 43% range at operating temperatures around 538°C (1000°F) for large central power stations with 100 to 1000 MW capacities. Small steam Rankine systems have relatively lower efficiencies. Current projections of small reciprocating engine and single-stage turbines in the 15 to 100 kWe range indicate a power conversion efficiency (including generator/alternator) around 20% at 538°C (1000°F) steam temperature. Advanced development of small steam Rankine systems incorporating a reheat cycle and higher pressure/temperature combinations may improve overall efficiencies to 30%, or higher. Typical steam Rankine power performance characteristics versus plant size are shown in Figure C-1, (Ref. C-4). The relative variation of efficiency with inlet steam temperature is shown in Figure C-2; here, relative efficiency is referenced to a 1000°F operating condition. Note that the theoretical steam Rankine efficiency rises less steeply with cycle temperature than does the Carnot cycle efficiency.

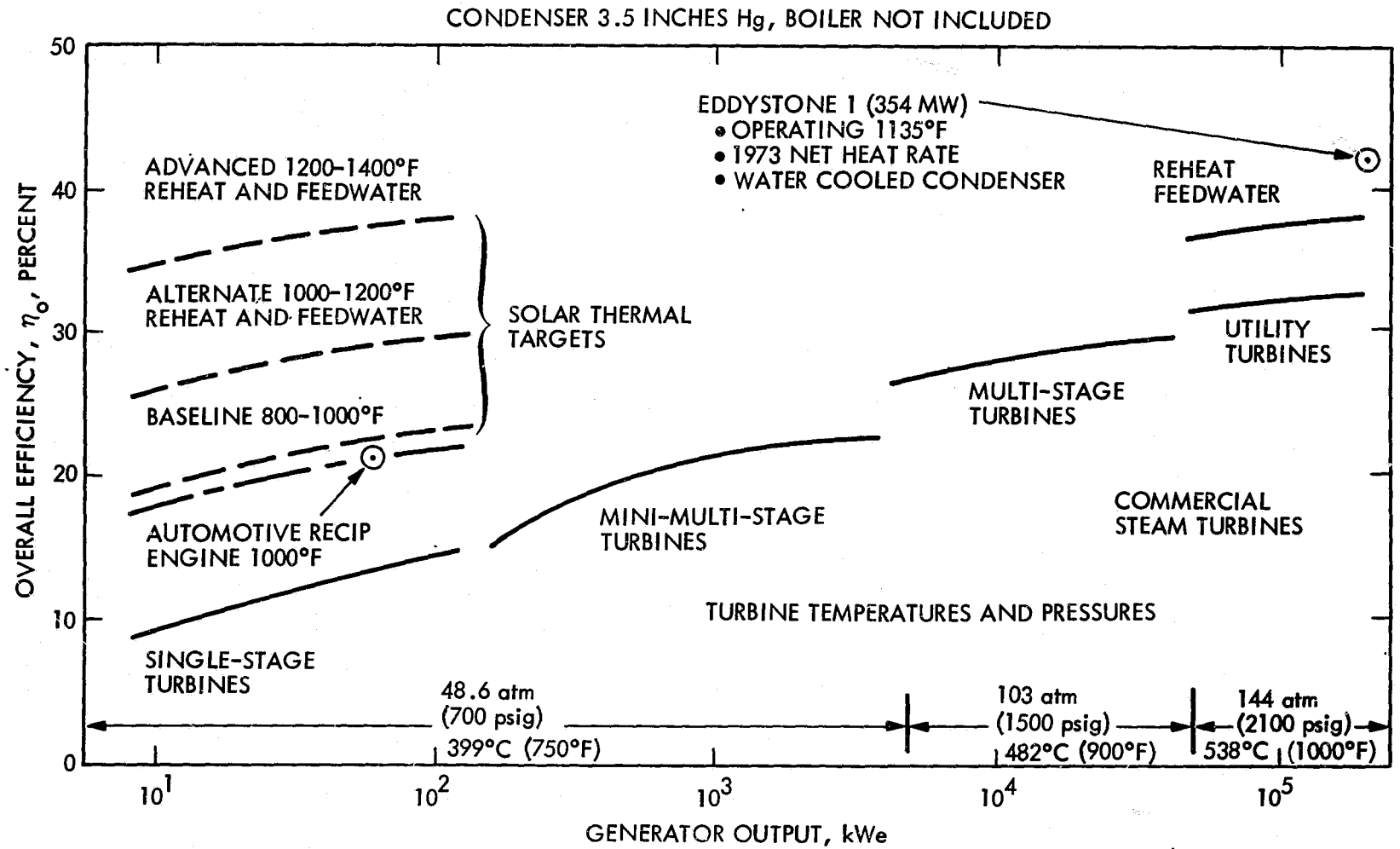

Figure C-1. Comparison of Performance of Advanced Steam Engine/Generator Sets with Commercial Steam Turbines

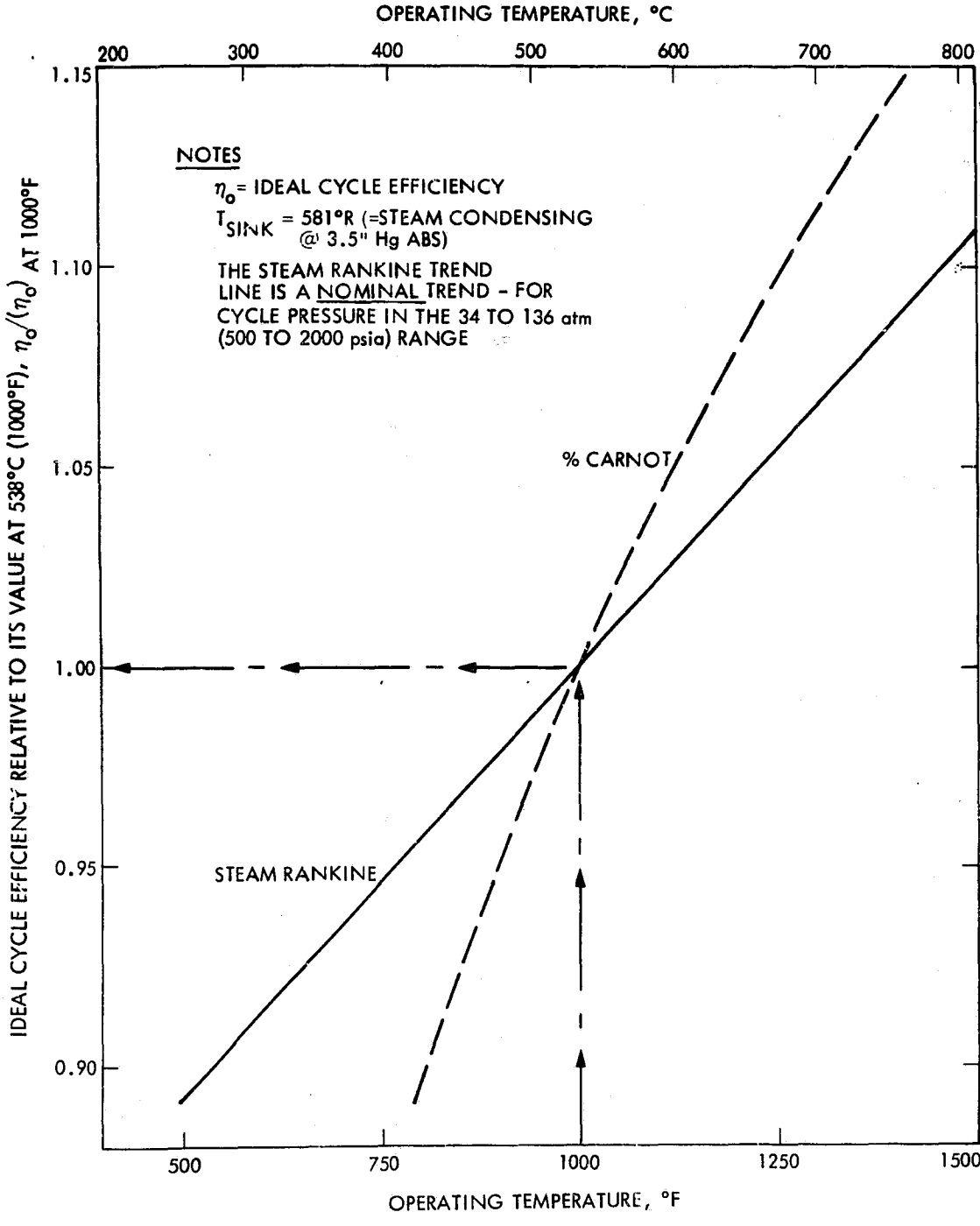

Figure C-2. Steam Rankine Power Conversion Efficiency versus Steam Temperature

B. GAS BRAYTON ENGINES

The Brayton cycle has been utilized extensively in the gas turbine, e.g., the jet engine. The engine efficiency depends on peak cycle temperature, pressure ratio, effectiveness of the recuperator, turbine and compressor mechanical efficiency, and ambient temperature. The operating principles of an ideal gas turbine cycle are well known. The working fluid is compressed isentropically to a pressure higher than the inlet value. Heat is then added (combustor or solar receiver) to increase the gas temperature at constant pressure. The high-temperature, high-pressure gas then undergoes insentropic expansion in the turbine producing the work necessary to drive the compressor, auxiliaries, and the load. The turbine exhaust is at a higher temperature than the compressor discharge so that it is usually advantageous to employ a recuperator to recover part of the exhaust heat, which is transferred to the compressed working fluid.

Brayton cycles may be operated as open (air) or closed systems. A number of working fluids, such as helium, argon, etc., that have better heat transfer properties than air, may be used in closed-cycled machines. Gas turbines commonly are used by utilities to generate electric power during peak demand. A large closed-cycle air turbine producing 60 MWe was assessed to have a power conversion efficiency around 42% at an inlet temperature of 1500°F (820°C) (Ref. C-5). The cycle efficiency of small Brayton engines at (820°C) was assessed to be 33.4% and 35.6% for open-air and closed-cycle helium systems respectively (Ref. C-6). Brayton cycle efficiency may be increased using higher inlet temperature, and improvements in turbine compression ratio and recuperator effectiveness (Ref. C-7). Large gas turbines may utilize multi-stage compressors, compressor stage intercooling, and turbine reheat to improve performance; Figure C-3 shows the estimated Brayton open-cycle performance vs. engine size. The dependence of Brayton cycle efficiency on engine operating temperature is illustrated in Figure C-4 along with the curve for the Rankine cycle (from Figure C-2). The Brayton curve has a steeper slope, which implies that Brayton cycle efficiency can be significantly improved using higher operating temperatures. Material cooling considerations limit the cycle temperature to about 1600 to 1800°F, at the present time. Higher temperatures require cooling of metallic turbine blades. Research in ceramic turbine blade technology may extend the operating temperature range to 2500°F, or higher.

The effectiveness of the recuperator, E, is another important factor governing the performance of the Brayton engine. Figure C-5 (Ref. C-7) shows the effects of recuperator effectiveness for different turbine inlet temperatures. Although high recuperator effectiveness is desirable, it also implies high cost and weight associated with the heat exchanger requirements.

Part-load characteristics of the candidate power conversion subsystems were discussed previously in the text (Section II, Part B).

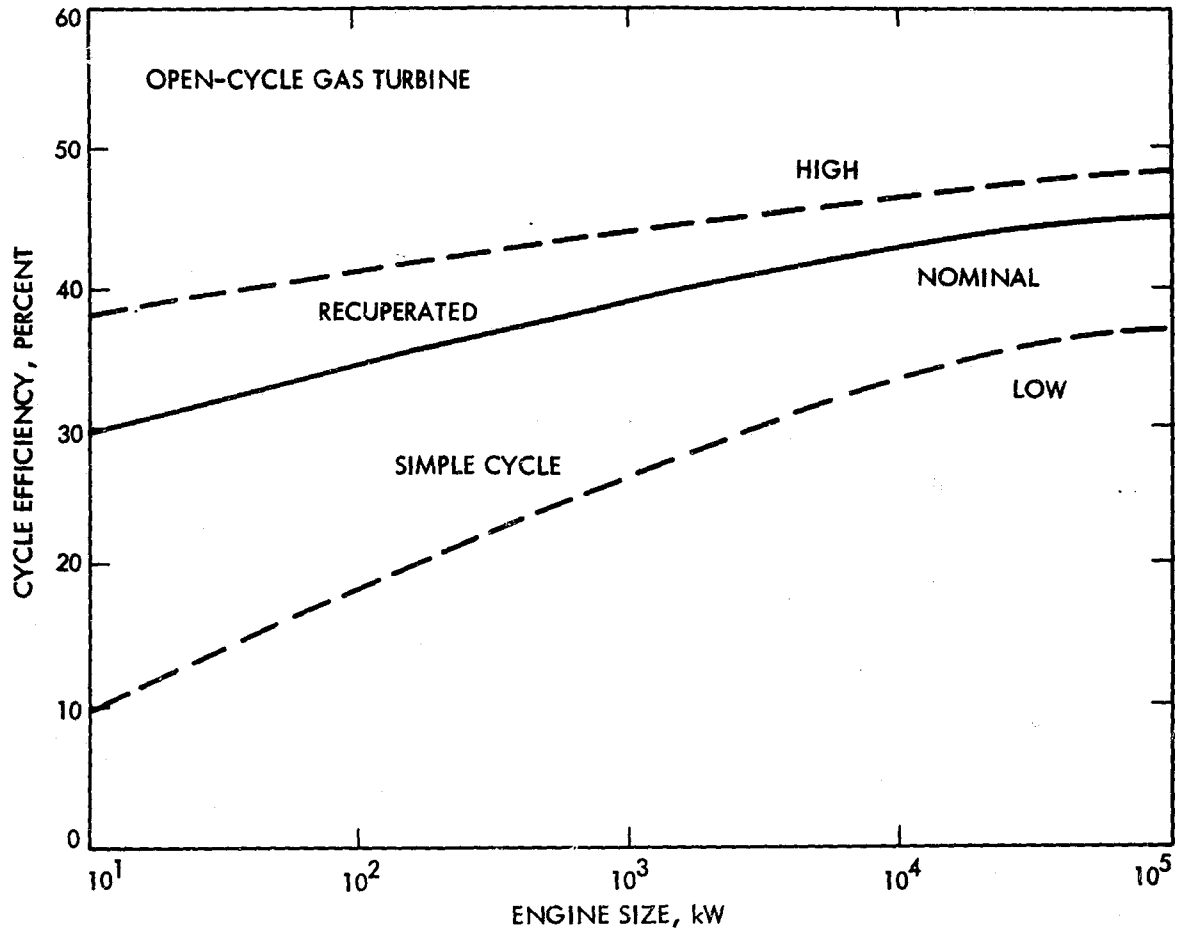

Figure C-3. Estimated Brayton Cycle Performance versus Engine Size

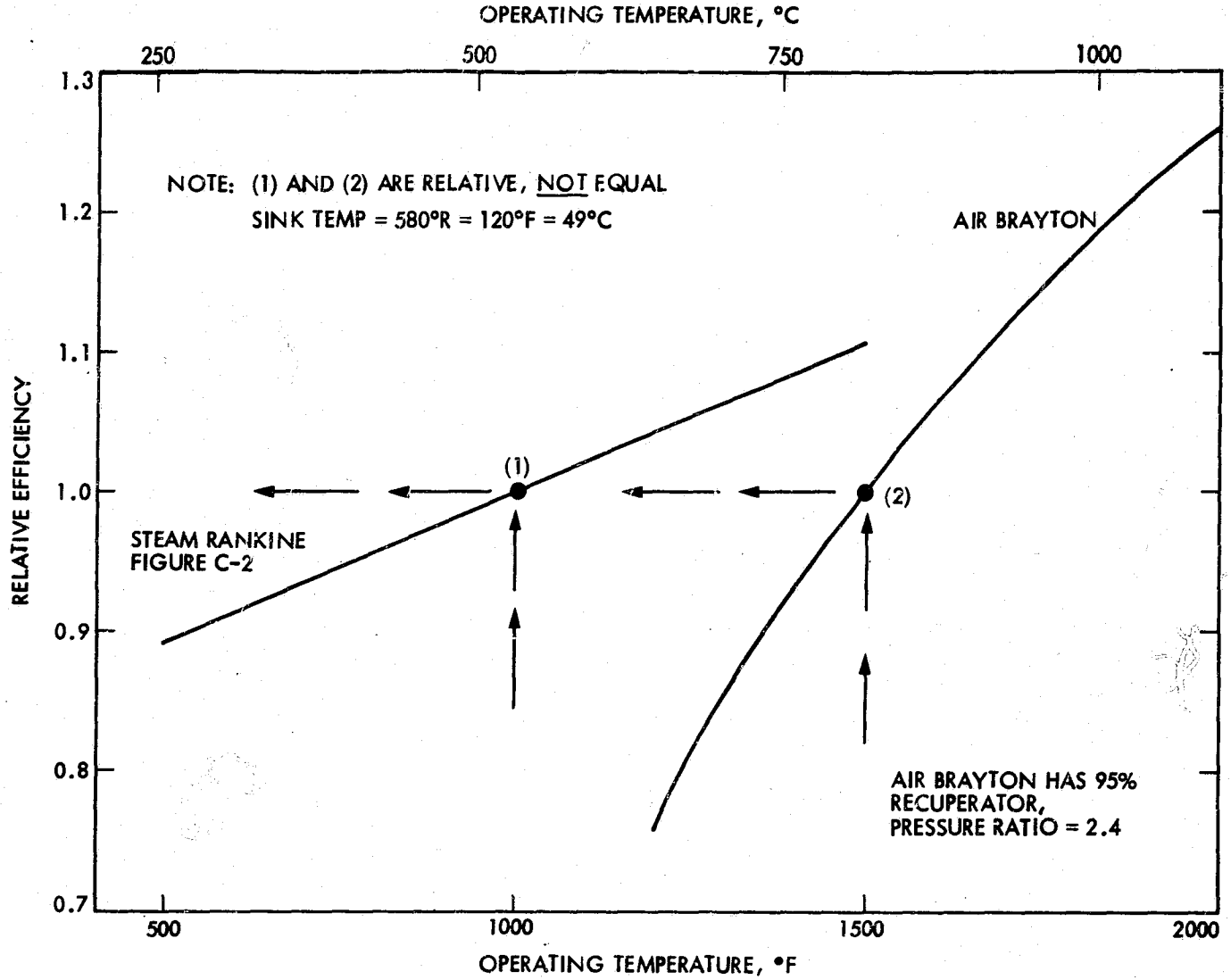

Figure C-4. Brayton Cycle Efficiency versus Operating Temperature

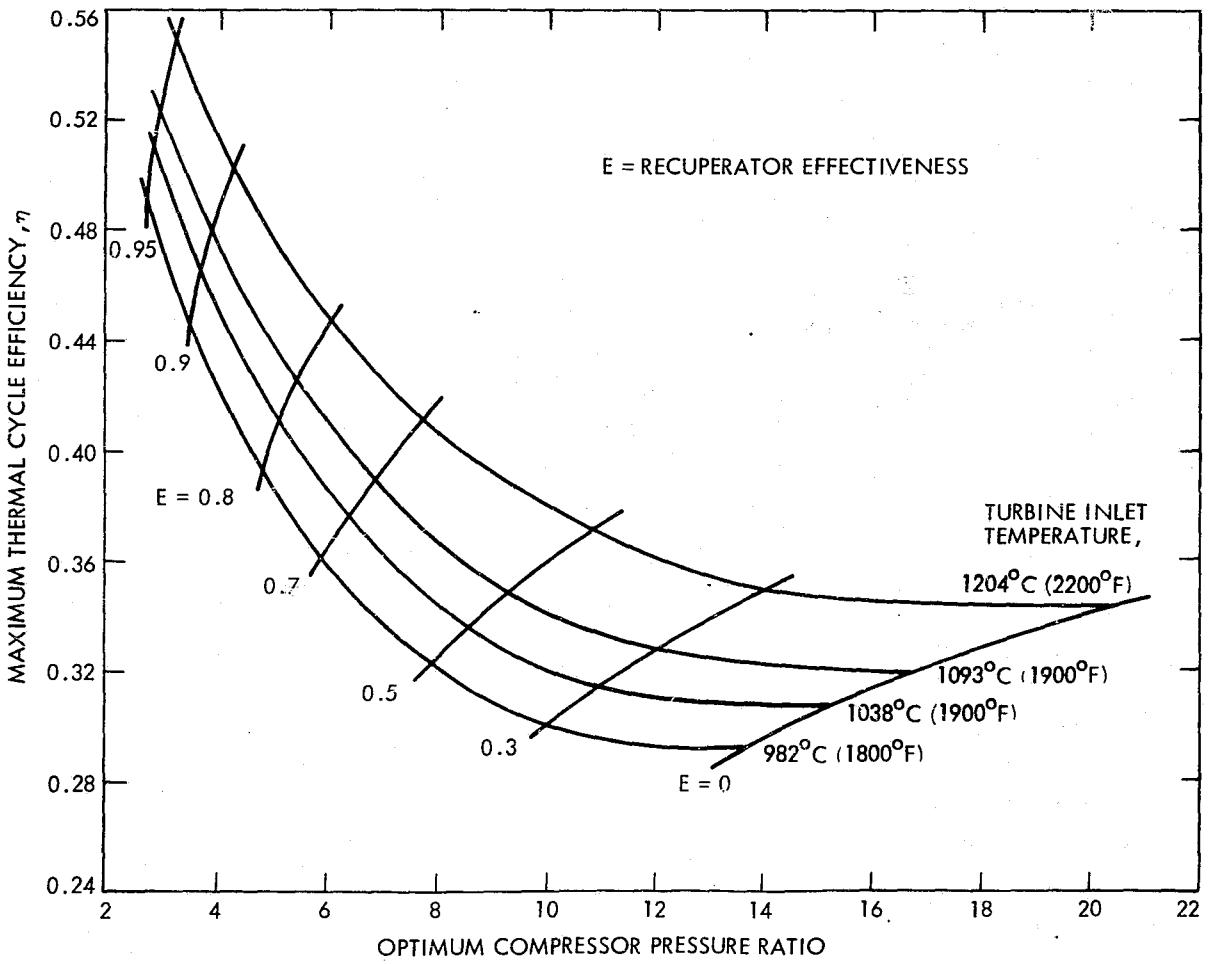

Figure C-5. Maximum Thermal Cycle Efficiency of Simple and Recuperated Gas Turbines

APPENDIX C

REFERENCES

C-1. "Application of Solar Technology to Today's Energy Needs," Vol. I, Office of Technology Assessment (OTA), Congress of the United States, June 1978.

C-2. Mroz, T., et al., "Handbook of Data on Selected Engine Components for Solar Thermal Applications," DOE/NASA-1060-78/1, NASA TM-79027, Advance Copy, NASA Lewis Research Center, Cleveland, Ohio, November 1978.

C-3. Fujita, T., et al., "Techno-Economic Projections for Advanced Dispersed Solar-Thermal Electric Power Plants to Years 1990-2000," DOE/JPL-1060-4, JPL Publication No. 78-12, November 1978. (See Appendix A, Survey of Advanced Energy Conversion Systems)

C-4. Bailey, M., private communication, NASA Lewis Research Center, Cleveland, Ohio, 1978.

C-5. Schroeder, J., "Advanced Central Receiver Concepts," Boeing Engineering and Construction paper presented at U.S. Department of Energy Semi-Annual Review, San Diego, California, March 2-3, 1978.

C-6. Heller, J. A., private communication, NASA Lewis Research Center, Cleveland, Ohio, 1978.

C-7. Bloomfield, H. S., and Calogeras, J. E., "Technical and Economic Feasibility Study of Solar/Fossil Hybrid Power Systems," NASA TM-73820, NASA Lewis Research Center, Cleveland, Ohio, Dec. 1977.